Ultrastructural Characterization of The Output of VIP Expressing Interneurons in Mouse Barrel Cortex

Dissertation

for the award of the degree

"Doctor rerum naturalium"

Faculty of Biology

of the Georg-August University Göttingen

within the doctoral program Sensory and Motor Neuroscience

of the Georg-August University School of Science (GAUSS)

submitted by

Xiaojuan Zhou

from Wuhan, China

Göttingen, March 31th, 2017

Thesis Committee

Prof. Dr. med. Jochen F. Staiger, Institute for Neuroanatomy, University Medical Center Göttingen

Prof. Dr. Thomas Dresbach, Institute for Anatomy and Embryology, University Medical Center Göttingen

Prof. Dr. Carolin Wichmann, Institute for Auditory Neuroscience & InnerEarLab, University Medical Center Göttingen

Members of the Examination Board

Referee: Prof. Dr. med. Jochen F. Staiger, Institute for Neuroanatomy, University Medical Center Göttingen

2nd Referee: Prof. Dr. Carolin Wichmann, Institute for Auditory Neuroscience & InnerEarLab, University Medical Center Göttingen

Further members of the Examination Board

Prof. Dr. Thomas Dresbach, Institute for Anatomy and Embryology, University Medical Center Göttingen

Prof. Dr. Siegrid Löwel, Department of Systems Neuroscience, Johann- Friedrich-Blumenbach-Institute of Zoology and Anthropology, University of Göttingen

Prof. Dr. Tim Gollisch, Department of Ophthalmology,
University Medical Center Göttingen

Camin Dean, Ph.D., Research group "Trans-synaptic Signaling",
European Neuroscience Institute Göttingen

Date of oral examination: May 15th, 2017

I, Xiaojuan Zhou, hereby certify that the present doctoral thesis has been written independently with no other sources than cited. All results presented here were the outcome of my own workings unless stated otherwise.

....

Göttingen, March 31th, 2017

Table of Content

Figures

List of Abbreviations

5HT	Serotonin
5HT3aR	Serotonin receptor type 3a
ANOVA	Analysis of variance
CCK	Cholecystokinin
ChAT	Choline acetyltransferase
CB	Calbindin
CR	Calretinin
CRF	Corticotropin-releasing factor
DAB	3,3'-Diaminobenzidine tetrahydrochloride
EM	Electron microscopy
FPF	False positive fraction
FNF	False negative fraction
GABA	Gamma-aminobutyric acid
GFP	Green fluorescent protein
POm	Posterior medial thalamic nucleus
PV	Parvalbumin
ROC	Receiver operating characteristics
SST	Somatostatin
TPF	True positive fraction
TNF	True negative fraction

V1   Primary visual cortex

VIP   Vasoactive intestinal polypeptide

VPm   Ventral posteromedial thalamic nucleus

YFP   Yellow fluorescent protein

1.   Introduction

Sensory and motor systems are crucial for rodents, mammal and human to perceive external stimuli and interact with the outside environment. For primary sensory cortex, it constantly receives information coming from the peripheral sensory organs in a bottom-up manner and integrates information coming from motor cortex in a top down manner when animals are doing an active exploration. This normal functionality of the cortex relies on complex neuronal circuits, the anatomy of which needs to be deciphered. There are two basic components of neuronal circuit: excitation and inhibition driven by excitatory neurons and inhibitory interneurons respectively. Nowadays, more and more researchers address their attention on interneurons and are astonished by their diversity. As a local regulator, interneurons also form diverse microcircuits, i.e. feedforward and feedback inhibition. It is important to study the microcircuit of each distinctive subtype of interneurons in order to gain knowledge on how they control local networks of the cortex in different behavioral conditions.

1.1   Barrel cortex and its connectivity

1.1.1   Whisker-to-barrel pathway

In rodents, the barrel cortex is a region of primary sensory cortex (S1) that corresponds to whisker related perception like shape, texture and distance. The term "barrel" comes from the barrel-like cytoarchitectonic morphology of neurons in layer IV and correlates to the cortical column (Mountcastle et al., 1955) when extending the barrel-like structure throughout the whole laminae. Each barrel-related column is the exact representation of a

single whisker (Woolsey and van der Loos, 1970). This intriguing correlation is based on the anatomical whisker-to-barrel pathway via the brain stem and thalamus. The whiskers on the snout of animals are organized in rows (A-E) and arcs (1-7). Each whisker grows in a follicle that is heavily innervated by axons of the neurons in the trigeminal ganglion that further project to the trigeminal nuclei in the brain stem. At this level, representation of whiskers forms a preliminary shape called barrelettes (Ma, 1991). The trigeminal nuclei further project to the ventral posteromedial thalamic nucleus (VPm) where single whiskers are represented as barreloids (Van Der Loos, 1976). Finally thalamic fibers project to barrel cortex in which the "barrels" are arranged in rows and columns correlating with the rows and arcs of whiskers (Schubert et al., 2007). By the whisker-to-barrel pathway, sensory information is transferred from the peripheral sensory system to the cortex.

1.1.2   Canonical microcircuit

The canonical microcircuit of the barrel cortex corresponds to the sensory information flows among principal cells across cortical layers initiated by thalamocortical input (Lübke and Feldmeyer, 2007; Feldmeyer et al., 2013). The two major thalamocortical inputs, known as lemniscal and paralemniscal pathways, target the barrel cortex in an almost complementary manner. For the lemniscal pathway, spiny stellate neurons, one type of excitatory neurons in layer IV (Schubert et al., 2003; Staiger et al., 2004a), receive the strongest innervation from VPm (Jensen and Killackey, 1987). Additionally, pyramidal neurons in layers III, Vb and VIa are innervated to a lesser extent (Meyer et al., 2010). For the paralemniscal pathway, the posterior medial thalamic nucleus (POm) innervates densely layers I, II/III, Va avoiding layer IV (Wimmer et al., 2010). Within the home column, axons of spiny stellate neurons then innervate layer II/III pyramidal neurons that further target pyramidal cells in layer V (Feldmeyer et al., 2002; Lefort et al., 2009). As the major output

2

layers, pyramidal neurons in layers V and VI project back to the thalamus (Cruikshank et al., 2010; Zingg et al., 2014). Besides the thalamo-cortico-thalamic loop, the barrel cortex is also connected reciprocally with other cortical regions, i.e. secondary somatosensory cortex (S2), primary motor cortex, as well as with subcortical areas (Koralek et al., 1990; Wright et al., 2001; Alloway, 2008).

1.2   Diversity of cortical interneurons

Inhibitory (i.e. GABAergic) interneurons represent approximately 15-20% of the neocortical neuronal population, leaving the rest majority population being the glutamatergic principal cells. Unlike the principal cells, which are often regarded as the projection neurons, most neocortical GABAergic interneurons are local circuit cells as their axons remain in the local cortical areas where their cell bodies and dendrites locate. They often use GABA in synaptic transmission and control the microcircuit of local areas by inhibiting the activity of the targeted cells, i.e. the surrounding pyramidal neurons. Although being a minority, GABAergic interneurons display a much greater phenotypic repertoire than glutamatergic principal neurons. This is due to the heterogeneity of interneurons in terms of morphological, electrophysiological, and molecular features which however do not necessarily make a consistent classification of neocortical interneurons (Markram et al., 2004; Ascoli et al., 2008; DeFelipe et al., 2013; Harris and Mrsic-Flogel, 2013; Jiang et al., 2015; Tasic et al., 2016). According to their molecular expression feature, there are three major non-overlapping classes: parvalbumin (PV) expressing, somatostatin (SST) expressing, and 5HT3a-receptor expressing interneurons, which account for around 40%, 30%, 30%, respectively, in the neocortex (Xu et al., 2010; Rudy et al., 2011; Pfeffer et al., 2013; Staiger et al., 2015).

1.3   Properties of VIP interneurons

1.3.1 Molecular feature of VIP cells

Vasoactive intestinal polypeptide positive (VIP) interneurons belong to the $5HT_{3a}$-receptor expressing class and account for around 12-17% of the interneuron population (Rudy et al., 2011; Pfeffer et al., 2013; Prönneke et al., 2015). Although VIP expression marks a specific class of interneurons that does not overlap with the two major other subpopulations, as a class they are heterogeneous since they coexpress several molecular markers and thus partially overlap with other types of interneurons. Besides VIP, the other molecular markers that can be expressed in VIP interneurons are, e.g. calretinin (CR), choline acetyltransferase (ChAT), cholecystokinin (CCK), and corticotropin-releasing factor (CRF) (Kubota et al., 2011; Cauli et al., 2014; Zeisel et al., 2015; Tasic et al., 2016). These secondary markers can coexpress in certain subpopulations of VIP interneurons, e.g. CR/ChAT or CRF/CCK expressing VIP cells. However, it is found that the secondary markers CR and CCK do not coexpress together in VIP cells (Kubota et al., 2011), and thus CR and CCK expressing VIP interneurons are considered as two major distinctive subtypes of VIP cells (He et al., 2016).

1.3.2 Morphology and distribution of VIP cells

VIP interneurons typically show a bipolar/bitufted dendritic morphology, however there are also tripolar, multipolar or atypical VIP cells in rat (Bayraktar et al., 2000) as well as mouse neocortex (Prönneke et al., 2015) and probably in most other species, including human (Lake et al., 2016). VIP cells often locate in cortical layer II/III, decrease in cell density when approaching deeper layers, and in rare cases exist in layer I. Represented as

4

the main subpopulation, bipolar VIP cells in layer II/III are so far the most studied, leaving the deep layer VIP cells, usually being multipolar shape less studied and known. Dendrites of bipolar layer II/III VIP cells remain in a narrow vertical column in their home layer, and additionally enter into layer I. Like the dendrites, their axons are also distributed within a narrow vertical column across all layers and the collaterals enter into deep layers besides the local innervation around their somata (Prönneke et al., 2015). Due to this narrow column-like distribution of dendritic and axonal morphology, VIP interneurons may regulate the circuitry of the entire cortical column at many different levels.

1.4 Circuits regarding VIP interneurons

1.4.1 Input of VIP interneurons

Input of VIP interneurons comes from many different sources, including local and long-range projections as well as subcortical innervations. Within the microcircuit of the barrel cortex, VIP interneurons receive excitatory input from local pyramidal neurons (Porter et al., 1998; Caputi et al., 2009). For long-range innervation, VIP interneurons in the barrel cortex are targeted by thalamic fibers as well as axons of projection neurons in motor cortex (Hájos et al., 1996; Staiger et al., 1996; Lee et al., 2013; Wall et al., 2016). As a subpopulation of $5HT_{3a}$ receptor expressing interneurons, VIP interneurons receive fibers coming from the raphe nucleus and can be depolarized by serotonin (Ferezou et al., 2002). In addition, they receive axonal projection from the basal nucleus of Meynert, correlating to their responsiveness to nicotinic stimulation (Porter et al., 1999). The input from the subcortical regions has a neuromodulatory effect on the activity of VIP interneurons in a widespread manner, depending on the brain state; however, for the local and long-range

input, VIP interneurons are recruited in a more spatially specific manner, depending on the sources of activation (Tremblay et al., 2016).

1.4.2   Disinhibitory motif

Output of VIP cells is more complicated than previously expected. VIP interneurons are preferentially considered to be interneuron-specific interneurons in the hippocampus (Klausberger and Somogyi, 2008). It was demonstrated by anti-GABA immunogold staining indicating that their axonal boutons in the hippocampus form synapses with GABAergic dendrites (Acsády et al., 1996). The largely overlapping population of CR interneurons also form synapses on the interneurons expressing calbindin (CB) in the hippocampus (Gulyás et al., 1996; Acsády et al., 1996). Later, innervation of VIP interneurons in rat barrel cortex was studied and shown to be also on CB interneurons that are now known to be SST expressing Martinotti cells (Staiger et al., 2004b). Thanks to the development of Cre mouse lines for GABAergic interneurons (Taniguchi et al., 2011), several functional studies using optogenetic stimulation found strong connectivity between VIP interneurons and SST expressing Martinotti cells and low connectivity between VIP interneurons and local pyramidal neurons in superficial layers of various neocortical regions (Lee et al., 2013; Pfeffer et al., 2013; Pi et al., 2013; Fu et al., 2014; Zhang et al., 2014; Walker et al., 2016). In addition, by in vivo recording of the neuronal firing in several behavioral paradigms, VIP interneurons are likely to be activated in the reinforcement phase with SST interneurons being inhibited and pyramidal neurons being activated (Fu et al., 2014). Due to the anatomical and functional evidence, VIP interneurons can play a disinhibitory net effect on the principal neurons via the recruitment of a VIP-to-Martinotti cell circuit motif. This motif should release pyramidal neurons from inhibition by Martinotti cells at their distal dendritic tufts (Pfeffer et al., 2014; Karnani et al., 2016; Walker et al.,

2016).

1.4.3   Beyond disinhibition

Besides disinhibitory connectivity, several studies claimed a direct connectivity of VIP interneurons to local pyramidal neurons. During arousal, VIP interneurons in frontal cortex strongly inhibit some pyramidal neurons while exciting others (Garcia-Junco-Clemente et al., 2017). Dual recordings done in the barrel cortex and primary visual cortex (V1) showed connectivity of layer II/III VIP interneurons to local pyramidal cells although with lower rates than to SST interneurons (Lee et al., 2013; Pfeffer et al., 2013). Another study using octuple recordings reported that bipolar and bitufted interneurons in layer II/III of V1, which were partially identified as VIP interneurons, have differential connectivity: the bipolar cells innervate only layer V interneurons while the bitufted cells target layer II/III pyramidal cells and local interneurons (Jiang et al., 2015). Studies on the output of CR interneurons (partially belonging to VIP cells) found different innervation pattern across laminae of rodent and monkey primary visual cortex: in superficial layers they primarily inhibit interneurons, while in deep layers they preferentially inhibit pyramidal neurons (Gonchar and Burkhalter, 1999; Meskenaite, 1997). In addition, some VIP interneurons expressing CCK were recently shown to belong to the small basket cells that form perisomatic synapses on pyramidal neurons (He et al., 2016). These studies, together with the heterogeneity of VIP interneurons, suggest that besides the disinhibitory motif, there exist other output circuits.

1.5   Scientific questions, Aims, and Experimental Plan

So far, morphological studies have quantified the connectivity between VIP interneurons and other types of interneurons and showed that it varied among different subcellular compartments and target cells (Staiger et al., 2004b; Dávid et al., 2007; Hioki et al., 2013). However, a quantitative study, which regards both interneurons and principal cells as targets of VIP neurons is still missing. Therefore, it is necessary to estimate their output connectivity with their potential targets in all layers of a cortical column. To reach the aim, a single cell study was initially planned using brain slices of transgenic mice of VIP-ires-Cre mouse line (Taniguchi et al., 2011). Based on the preliminary result, a quantitative EM study, as the main part of the present work, was carried out on VIP_{cre}/YFP transgenic mice. Pre-embedding anti-YFP (yellow fluorescent protein) staining was used to visualize VIP cells at the population cell level, and post-embedding anti-GABA staining was used to localize GABA in each targeted subcellular compartment (Ottersen, 1987; Acsády et al., 1996; Staiger et al., 1996). Sensitivity and specificity of anti-GABA staining were further evaluated by employing the receiver operating characteristic (ROC) analysis and the optimal cut-off points were obtained as the thresholds for identifying GABA-immunopositive and GABA-immunonegative subcellular structures among the targets. Moreover, by retrograde tracing, pyramidal cells were labeled with rabies virus expressing GFP and stained together with VIP cells by double immunostaining. The potential synaptic contact of VIP interneurons to principal neurons was then verified by correlated light and electron microscopy investigation.

8

2 Materials and Methods

2.1 Animal and tissue preparation

2.1.1 Animals

Homozygous Vip-ires-cre (VIP[tm1(cre)Zjh], The Jackson Laboratory, Bar Harbor, USA) mice were crossed with different reporter lines: Ai9 mice (floxed tdTomato mice: B6.Cg-Gt(ROSA)26Sortm9[(CAG-tdTomato)Hze]/J) and Ai3 mice (floxed YFP mice: B6.Cg-Gt(ROSA)26Sortm3(CAG-EYFP) (Madisen et al., 2010) to generate VIP_{cre}/tdTomato and VIP_{cre}/YFP mice. Only the heterozygous offspring was used in the experiments. Young adult, 21-36 days old, VIP_{cre}/tdTomato mice were used for targeting single VIP cells, and another three adults (12 weeks old) were used for double immunostaining. Five, 4-6 month old, male VIP_{cre}/YFP mice were used for quantitative EM study. All animals were bred at the animal facility of the University Medical Center Göttingen (Göttingen, Germany). The experimental procedures were performed in accordance with German laws on animal research (TierSchG und TierSchVersV 2013).

2.1.2 Fixation of biocytin-filled single VIP cells

This part was done by Dr. Alvar Prönneke. 300 µm-thick slices from VIP_{cre}/tdTomato transgenic mice were used to record electrophysiologically single VIP cells. After that, 0.3% - 0.5% biocytin was added to patch-clamp recording solutions (Prönneke et al., 2015). According to Staiger et al (2004), for the purpose of ultrastructure

preservation, fixation solution (4% formaldehyde in PB) was added with 0.5% glutaraldehyde, and the slices were fixed in the solution overnight in 4 °C. To stop fixation, the slices were rinsed 3 times with PB and 1% H_2O_2 was added to the rinsing buffer as an intermediate step to block endogenous peroxidase activity. After that, the slices were incubated in a cryoprotectant (25% saccharose and 10% glycerol in PB) for 1 hr at room temperature, and then frozen and thawed over liquid nitrogen for 3 times. After that, the cryoprotectant was washed out with PB.

2.1.3 Stereotactic injection of rabies virus

This part was done by a PhD student (Georg Hafner). Three VIP_{cre}/tdTomato mice were injected with rabies virus SAD DeltaG-EGFP (CVS-G), which was kindly provided by Dr. Karl-Klaus Conzelmann (Gene center Munich). The virus was produced like in the description in Wickersham et al (2007) with titers of about 1 x 10^7 particles/ml and injected at Bregma 3.25 mm lateral and Bregma -1.6 mm posterior. To test the virus transfection efficiency, three different volumes, 50 nl, 150 nl, 300 nl, were used on each animal. Animals were kept in their home cages for 10 days to enable virus transfection before perfusion.

2.1.4 Perfusion and vibratome sectioning

All animals were intraperitoneally injected with an overdose of Ketamin (0.1 ml 10% Ketamine for 10g body weight). VIP_{cre}/YFP mice were perfused according to the slightly modified protocol (Sloviter et al., 1989). It started with 0.9% sodium chloride for 2 min, then acidic fixative (2% PFA, 1% GA, in sodium acetate buffer, pH 6.0) for 2 min, followed by basic fixative (2% PFA, 1% GA, in borate buffer, pH 8.5) for 60 min. The mouse brains were collected and stored in 0.1 M phosphate buffer (PB; pH 7.4) for

10

sectioning. For VIP$_{cre}$/tdTomato mice, the protocol was: 0.9% sodium chloride for 2 min, then fixative (4% PFA, 0.2% GA, in PB, pH 7.4) for 20 min, followed by 2 hr post-fixation in the same fixative. After that, the brains were rinsed 3 times extensively in PB and subjected to sectioning. The brains were cut into 50 μm-thick coronal sections with a vibratome (VT 1200S, Leica, Germany) harvesting the barrel field from Bregma -1.06 mm to Bregma -1.94 mm.

Before immunohistochemical staining, sections from all brains were first incubated in the cryoprotectant (25% saccharose, 10% glycerol in 0.01 M PB) overnight at 4°C, and freeze-thawed over liquid nitrogen 3 times. Then they were rinsed first with 0.1 M PB and then 2 times with 0.05 M Tris-buffer saline (0.05% TBS; pH 7.6). The sections from VIP$_{cre}$/tdTomato mice were treated with an extra step: 1% H_2O_2 (diluted in TBS) for 15 min to block endogenous peroxidase. Followed by 3 times 15 min rinse in TBS, all of the sections were ready for immunostaining.

2.2   Staining procedures

2.2.1   Staining of biocytin-filled VIP cells

The slices were incubated overnight in avidin-biotin complex (ABC; Vector Laboratories, California) with 1:200 dilution at 4 °C. Then the slices were incubated for 10 minutes in 1 mg/mL 3,3'-diaminobenzidine tetrahydrochloride (DAB; Sigma, Deisenhofen, Germany) diluted in PB. 30% H_2O_2 (Merck, Darmstadt, Germany) was added to reach 0.01% final concentration to start the reaction. The reaction lasted for 7-10 min until somata of VIP cells became clearly stained under the stereoscope. After reaction, the slices were rinsed thoroughly with PB.

2.2.2   Pre-embedding anti-YFP immunohistochemistry

The sections from VIP$_{cre}$/YFP transgenic mice were stained with pre-embedding anti-YFP staining. They were incubated in a blocking solution (0.25% BSA, 0.1 M DL-lysin, 10% normal goat serum in TBS) for 4 hr at room temperature. Polyclonal rabbit anti-GFP (Invitrogen, A11122) was used as primary antibody (1:1000 diluted in the blocking solution) as it can detect GFP and other fluorescent protein variants, such as YFP. The sections were incubated for 72 hr at 4°C and rinsed in TBS (4 × 60 min). Biotinylated goat anti-rabbit was used as the secondary antibody (1:200 diluted in the blocking solution, Vector Laboratories, California). Incubation lasted overnight at 4°C, followed by rinsing in TBS (4 × 30 min). Afterward, the sections were incubated overnight in avidin-biotin complex (1:400 diluted in TBS with 1% BSA) at 4°C, followed by 2 times rinsing in TBS and 2 times in TB. For visualization, the sections were pre-incubated in 0.5% DAB (diluted in TB) for 10 min. The reaction was started by adding hydrogen peroxide (30% H_2O_2) to a final concentration of 0.01% and lasted for 7-10 min until somata of VIP cells became clearly stained under the stereoscope. The sections were thoroughly rinsed in TB, followed by phosphate-buffered saline (PBS; pH 7.4).

2.2.3   Pre-embedding double immunohistochemistry

The sections from VIP$_{cre}$/tdTomato transgenic mice were treated with double immunostaining. They were incubated in a 1st blocking solution (0.25% BSA, 0.1 M DL-lysin, 10% normal horse serum in TBS) for 4 hr at room temperature. For detecting VIP cells, polyclonal mouse anti-RFP (Rockland, 200-301-379) was used as the primary antibody (1:1000 diluted in the 1st blocking solution). For detecting retrogradely infected cells, polyclonal rabbit anti-GFP (Invitrogen, A11122) was used as the primary antibody (1:1000 diluted in the 1st blocking solution). The sections were incubated in the solution

12

containing both primary antibodies for 72 hr at 4°C. After intensive rinsing in TBS (4 × 60 min), they were stained in the secondary antibody solution, biotinylated horse anti-mouse, (1:200 diluted in the 1st blocking solution, Vector Laboratories, California), overnight at 4°C. After rinsing in TBS (4 × 30 min), the sections were incubated overnight with avidin-biotin complex (1:400 diluted in TBS with 1% BSA) at 4°C. After rinsing in TBS (3 × 30 min) and TB (pH 8.2; 3 × 10 min), DAB-nickel staining was carried out for visualizing VIP cells. The sections were pre-incubated in a DAB-nickel solution (0.015% DAB, 0.4% ammonium nickel sulfate, diluted in TB pH 8.2) for 10 min, and then 30% H_2O_2 was added to a final concentration of 0.005% to start the reaction. The reaction lasted for 3-5 min until somata of VIP cells appeared under the stereoscope. The sections were rinsed in TB (pH 8.2; 2 × 10 min), followed by TBS (pH 8.2; 2 × 10 min).

For visualizing retrogradely infected cells, the sections were incubated in a 2nd blocking solution (0.25% BSA, 0.1 M DL-lysin, 10% normal goat serum in TBS pH 8.2) for 2 hr. Biotinylated goat anti-rabbit was used as the secondary antibody (1:200 diluted in the 2nd blocking solution). Incubation lasted overnight at 4°C, followed by rinsing in TBS (pH 8.2, 4 × 30 min). Afterward, the sections were incubated overnight in avidin-biotin complex (1:400 diluted in TBS pH 8.2 with 1% BSA) at 4°C. After rinsing in TBS (pH 8.2; 3 × 30 min) and TB (pH 7.6; 3 × 10 min), the sections were pre-incubated in a DAB solution (0.5% DAB diluted in TB pH 7.6) for 10 min, and then 30% H_2O_2 was added to a final concentration of 0.01% to start reaction. The reaction lasted around 5 min. The sections were rinsed in TB (pH 7.6; 2 × 10 min), followed by PB (pH 7.4; 2 × 10 min).

2.2.4 Post-embedding anti-GABA immunogold labeling

Post-embedding anti-GABA immunostaining was carried out with a modified

protocol of Somogyi and Hodgson (1985). Nickel grids with ultrathin sections were pre-treated with 1% periodic acid for 10 min for etching the osmium and 1% sodium periodate for 10 min for etching the resin. Immunoreaction was performed in a humid petri dish with grids being placed upside down on drops of reagents on a parafilm. The grids were washed with distilled water for 3 × 3 min, followed by TBS (pH 7.4) for 3 min. For blocking, they were incubated with 1% ovalbumin in TBS for 30 min. Primary antibody was polyclonal rabbit anti-GABA serum (Sigma-Aldrich, A2052), diluted in TBS at 1:500. After 90 min incubation, the grids were washed 4 × 5 min in TBS. Secondary antibody was 12 nm gold conjugated to goat anti-rabbit (Dianova; No. 111-205-144), diluted in TB (pH 7.4) at 1:40 with 1% BSA and 0.5% Tween 20. The grids were incubated for 90 min in a dark moist chamber and washed 3 × 5 min with distilled water. After that, the grids were contrast-stained with 10% uranyl acetate for 30 min and quickly rinsed 4 times in distilled water.

2.3   Electron microscopy sample preparation

2.3.1   Osmification, dehydration and embedding

After biocytin staining, the slices from VIP_{cre}/tdTomato mice containing filled VIP cells were osmified with 0.04% osmium tetroxide in PBS. After 1 hr osmification, they were rinsed with PBS for 3 × 15 min. Next, the slices were dehydrated in ascending concentrations of alcohols and infiltrated with epoxy resin with the protocol as follows: 30% 5 min, 50% 5 min, 70% 30 min, 90% 10 min, 100% 10 min, isopropanol 10 min, propylene oxide 2 × 10 min, propylene oxide/epoxy resin (1:1) 60 min, epoxy resin overnight, and fresh epoxy resin 4 hr. Afterward, the slices were flat-embedded in epoxy

14

resin on glass slides, covered by a cover slide, and polymerized in an oven for 2 days at 60°C.

After pre-embedding anti-YFP staining, the sections from VIP$_{cre}$/YFP mice were osmified with 0.5% osmium tetroxide in PBS for 1 hr, and then washed with PBS for 3 × 15 min. The sections from VIP$_{cre}$/tdTomato mice after pre-embedding double immunostaining were osmified with 0.25% osmium tetroxide (with 2.5% matured D-glucose in PB) for 1 hr, followed by 3 × 15 min rinse in PB. All sections were dehydrated and infiltrated with the same protocol used for the slices (see above). Afterward, they were flat-embedded in epoxy resin on glass slides covered by a piece of plastic film (Aclar) and polymerized in the oven for 2 days at 60°C.

2.3.2   Preparation of sample blocks for ultramicrotomy

For single VIP cells, hydrofluoric acid was used to etch the cover slides and expose the embedded slices. The barrel field was detached from the glass slides using capsule blocks filled with pure epoxy resin. Then the block surface was trimmed into a trapezoid shape including the area of interest (i.e. the stained VIP cell) by razor blades under a stereomicroscope. After that, the block was ready for correlated light and electron microscopy procedure (see the following section). For the quantitative EM study, 2-3 sections from each VIP$_{cre}$/YFP animal with good pre-embedding immunostaining were chosen for the ultramicrotomy. As described above, the barrel field was detached and the block face was trimmed either into ca. 1200 μm × 300 μm trapezoid pyramids containing all cortical layers or into small ones ca. 750 μm × 200 μm for studying either superficial or deep layers. After trimming, the blocks were ready for ultrathin sectioning (Reichert Jung Ultracut, Leica, Germany). For large blocks, 2-3 consecutive ultrathin sections were

cut at 60-80 nm thickness and mounted on a formvar-coated single-slot nickel grid. For small blocks, around 25 serial ultrathin sections of the same thickness were cut with 5-6 serial sections being picked up on each grid. All nickel grids were used for anti-GABA immunogold staining.

2.3.3 Correlated light and electron microscopy procedure

The correlated light and electron microscopy method was initially developed to facilitate the localization of axonal boutons of single VIP cells and was also used to verify putative VIP synapses onto pyramidal neurons for the sections after double immunostaining. The procedure was as follows: 2 μm-thick semithin sections were cut from the sample blocks, prepared either from 300 μm-thick slices or 50 μm-thick sections (as described in section 2.3.2). Semithin sections were transferred onto glass slides using water droplets. They were dried on a hot plate at 65°C and stained with Richardson's staining (1% Azure II, 1% Methylene blue, 1% Borax; Richardson et al., 1960) for 3 min. The regions of interest (i.e. the axonal boutons of VIP cells) of the semithin sections were imaged using a 40x objective lens (NA 0.75) at an Axioskop (Zeiss). The sections were then detached from the glass slides using the capsules blocks and trimmed further into small sample blocks (having only the regions of interest) for doing serial ultrathin sectioning. 60-80 nm serial ultrathin sections were cut and mounted on formvar-coated single-slot copper grids. The copper grids were stained with 0.5% uranyl acetate for 30 min and 3% lead citrate for 4 min using a Leica EM AC20. After contrast staining, the grids were ready for ultrastructural observation in EM.

2.4   Bright field imaging

2.4.1 Imaging and reconstruction of single cells

After osmification and embedding before EM preparation, biocytin-filled single VIP cells with intensive staining of neurites and no obvious truncation of processes were chosen for imaging and reconstruction. The cells were imaged with a 63x oil immersion objective lens (NA 1.4) of an upright epi-fluorescence microscope (AxioImager.M2; Zeiss; Jena, Germany) the setup of which was controlled by the software Neurolucida (MBF Bioscience; Colchester, VT). The Visual Tissue module was used to acquire 3D image stacks for reconstruction. Reconstruction was also done using Neurolucida. VIP-positive axonal structures were differentiated from dendritic processes according to the principles described by Prönneke et al (2015). In addition, the rabies virus labeled pyramidal neurons were imaged and reconstructed in the same way except for using a 63x water immersion objective lens (NA 1.2) of the microscope to avoid tissue damage by the infiltration of oil.

2.4.2 Bright field imaging of cells at population level

After embedding and before ultramicrotomy, VIP cells stained by anti-YFP staining were imaged in the bright field. For an overview imaging, a 10x objective lens (NA 0.30) of a light microscope (Axioskop; Zeiss; Germany) was used. In order to have a homogeneous illumination across cortical layers, EnfuseGUI software was used to blend the images taken at different exposure times. The overview image was generated from 24 original images including 2 tiles, 6 exposure times and 2 planes of focus. 2 focus planes were merged using a minimum intensity projection algorithm (Fiji; Schindelin et al., 2012). For high resolution, VIP cells were imaged using a 40x objective lens (NA 0.75) on an upright microscope (AxioImager.M2; Zeiss; Germany) using Visual Tissue module of Neurolucida (MBF Bioscience; Colchester, VT). The generated stacks were also

merged with the minimum intensity projection feature of Fiji.

2.5   Evaluation of anti-GABA staining

2.5.1   Labeling over subcellular profiles of GABAergic and non-GABAergic neurons

In order to evaluate the anti-GABA staining, first of all, different subcellular profiles of GABAergic and non-GABAergic neurons were sampled according to their ultrastructure, as described in textbooks. For the ones from GABAergic neurons, these were 59 presynaptic axonal terminals forming symmetric Type II synapses, 59 interneuron dendrites and 16 interneuron somata as postsynaptic structures. Interneuron somata were identified by having nuclear membrane indentations. Interneuron dendrites were originating from such somata and had no appearance of spines. For the ones from non-GABAergic neurons, these were 92 presynaptic axonal terminals forming asymmetric Type I synapses, 80 spines and 12 pyramidal cell somata as postsynaptic structures. Since spines usually come from the protrusion of dendrites of principal cells, they were sampled as an equivalent of those dendrites. Gold grain density of these profiles was calculated by dividing the number of gold grains over one profile by its area (μm^2) (measured with Fiji). The grain density of interneuron dendrites and spines were plotted into histograms and fitted with log-normal and exponential distributions. The goodness of fit was tested with a Chi-square test. Mann-Whitney U test was used to compare pairwise the grain density of different profiles.

2.5.2   Generation of ROC curves and GABA-immunopositive thresholds

ROC analysis (Fawcett, 2006) was used to evaluate the anti-GABA staining efficiency and obtain the optimal cut-off points corresponding to GABA-immunopositive thresholds. Since dendrites were the main target of VIP interneurons (Acsády et al., 1996), the dendritic ROC curve was first generated using the grain density of interneuron dendrites and spines as the putative positive and negative classes. In addition, the somatic ROC curve was also generated using the grain density of interneuron somata and pyramidal cell somata as the positive and negative classes. The ROCR package in R software (Sing et al., 2005) was used to generate the ROC curves and calculate the area under ROC (AUC). The optimal cut-off point was determined by the most frequently used method "closest point to (0,1)". For comparison, additional three methods were used to generate other possible cut-offs. For each method, the corresponding false positive and false negative errors were calculated.

2.6 Quantitative analysis of the targets

2.6.1 Systematic sampling of axonal boutons

A transmission electron microscope (LEO 906E; Zeiss, Germany) equipped with a wide-angle dual speed 2K CCD camera (TRS, Germany) was used to observe and sample the axonal boutons of VIP interneurons that formed synapses. A systematic sampling method was adopted: the axonal boutons were searched at low magnification (2,100 ×) by scanning the whole ultrathin sections, i.e. from a random start in layer I to layer VI, with an interval of 50 µm. Once a putative axonal bouton being found, higher magnification (21,000 ×) was used to check whether it formed a synapse or not. Since VIP cells are interneurons (Rudy et al., 2011), they should form symmetric synapses that

have three main features according to Colonnier (1968): (i) a cluster of synaptic vesicles close to presynaptic membrane, (ii) parallel appositions between pre- and postsynaptic membranes and widening of the extracellular space at the putative synaptic cleft and (iii) postsynaptic membrane thickening, although the feature is mostly very subtle in symmetric synapses compared to asymmetric synapses. Consecutive sections were also checked for verifying a putative synapse.

In total, 200 axonal boutons were collected across all cortical layers: layer I (n = 12), layer II/III (n = 74), layer IV (n = 45), layer V (n = 37), and layer VI (n = 32). Among them, 18 boutons were observed in complete or almost complete serial ultrathin sections. Some of them were reconstructed using TrakEM2 of Fiji, and the 3D structures were rendered into 2D images using Blender (v2.7). For differentiating postsynaptic subcellular profiles in ultrastructure, dendrites were recognized by containing mitochondria and microtubules. Spines were of smaller size compared to dendrites and sometimes contained a spine apparatus (smooth endoplasmic reticulum) but no mitochondria. Somata, regardless of the presence of nuclei, were identified by their specific morphology and content of organelles, like ribosomes, rough endoplasmic reticulum and Golgi apparatus.

2.6.2   GABA immunoreactivity among the postsynaptic targets

GABA-immunopositive threshold was used to calculate GABA-immunopositive ratio among the postsynaptic targets. The thresholds for dendrites and somata were different, and since spines originate from dendrites of principal cells, they shared the same threshold as the dendrites. To compare GABA immunoreactivity of the dendritic targets across cortical layers, original and normalized gold grain density were analyzed by the following statistic procedures. Since they did not follow a normal distribution, the data

20

were described by 25% Quartile (Q_{25}), 50% Quartile (Q_{50}), and 75% Quartile (Q_{75}). Normalization was performed by dividing the original grain density of a targeted dendrite by the mean density of the surrounding spines. Kruskal–Wallis one-way analysis of variance (ANOVA) on ranks was used to test the original and normalized grain density for a layer-dependent difference. Post hoc Dunn's test was used to compare the normalized grain density between cortical layers and was treated with Bonferroni correction due to multiple comparisons. Afterward, Mann-Whitney U test was used to compare the grouped normalized grain density between superficial and deep layers. All graphs and analysis were done using either Libreoffice calc or R.

3 Results

3.1 VIP interneuron morphology in light and electron microscope

Being a heterogeneous population, each VIP cell might have a distinct morphology and unique targeting property, thus, a single cell study was initially planed and carried out using correlated light and electron microscopy methodology. However, only a limited number of VIP cells were sampled due to a low recovery rate of cell morphology. To overcome the sample size limitation, VIP interneurons were also stained at population level and their morphology was characterized in both light and electron microscope.

3.1.1 Correlated light and electron microscopy study of single VIP cells

Three biocytin-filled VIP neurons in layer II/III were stained and reconstructed from 300 μm thick slices, and one of them was re-sectioned for studying the synaptic ultrastructure. The reconstruction (Figure 1A) was superimposed over the slice at its original location (Figure 1B). Laminae were delineated in the slice by referring to the measurement of the layer thickness in the study of Prönneke et al (2015). The neuron was a typical bipolar VIP cell. It had extensive axonal arborizations in the home layer, layer II/III, and sent its axonal collaterals to layer I and deep layers, respectively. In total it had 1348 axonal boutons that existed in all layers except layer VI as the axon did not enter into layer VI. To facilitate observation of the synaptic ultrastructure in EM, two steps of correlation were used: (i) correlation of semithin sections to the slice (Figure 1), followed

22

by (ii) correlation of ultrathin sections to semithin sections (Figure 2). For the 1st correlation, three characteristic points were used for aligning semithin sections to the slice: two origins of blood vessels at the pial surface and one intersection of two blood vessels. After the 1st correlation, laminae were delineated in the semithin sections as well (Figure 1C). Any VIP neuronal processes that appeared in the semithin sections were localized to their original location in the reconstruction. In this way, dendritic varicosities were differentiable from axonal boutons at the level of semithin sections.
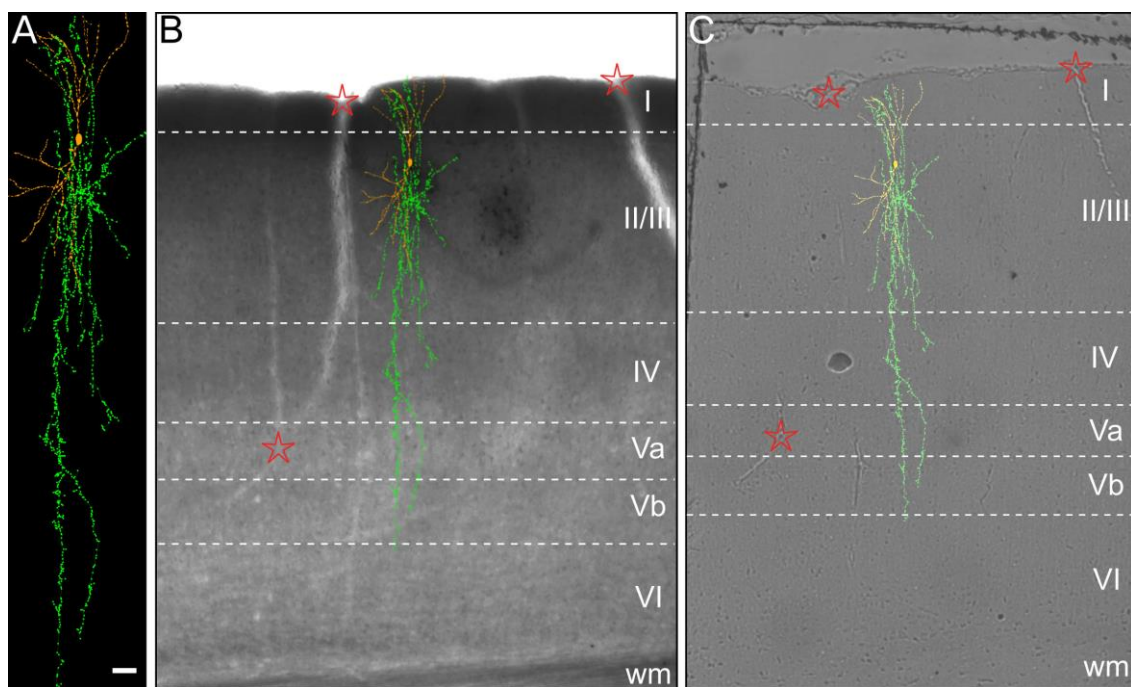
Figure 1. 1st correlation: semithin sections to the slice.
(A) The reconstruction of a bipolar VIP cell. Soma and dendrite are in orange; axons are in green. Axonal boutons are indicated by the green dots on the axonal branches. (B) Bright field picture of the brain slice. The reconstruction of the cell has been superimposed on its exact original place on the slice. Three characteristic points are determined and marked by red stars. (C) Using the three characteristic points, the semithin section is then aligned to the slice. Scale bar = 10 μm in A.

The 2nd correlation was used to localize the boutons of VIP cells found in ultrathin sections to the semithin sections, and thus indirectly to the reconstruction. Richardson's staining, typically used for staining the neuropil of resin embedded semithin sections

(Richardson et al., 1960), was taken as an intermediate procedure to help the correlation process. After the staining, cell bodies of neurons in the semithin section were stained in blue. In addition, proximal apical dendrites were also stained (Figure 2B). However, Richardson's staining failed to label neurons in a Golgi-like manner and the other neuronal processes including distal dendrites, spines and axons were unstained. For the 2nd correlation, three somata of layer II/III pyramidal cells were used as the characteristic points. After aligning the electron micrograph (yellow inset in Figure 2C) to its semithin section (white inset in Figure 2B), a putative bouton was found in EM at low magnification. The bouton located in the vicinity of an oblique dendrite which was likely to belong to a pyramidal neuron due to its orientation and thickness (Figure 2D). The bouton formed a symmetric synapse on the dendrite, which was verified by the synaptic ultrastructure in the electron micrograph taken at high magnification (Figure 2E).

In total 20 axonal boutons in layer II/III of the VIP bipolar cell were examined using correlated light and electron microscopy method. All of the boutons formed symmetric synapses on other non-VIP expressing neuronal profiles: 18 boutons synapsed onto dendrites and 2 onto somata. For the targeted dendrites, some of them likely belonged to the apical dendrites of pyramidal cells as they had relatively large caliber and extended almost perpendicularly to the pial surface. For the somatic innervation, one of the two innervated somata was found to have indentations in its nuclear membrane. This typical morphology indicates it belonged to an interneuron (Peters et al., 1991). The findings of the single cell study suggest VIP interneurons might not only innervate other interneurons but also non-GABAergic excitatory cells at different subcellular compartments. The preliminary work initiated the following quantitative EM study for mapping the output of VIP cells.

24
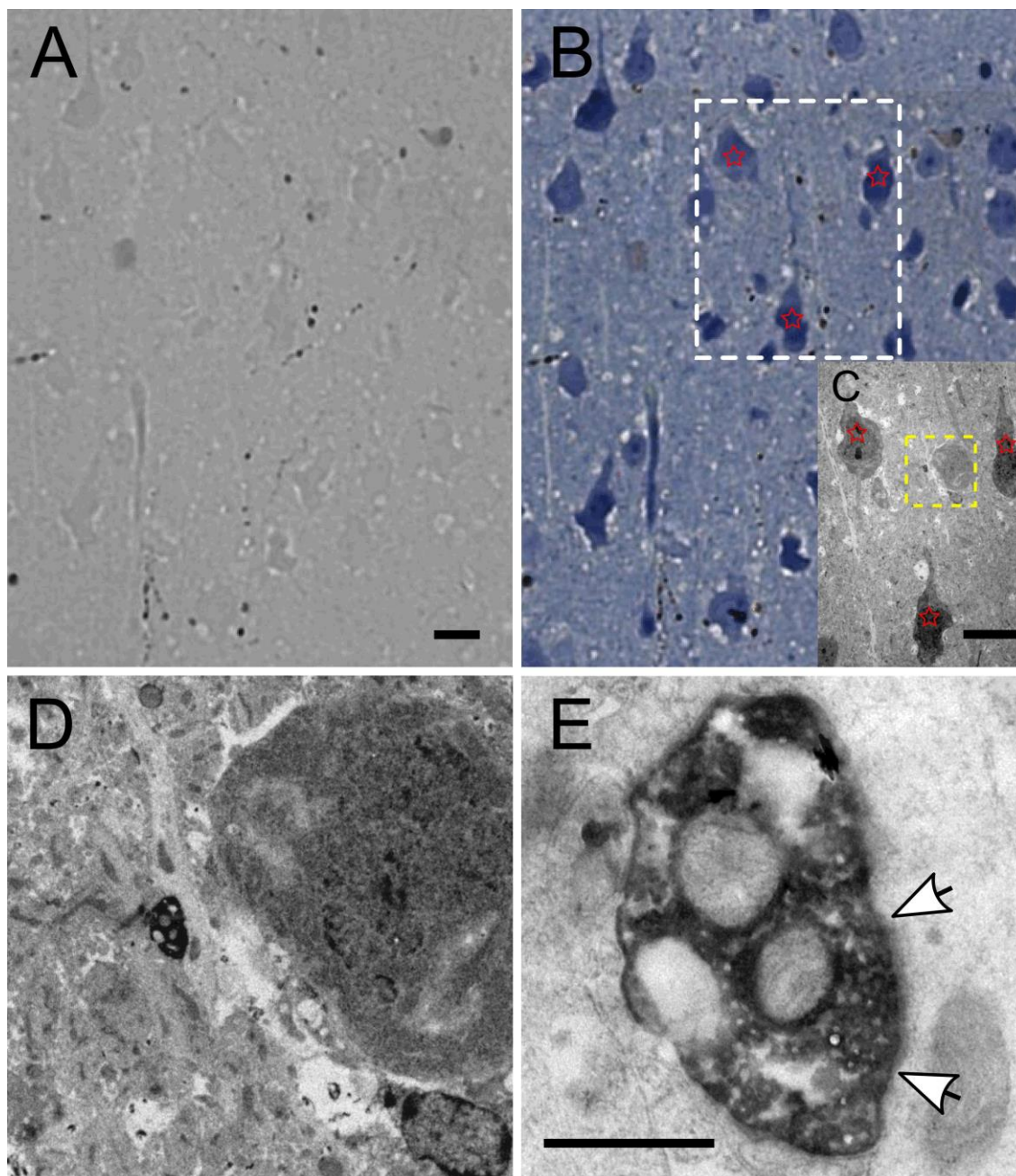
Figure 2. 2nd correlation: ultrathin sections to semithin sections.

(A) 2 μm-thick semithin section shows distribution of some processes of VIP neurons (black dots) in layer II/III. Most of them are axonal boutons according to the 1st correlation. (B) The semithin section after Richardson's staining. (C) The corresponding EM image at low magnification of the white inset in (B). Red stars mark the characteristic points that are used for correlating electron micrograph of an ultrathin section to its semithin section. (D) The corresponding EM image at middle magnification of the yellow inset in (C). (E) High magnification EM image shows the bouton forms a symmetric synapse (white arrows) on a dendritic segment. Scale bars = 10 μm in A, C; 0.5 μm in E.

3.1.2   Pre-embedding anti-YFP staining of VIP cells

Distribution and morphology of VIP interneurons at the light microscopic level suggests specific and comprehensive labeling

Pre-embedding anti-YFP immunostaining was performed to label the entire population of VIP interneurons in the mouse barrel field using VIP_{cre}/YFP transgenic animal. Across all mice used in this study (n=5), the distribution of VIP neurons was similar, if not identical (Figure 3A). Most of the cell bodies were located in layers II to IV and only a few in layers I, V and VI, which was consistent with previous findings in a similar mouse line (Prönneke et al., 2015). The staining was good enough in visualizing all VIP cell somata as well as their dendrites and axons in a Golgi-like manner. Importantly, in the neuropil dense punctate labeling, suggestive of rich bouton labeling, was prominent throughout all layers at higher magnification (Figure 3B-C). However, this needed to be proven by correlated light and electron microscopy investigation. Since the background of the sections was not strong (light brown, although not visible in black and white images), cell morphology and cell density information were used to delineate cortical layers.

In accordance with previous classification (Bayraktar et al., 2000; Prönneke et al., 2015), bipolar somatodendritic shape was most often typical for VIP interneurons in layer II/III (Figure 3B). Their somata were small and in oval shape, and oriented perpendicular to the pial surface with their primary dendrites (Figure 3B). Multipolar VIP cells were far less prominent and usually found in deep layers (Figure 3C). They possessed large somata in triangular or polygonal shape with 4 or more primary dendrites extending in different directions. Their main axis was oblique to the pial surface (Figure 3C). Other somatodendritic types were also observed, including single tufted, bitufted, modified

bipolar, and atypical shapes (e.g. horizontally oriented bipolar). In sum, the pre-embedding staining was complete in homogeneously labeling all morphological types of VIP cells, therefore enabled the study of their innervation properties without sample bias.
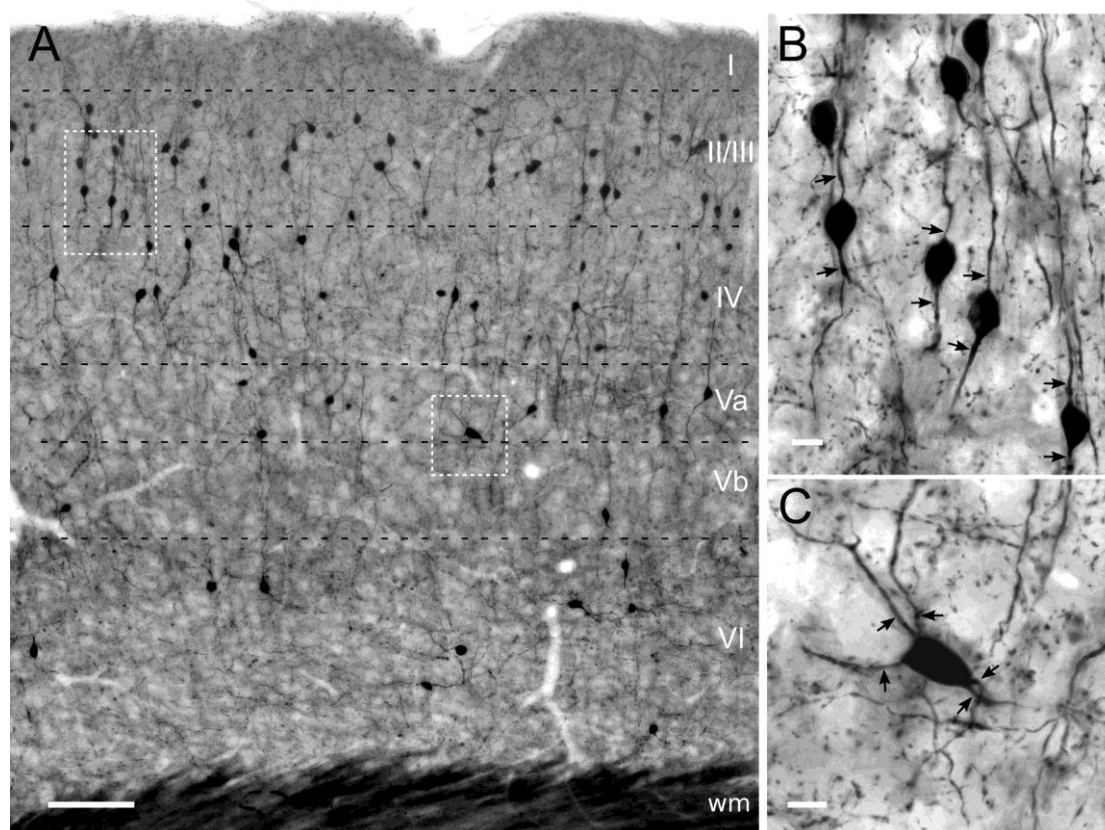
Figure 3. Light microscopic characterization of YFP-immunolabeled cells in the barrel cortex of the VIP$_{cre}$/YFP mouse.

(A) Distribution of the population of VIP cells in mouse barrel field shown in a 50 μm-thick, osmium-intensified and resin-embedded section. Most cells are located in superficial layers II to IV whereas much fewer are found in layers I, Va, Vb and VI. (B) Morphology of a cluster of bipolar VIP cells in layer II/III (left inset in A). (C) Multipolar VIP cell in layer Va (right inset in A). Arrows indicate primary dendrites. Scale bars = 100 μm in A; 10 μm in B, C.

Correlated light and electron microscopy discloses typical features of subcellular compartments of VIP interneurons

In the anti-YFP staining, DAB precipitate was very intensive and somehow prevented observation of structure in detail. Correlated light and electron microscopy

method helped to differentiate subcellular compartments of VIP cells, especially large axonal boutons from dendritic varicosities in the electron micrographs. The 2 μm-thick semithin section containing several VIP expressing cell bodies as well as dendritic and axonal segments was stained with Richardson's staining which assisted the correlation process (Figure 4A). Figure 4B shows the correlated ultrastructure of the somatodendritic domain of a layer II/III bipolar VIP cell (Figure 4A, inset). The cytoplasm of the soma was darkly stained, leaving the nucleus unstained. The nucleus was indented (double arrows), a feature typical for interneurons (Peters et al., 1991). In the light microscope, the axons appeared more curly and finer than the dendrites; the axonal boutons were roundish and smaller than the more fusiform shaped dendritic varicosities (Figure 4A-B). In the electron microscope, a cluster of unstained synaptic vesicles was visible in the axonal boutons, which accumulated near the active zone (Figure 4C1-C8). This bouton was followed in 9 serial ultrathin sections forming a symmetric synaptic junction in three of them (Figure 4C4-C6).

28
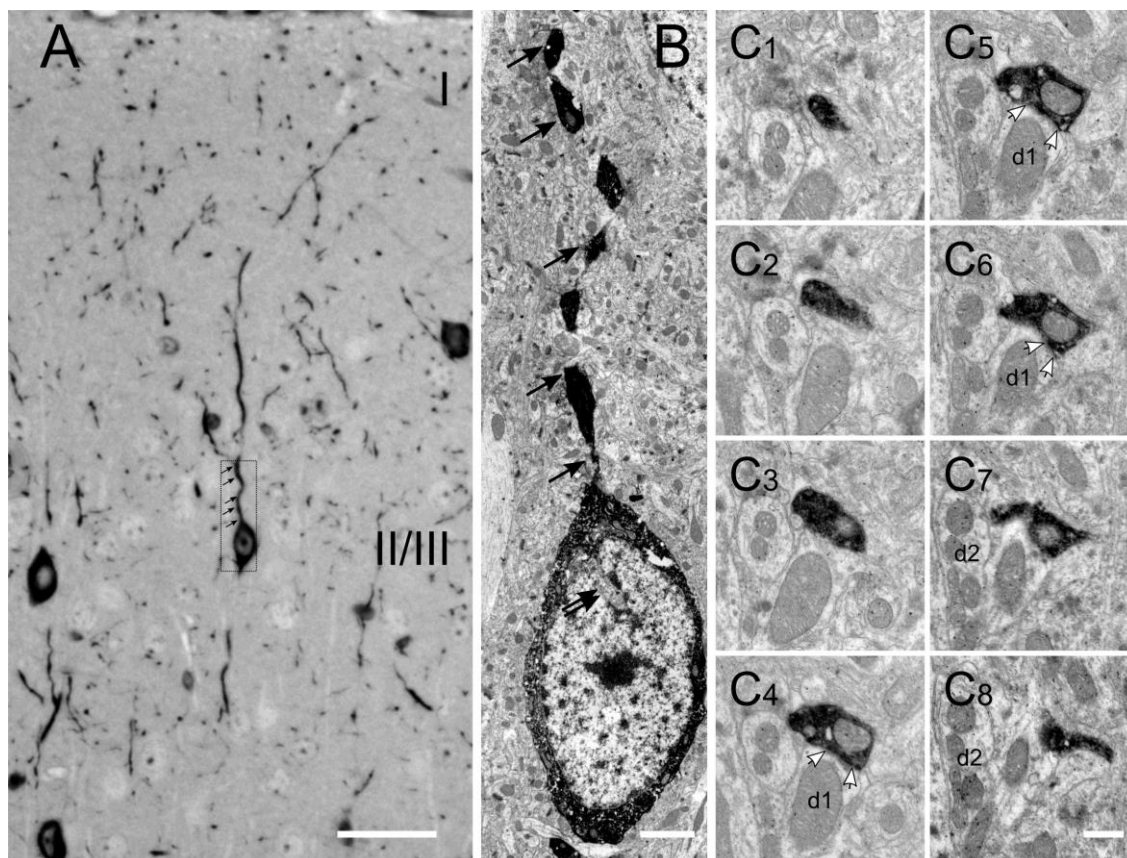
Figure 4. Ultrastructure of different subcellular compartments of VIP cells.

(A, B) Correlative light and electron microscopic images of the soma and ascending primary dendrite of a bipolar VIP cell in layer II/III. The typical indentation of the nucleus is indicated by double arrow, single arrows show the same dendritic segment. (C1-8) Serial sections through a large, mitochondrium-containing bouton clearly showing a synaptic specialization on a putative GABA-immunonegative dendrite (d1; white arrows show the active zone). d2 labels a putative GABA-immunopositive dendrite as gold grains accumulate over its mitochondria as well as cytoplasm (C7-8). Scale bars = 20 µm in A; 2 µm in B; 0.5 µm in C8 (applies to C1-7).

Through complete or almost complete serial sectioning of 18 axonal boutons of VIP cells, it was found that most of them formed symmetric synapses (90%, 16 /18) on identified target structures. For 2 boutons no obvious synaptic contact was observed, which might be caused by a disadvantageous orientation of the synaptic specialization to the cutting (and thus imaging) plane. In addition, the majority of the serially sectioned boutons (87.5%, 14 /16) formed one synaptic contact with their targets. Figure 5A shows the reconstruction of a symmetric synapse formed by a bouton followed through 14 serial

ultrathin sections. After anti-GABA immunogold staining (described in the section 3.2), the postsynaptic target was revealed as a putative GABAergic dendrite as gold grains labeled it across serial sections (e.g. the 1st, 4th, 9th, 13th ultrathin sections). The putative GABAergic dendrite received an excitatory synapse in addition to the inhibitory VIP expressing synapse. Among the serially sectioned boutons, it was of a low incidence that they formed two synapses (12.5%, 2 /16) and no triple synapse existed. However, since it is difficult to identify synapses when the synaptic cleft has an orientation in parallel to or at a low angel with respect to the plane of sectioning (Kubota et al., 2009), this might have led to an underestimation of the synapse numbers formed by the axonal boutons. Figure 5B shows the incomplete reconstruction of a large bouton forming two synapses on two distinct dendrites. This large bouton had more than 18 serial ultrathin sections. From the visual inspection of the gold grains, both targeted dendrites belonged to non-GABAergic ones, which is in agreement with their morphology as one dendrite had a spine protrusion as shown by serial EM images and reconstruction. In the following section, GABA immunogold labeling was quantitatively evaluated in order to quantify the GABAergic targets of VIP cells.
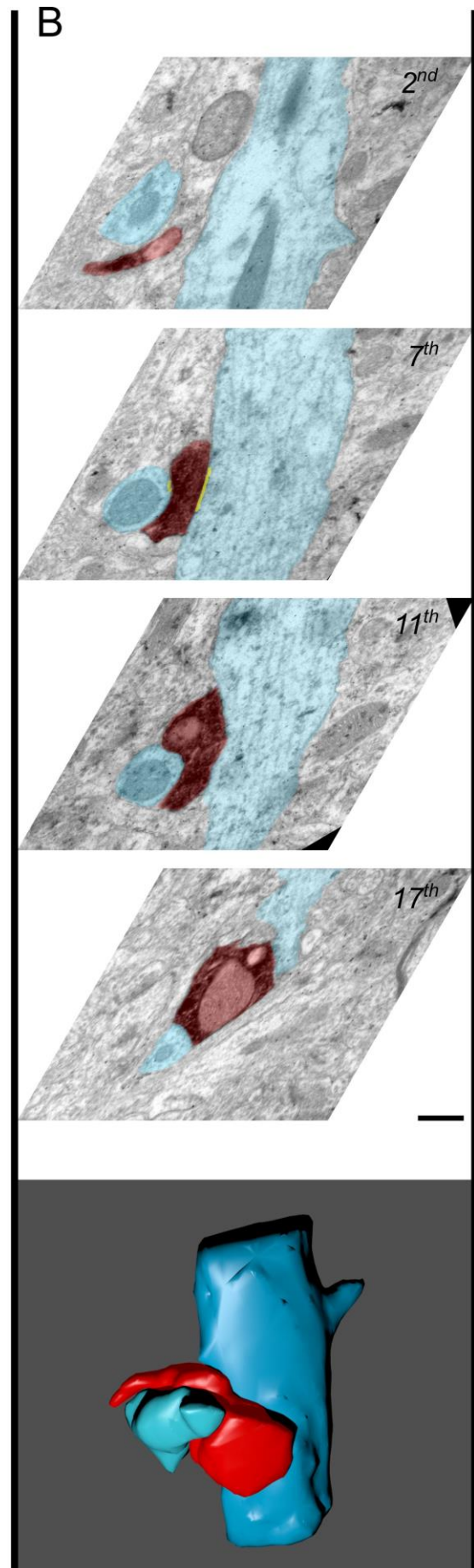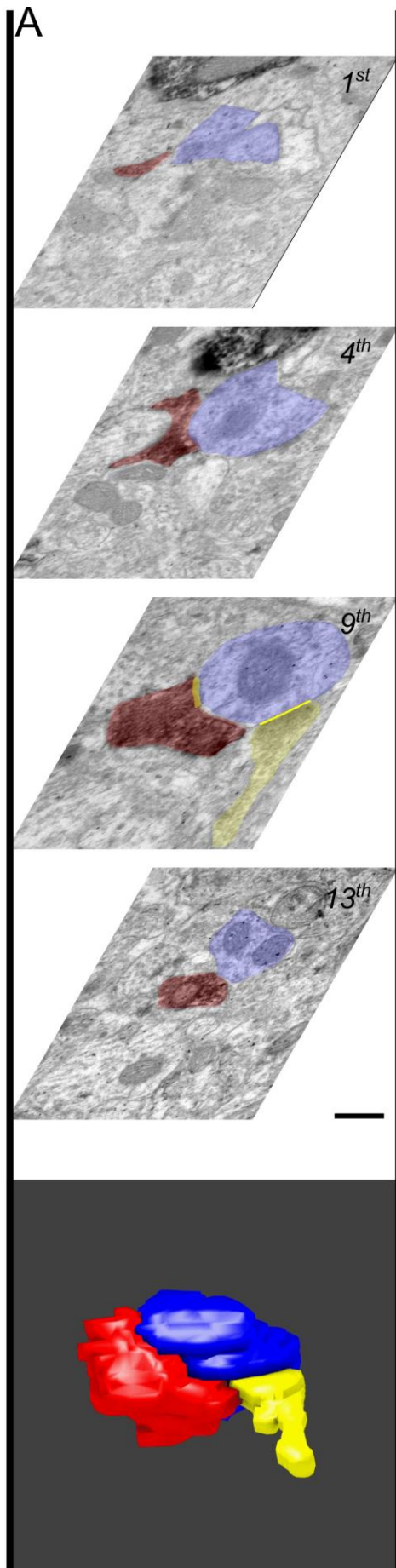
Figure 5. 3D reconstruction of VIP-positive synapses from serial ultrathin sections.
(A) A symmetric synapse formed by an axonal bouton (red) on a putative GABAergic dendrite (blue) which is additionally targeted by an excitatory axonal terminal (yellow). Both active zones (yellow lines) appear in the 9th ultrathin section. (B) Double synapses formed by a large bouton (red) on two putative non-GABAergic dendrites (cyan). A spine protrudes from the large dendrite. Active zones (yellow lines) appear in the 7th ultrathin section. Scale bars = 0.5 μm in A and B.

3.2   Evaluation of anti-GABA immunogold staining

By visual inspection of the gold grain labeling, it is possible to qualitatively differentiate GABAergic and non-GABAergic profiles. However, the identification is subjective and lacks an estimation of the staining which exists ubiquitously in every immunostaining. An unspecific staining leads to false positive error and vice versa when a staining is not sensitive enough it causes false negative error. Therefore, before quantification, a statistically valid method "ROC analysis" was adopted in order to evaluate the staining efficiency. Furthermore, based on the analysis, the GABA-immunopositive thresholds were generated for different subcellular profiles, determined by the optimal cut-off points.

3.2.1   Establishing ground truth for GABA immunogold labeling

In order to unequivocally identify the GABAergic postsynaptic targets of VIP cells, a quantitative method was established to evaluate the efficiency of anti-GABA immunogold staining. As a first step, subcellular profiles of GABAergic and non-GABAergic neurons were identified by their ultrastructure in electron micrographs (Figures 6 to 7). The profiles from non-GABAergic neurons were axonal terminals forming Type I synapses (AT-I), pyramidal cell somata (PYR-SO), and spines which in the cortex originate from dendrites of principal neurons. The profiles from GABAergic

interneurons were axonal terminals forming Type II synapses (AT-II), interneuron somata (IN-SO) and interneuron dendrites (IN-D) in continuity with them. GABA labeling over "AT-I", "Spine", and "PYR-SO" was regarded as the background for the labeling over "AT-II", "IN-D", and "IN-SO", respectively (Table 1). A significantly higher gold grain density was found in each GABAergic subcellular profile compared to the corresponding background by Mann-Whitney U test (Figure 8A; Table 1). It should be noted that, however, the GABA labeling was not equally intensive among different subcellular compartments of interneurons. Their presynaptic axonal terminals had higher gold grain density than the dendrites (U = 2881, p < 0.001) and somata (U = 838, p < 0.001); between the dendrites and somata, there was no difference (U = 610.5, p = 0.07). In addition, there was a difference in background labeling: gold grain density was higher in the axonal terminals than spines (U = 4322, p = 0.05), and there was no difference between spines and somata (U = 606, p = 0.58). In sum, this result gives the first evidence that the anti-GABA staining can differentiate GABAergic profiles from the non-GABAergic ones.

The histograms of gold grain density of interneuron dendrites and spines showed there existed an overlap between the positive and background labeling (Figure 8B). The overlapping area can be estimated after fitting the GABA labeling of interneuron dendrite and spine with log-normal and exponential distributions, respectively (Figure 8C-D). The function and parameter for the fitted distributions are shown in Table 2. The goodness of fit was tested by Chi-square test for both distributions (IN-D: Chi-square = 3.94, df = 6, p = 0.68; spines: Chi-square = 4.03, df = 4, p = 0.40). Due to the small sample, labeling over somata had not been fitted.
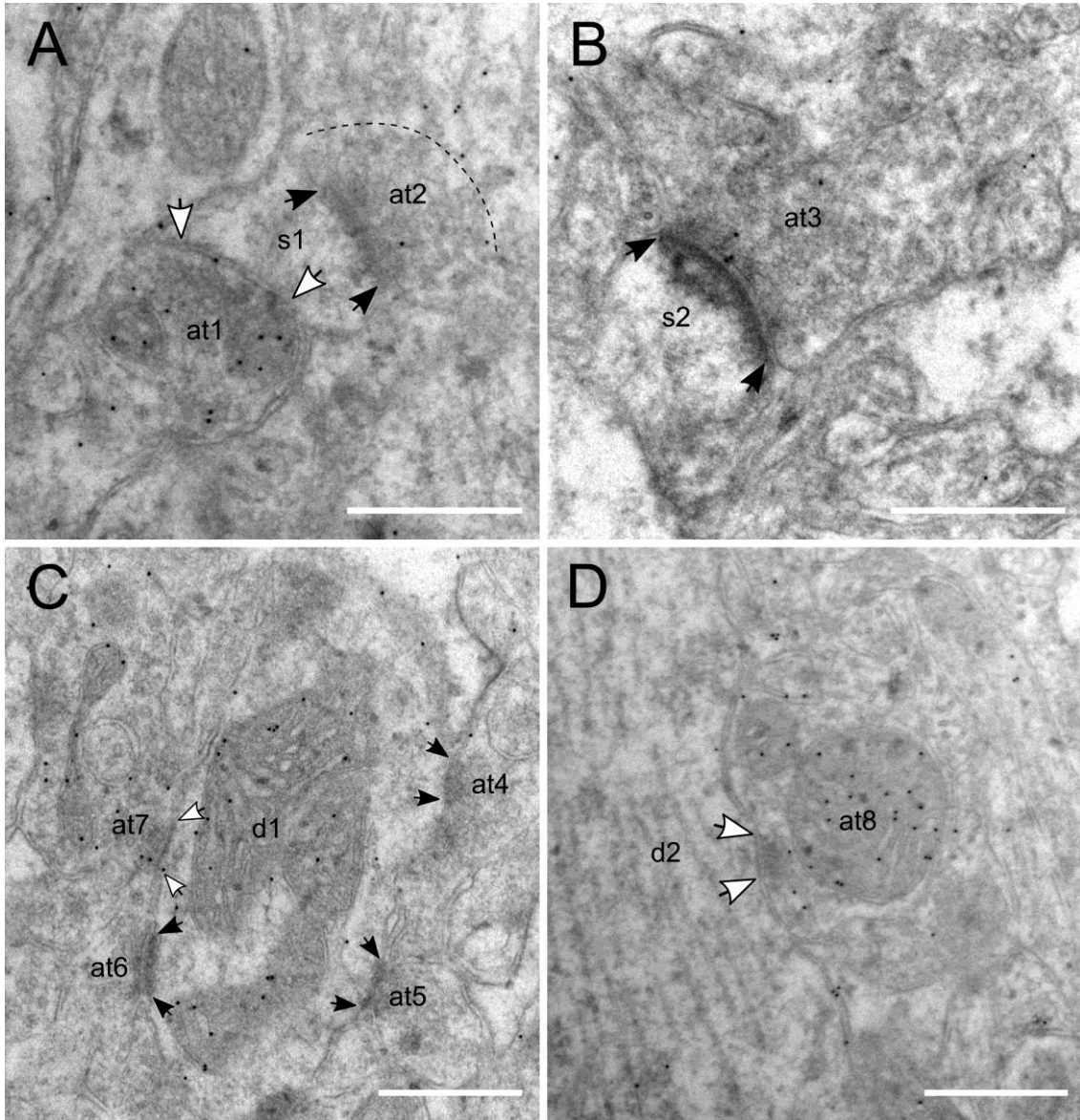
Figure 6. GABA labeling over symmetric (white arrows) and asymmetric (black arrows) synapses.

(A) Dual synaptic junction on a gold grain-free spine (s1), formed by an inhibitory and an excitatory axonal terminal (at1, at2). At1 has many gold grains, however, at2 has only very few. Dashline delineates the border of at2 and a labeled profile at the upper right. (B) Asymmetric synapse formed by at3 on s2. Both profiles are very likely from excitatory neurons and thus virtually lacking gold grain labeling. (C) A densely labeled GABAergic dendrite receives synaptic innervation by 3 excitatory terminals (at4, at5, at6) and 1 inhibitory terminal (at7). (D) Short segment of a large symmetric synapse formed by densely labeled at8 on a putative pyramidal cell dendrite (d2). Scale bars = 0.5 μm in A-D.
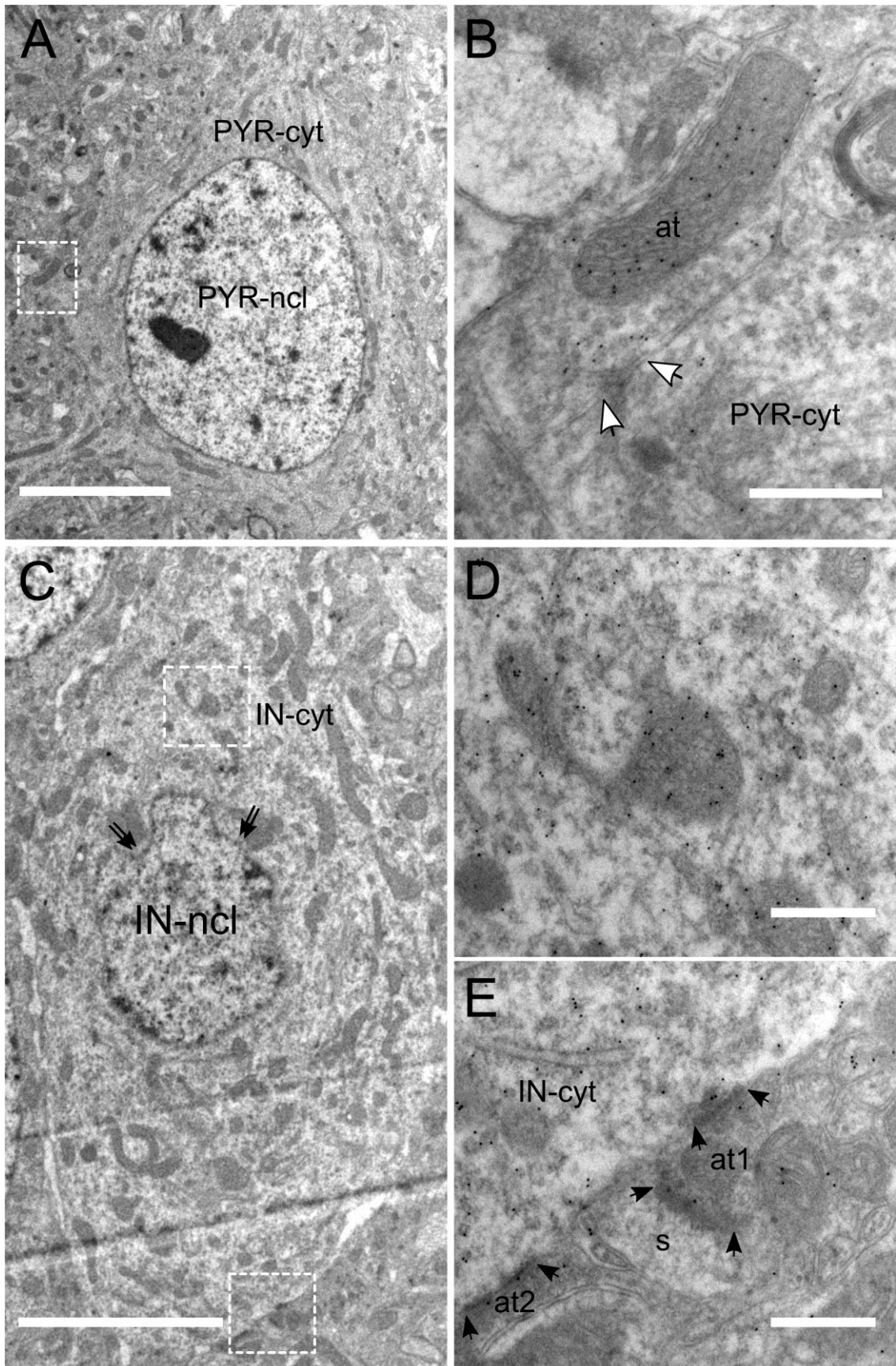
Figure 7. GABA labeling over somata and somatic synapses.

(A) Ultrastructure of the cell body of a pyramidal neuron with its nucleus (PYR-ncl; without indentations of the nuclear membrane) and cytoplasm (PYR-cyt). (B) Higher magnification of the inset in (A) shows an inhibitory synapse on the soma (white arrows). The presynaptic terminal (at) is densely labeled by gold grains whereas the cytoplasm of the soma is devoid of gold grains. (C) Structure of the cell body of an interneuron. The nuclear membrane indentations are marked by double arrows. (D) Upper inset in (C) shows the dense labeling over the cytoplasm. (E) Lower inset in (C) shows two asymmetric somatic synapses (at1, at2), both of which are hardly labeled. At1 also forms an asymmetric synapse on a spine (s). Scale bars = 5 μm in A, C; 0.5 μm in B, D, E.
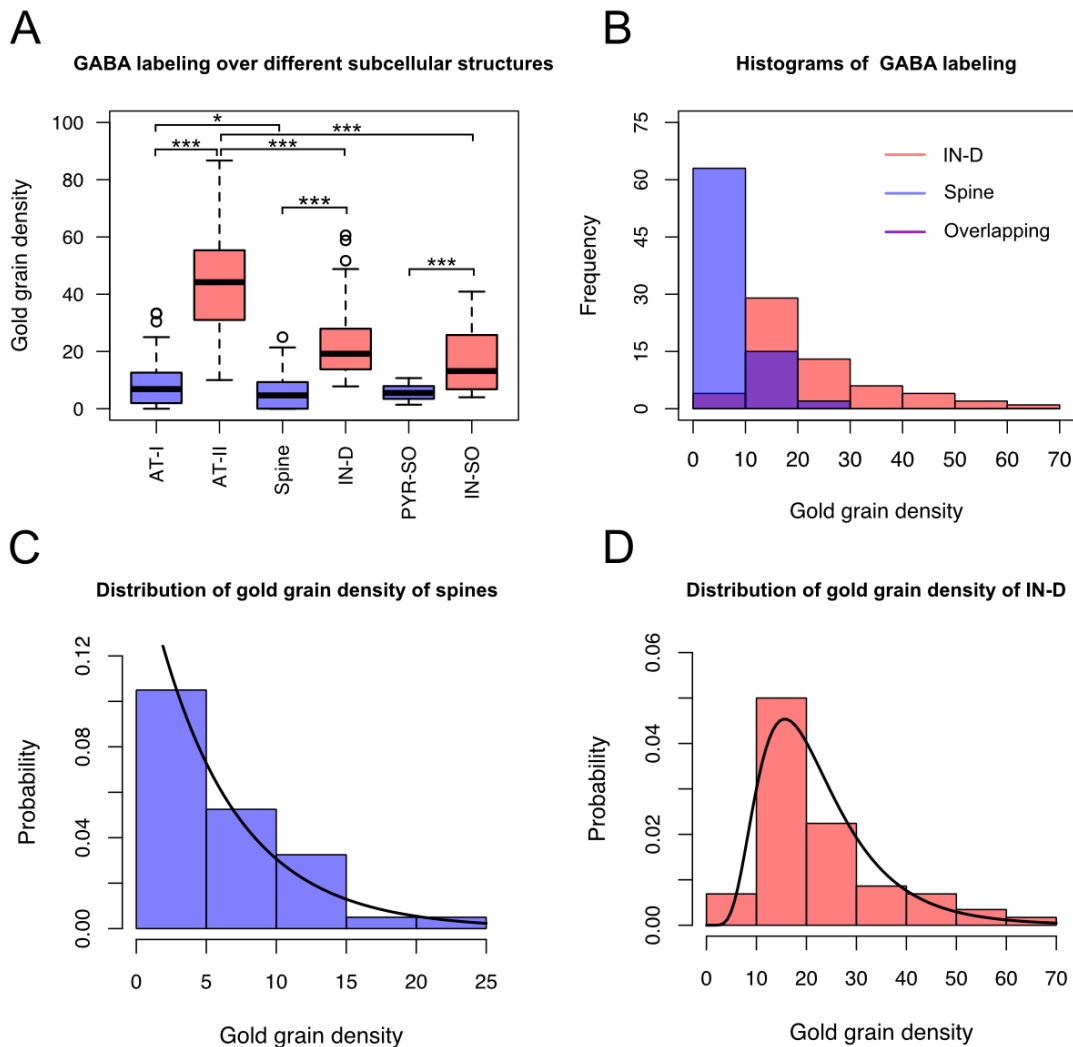
Figure 8. Distribution of gold grain density of different subcellular profiles.

(A) Box plot of gold grain density (gold grains/μm²) of ultrastructurally-defined GABAergic (red boxes; n=134) and non-GABAergic (blue boxes; n=184) profiles. Mann-Whitney U test shows

significant differences in gold grain density between groups: AT-I (n=92) vs AT-II (n=59), Spine (n=80) vs IN-D (n=59), PYR-SO (n=12) vs IN-SO (n=16), AT-II vs IN-D, AT-II vs IN-SO (***, p < 0.001), and AT-I vs Spine (*, p = 0.05). AT-I: axonal terminals forming Type I synapses; AT-II: axonal terminals forming Type II synapses; IN-D: interneuron dendrites; IN-SO: interneuron somata; PYR-SO: pyramidal cell somata. (B) Histograms of gold grain density of interneuron dendrites and spines. The two groups were taken as GABAergic and non-GABAergic reference datasets for generating the classifier which was used for further quantiative analysis. (C-D) Histograms in (B) were fitted with exponential (C) and log-normal (D) distributions. Goodness of fit was evaluated by Chi-square test. Since both p values (0.68, 0.40) are much higher than 0.05, the two distributions fit well the empirical datasets.

Table 1. Labeling over GABAergic (positive) and non-GABAergic profiles (background)

Background	Density (grains/µm²)	Example	Positive	Density (grains/µm²)	Example	Mann-Whitney U
AT-I (n = 92)	$Q_{25} = 2.0$ $Q_{50} = 6.8$ $Q_{75} = 12.6$	Figure 6A-C, 3E	AT-II (n = 59)	$Q_{25} = 31.0$ $Q_{50} = 44.2$ $Q_{75} = 55.3$	Figure 6A,C,D, 3B	$U_{\text{AT-I vs AT-II}} = 152.5$, $p < 0.001$
Spine (n = 80)	$Q_{25} = 0$ $Q_{50} = 4.7$ $Q_{75} = 9.2$	Figure 6A-B, 3E	IN-D (n = 59)	$Q_{25} = 13.8$ $Q_{50} = 19.2$ $Q_{75} = 28.0$	Figure 6C	$U_{\text{Spine vs IN-D}} = 307$, $p < 0.001$
PYR-SO (n = 12)	$Q_{25} = 3.9$ $Q_{50} = 5.5$ $Q_{75} = 7.6$	Figure 7A-B	IN-SO (n = 16)	$Q_{25} = 7.0$ $Q_{50} = 13.2$ $Q_{75} = 25.0$	Figure 7C-E	$U_{\text{PYR-SO vs IN-SO}} = 36$, $p = 0.005$

Table 2. Fitted distributions for positive and background labeling

Dataset	Distribution	Probability density function	Parameter
Spine	*exponential*	$f(x, l) = l\, e^{(-l/x)}$	$l = \dfrac{1}{mean} = 0.1727$
IN-D	*log-normal*	$f(lnx, m, s) = \dfrac{1}{s\sqrt{2p}} e^{-\frac{(lnx-m)^2}{2s^2}}$	$m = 3.0064$ $s = 0.4951$

3.2.2   ROC curves and the optimal cut-off points

ROC analysis is frequently used for evaluating diagnostic tests in clinical medicine, and it was adopted in the present study to evaluate anti-GABA immunogold labeling over subcellular profiles (Fawcett, 2006). Since VIP interneurons are likely to form synapses on dendrites (Markram et al., 2004), a ROC curve was first generated for the labeling over dendrites. Figure 9 shows how it was plotted using the fitted distributions. When moving the cut-off line along the x-axis of the distributions (0 to 70 grains/μm^2), they were separated into four areas: true positive fraction (TPF), false positive fraction (FPF), false negative fraction (FNF), and true negative fraction (TNF). Dendritic ROC curve was generated by plotting each TPF (sensitivity) against each FPF (1 - specificity) using either the fitted distributions or the experimental data (both are shown in Figure 10). The area under the ROC curve ($AUC_{dendrite}$) indicates the efficiency of a diagnostic test, and was high (0.93) when measured from the empirical dendritic ROC curve. It means a randomly selected GABAergic dendrite can be discriminated from non-GABAergic ones with a probability at 0.93 when using the anti-GABA labeling for identification. Furthermore, a somatic ROC curve was generated from the GABA labeling over interneuron somata and pyramidal cell somata (data not shown). The AUC_{soma} was 0.82. In summary, ROC analysis indicated a reliable performance of the GABA immunogold staining in identifying different GABAergic subcellular compartments.
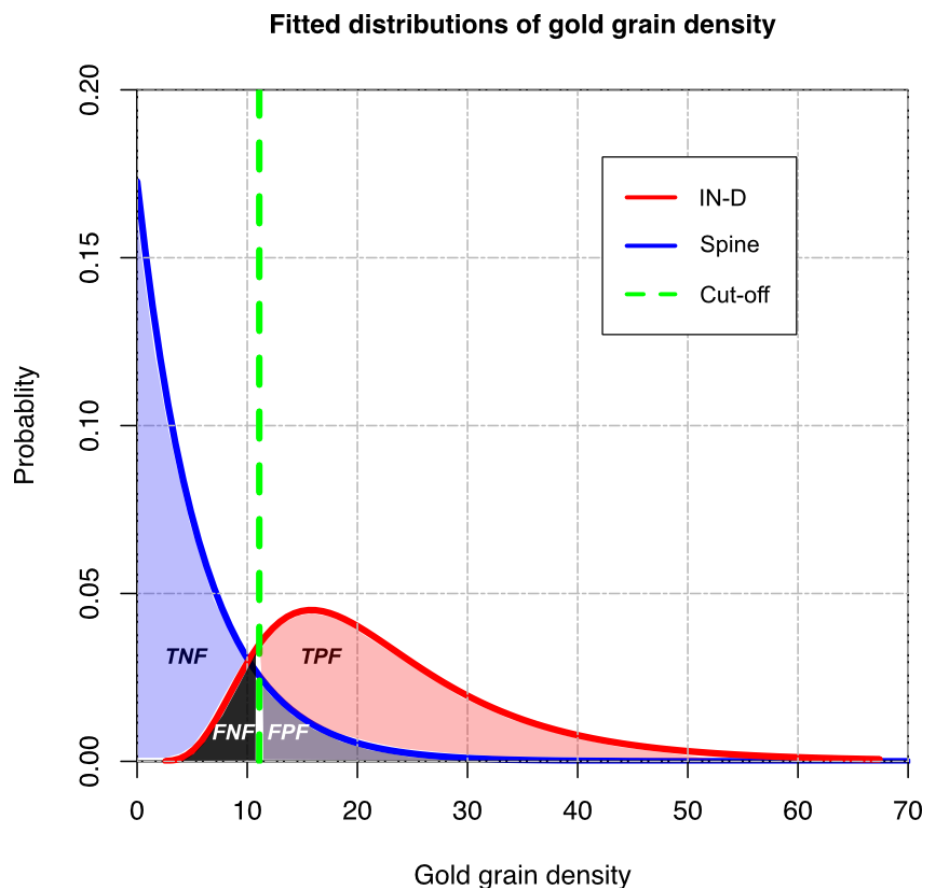
Figure 9. Generation of the dendritic ROC curve.
FPF and FNF are in grey and black, respectively; TPF is the area in red plus grey; TNF is the area in blue plus black. TNF = 1 – FPF; TPF = 1 – FNF.

Based on the ROC curve, there exist various methods with different underlying principles for defining the optimal cut-off point that was also called as GABA-immunopositive threshold in the thesis. Since there is always a trade-off between sensitivity and specificity, it is preferred to consider the specific purpose and constraints of an experiment in order to decide which cut-off method is preferred. For the present study, due to the technical limitation (see discussion 4.1.2), having higher sensitivity (lower false negative ratio) is considered as more important than having higher specificity (lower false positive ratio) when identifying the targeted GABAergic profiles. Thus, one of the most frequently used methods "closest point to (0,1)" was adopted (Perkin and Schisterman, 2006). It chooses the point on the ROC curve that is closest to the perfection

which has zero false positive and perfect sensitivity. Using this method, the GABA-immunopositive threshold for dendrites as well as spines was defined on the dendritic ROC curve at 11.1 gold grains/µm² with 0.86 TPF and 0.16 FPF (Figure 10). Any dendrite or spine that had the labeling higher than 11.1 gold grains/µm² was regarded as GABA-immunopositive with 0.16 probability of making false positive error (type I error); while any dendrite or spine with the labeling lower than 11.1 gold grains/µm² was taken as GABA-immunonegative with 0.14 probability of making false negative error (type II error). The method was also used to determine the optimal cut-off point on the somatic ROC curve and gave the GABA-immunopositive threshold for somata at 8.5 gold grains/µm² with 0.17 FPF and 0.29 FNF.
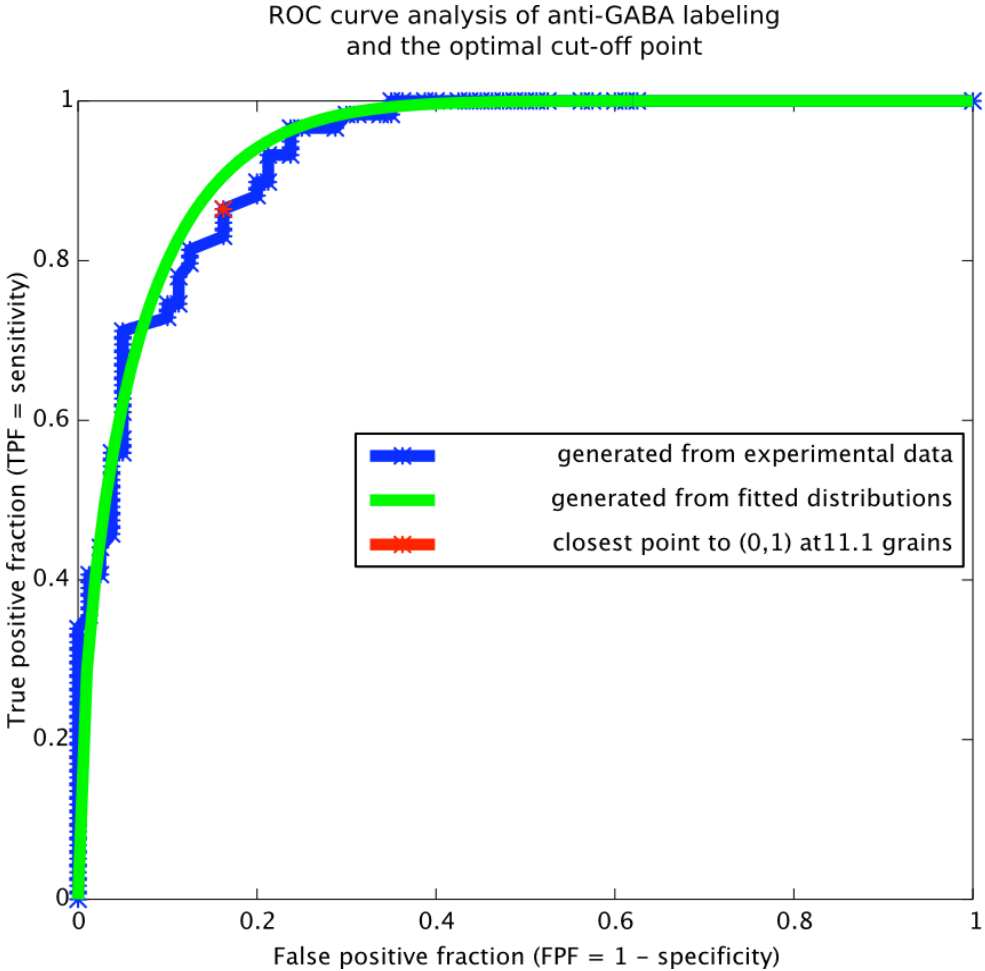
Figure 10. The optimal cut-off point on the ROC curve.

40

The method "closest point to (0,1)" generates the dendritic GABA-immunopositive threshold at 11.1 gold grains/µm² (red point).

3.2.3   Other cut-off methods

To show how the quantification varies along with the statistically defined GABA-immunopositive thresholds, several other cut-off methods were additionally employed on the dendritic ROC curve.

"Equal false rate"

The method "equal false rate" balances the sensitivity and specificity by making FPF and FNF equal. The generated threshold for dendrites (spines) was at the value 12.0 gold grains/µm² with 0.15 FPF and FNF (Figure 11). The value was very close to the optimal cut-off point. Using this cut-off method, any dendrite (spine) with a density over 12.0 gold grains/µm² was regarded as GABA-immunopositive with 0.15 probability of making type I error; vice versa, the structure with the density below 12.0 gold grains/µm² was regarded as GABA-immunonegative with 0.15 probability of making type II error. It gave the threshold for GABA-immunopositive somata at 7.9 gold grains/µm².
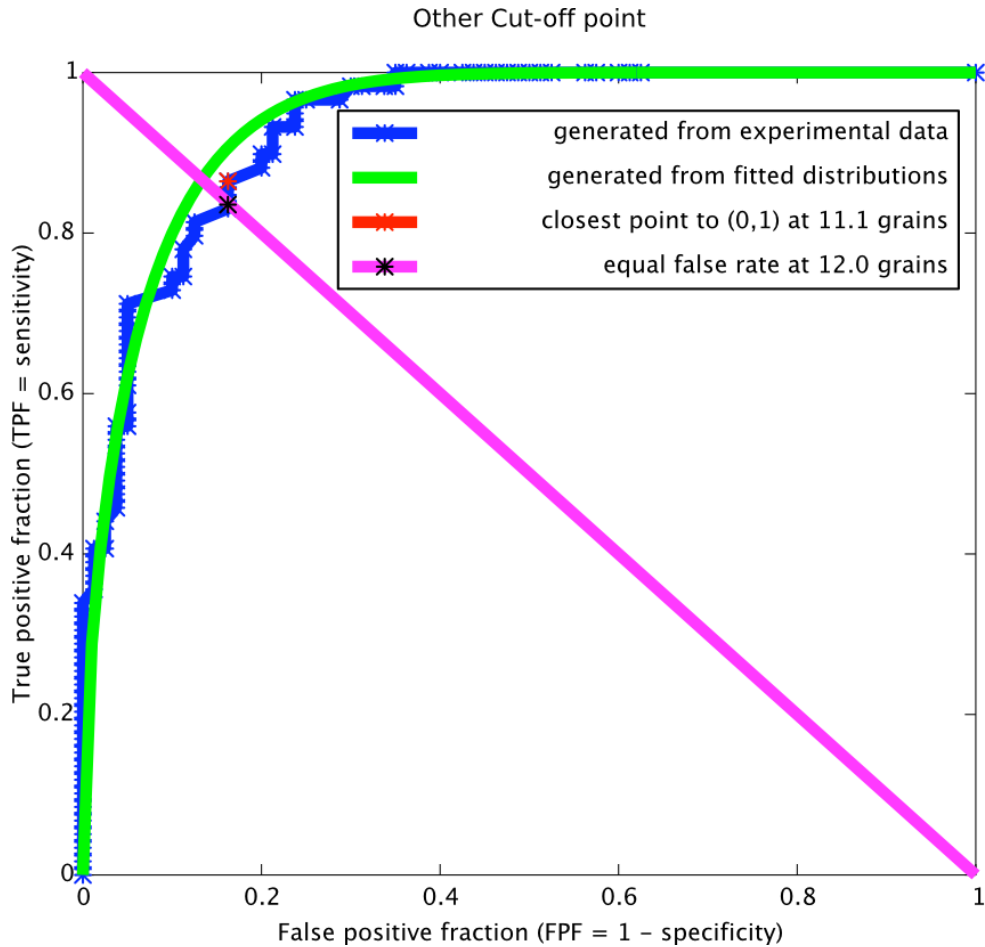
Figure 11. A cut-off method: "equal false rate".

"Double thresholds at 0.1 false rate"

"Double thresholds at 0.1 false rate" generates two thresholds: one for GABA-immunopositive profiles and one for GABA-immunonegative profiles, determined respectively by setting both FPF and FNF at 0.1. Using the method, the GABA-immunonegative threshold was found at 10.8 gold grains/μm² and the GABA-immunopositive threshold at 14.0 gold grains/μm² on the dendritic ROC curve (Figure 12). Any dendrite (spine) that had the density below 10.8 gold grains/μm² or above 14.0 gold grains/μm² was regarded as the real GABA-immunonegative or GABA-immunopositive with 0.1 probability of making type II or type I errors, respectively. Between 10.8 gold grains/μm² to 14.0 gold grains/μm², was the gray zone where data

42

were not counted. For the somata, the double thresholds were at 9.0 gold grains/µm² and

4.2 gold grains/µm² for GABA-immunopositive and GABA-immunonegative.
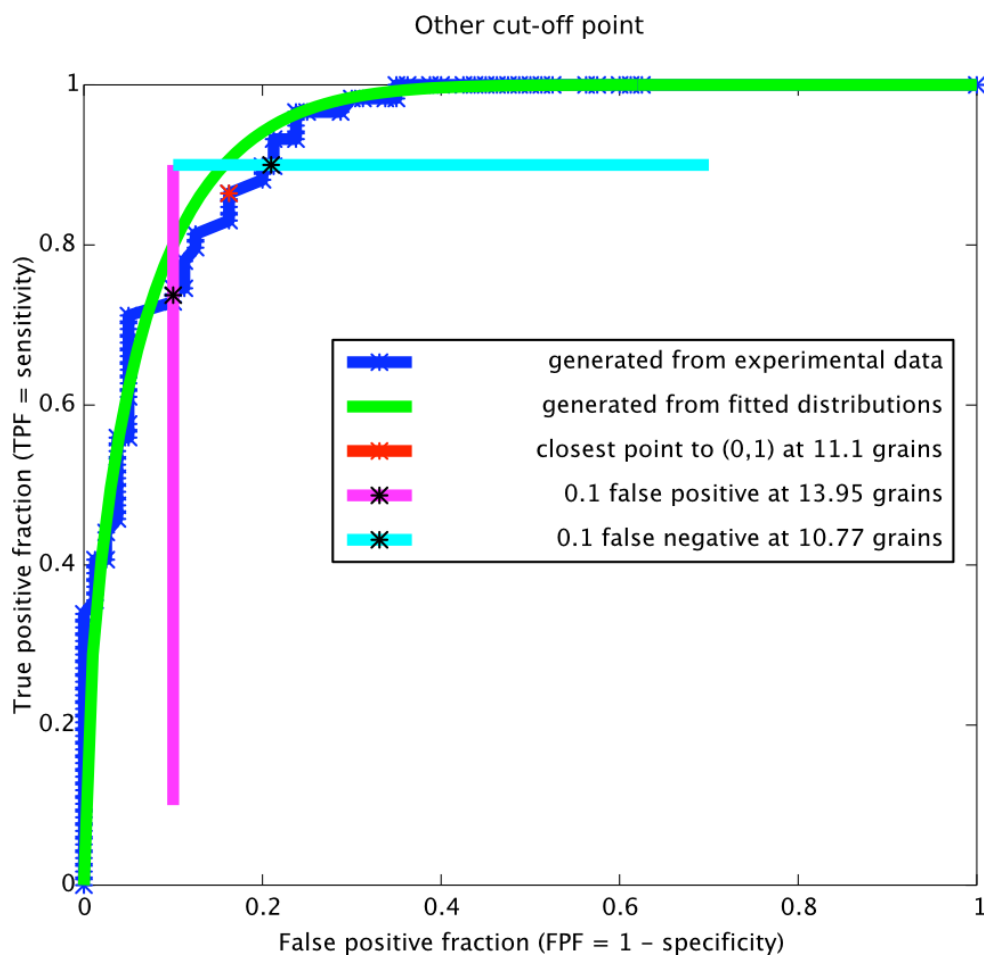
Figure 12. A cut-off method: "double thresholds at 0.1 false rate".
The pink and cyan lines depict 0.1 FPF and 0.1 FNF respectively. Their intersections with the
dendritic ROC curve give corresponding thresholds for GABA-immunopositive and GABA-
immunonegative.

"Prevalence based adaptive threshold"

The above three methods were based on the principle that the prevalence of non-

GABAergic (spines) and GABAergic structures (interneuron dendrites) are equally 50%

as shown by the distributions in Figure 9. However, in real case, the prevalence might not

always be equal, and thus the generated threshold may not be able to estimate the real

positive presence, i.e. the prevalence of GABA-immunopositive profiles among the

targets. This method is improved based on the method "equal false rate" with consideration of the prevalence. Therefore, the following algorithms were developed to find an adaptive threshold that could end up with the estimated GABA-immunopositive prevalence as close as possible to the real GABA-immunopositive prevalence in the tissue.

Definitions:

- P(A) prevalence of being GABA-immunopositive, the real fraction in the tissue
- P(B) GABA-immunopositive probability, estimated by the gold grains above the threshold

$$P(B) = \ TPF \times P(A) + FPF \times \left(1 - P(A)\right)_{(1)}$$

In the equation (1), the measured P(B) is the sum of true and false positive probabilities of GABA-immunopositive prevalence. The best condition for defining the threshold is to set the *P(B) = P(A)*, therefore,

$$P(A) = \ TPF \times P(A) + \ FPF \times \left(1 - p(A)\right)_{(2)}$$

transformation of equation (2) shows the equations (3), which means the false negative probability has been set equal to false positive probability.

$$(1 - TPF) \times P(A) = FPF \times \left(1 - p(A)\right)_{(3)}$$

Another transformation of equation (2) shows a line in ROC space which descends from the optimal point (0,1) and the slope of which is the odds against prevalence.

$$TPF \ = 1 - \frac{1 - p(A)}{p(A)} \times FPF_{(4)}$$

Its intersection with the ROC curve defines the optimal threshold for a given P(A).

The iterative procedure to find the prevalence P(A) is as follows.

1. Have all measurements available for analysis.

2. Make the initial guess on P(A), e.g. P(A) = 0.5.

3. Intersect the ROC curve using equation (4) and lookup the threshold.

44

4. Evaluate P(B), the fraction above the threshold.

5. If P(B) still differs significantly from P(A) assume that P(B) is only an improved estimate of P(A). So set P(A) = P(B) and continue with step 3) above.

Using the iterative procedure on the two distributions in Figure 9, the real GABA-immunopositive prevalence was found at 0.45, which gave the threshold at 12.4 gold grains/μm² for dendrites (spines) (Figure 13). The somatic threshold was found at 6.7 gold grains/μm². It should be noted that the threshold by this method is adaptive: when adopting the iterative procedure to other datasets, e.g. the grain density of the targeted dendrites in different layers, the GABA-immunopositive threshold might vary across layers. For the dataset with higher GABA labeling immunoreactivity, the GABA-immunopositive threshold is tuned to become lower in order to let false positive probability equal false negative probability; vice versa, for the dataset with lower GABA labeling immunoreactivity, the GABA-immunopositive threshold is tuned to become higher.
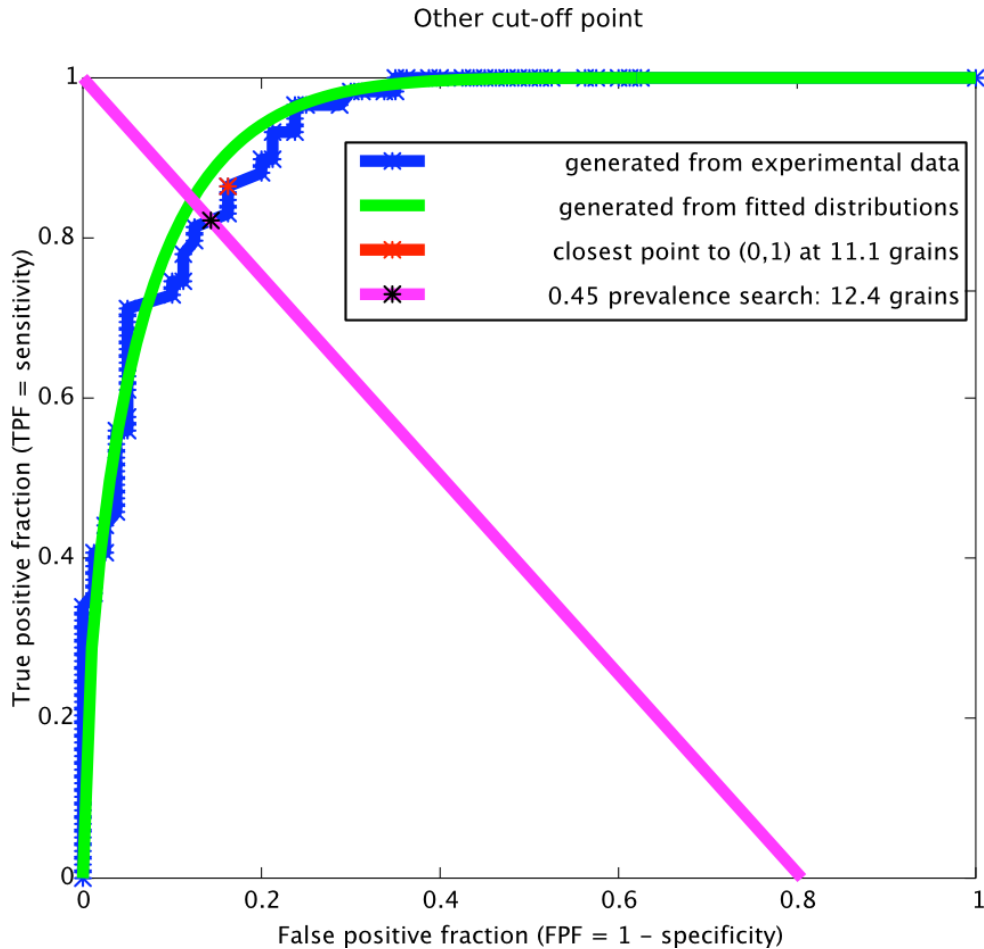
Figure 13. A cut-off method: prevalence based adaptive threshold.
The pink line depicts the threshold found by the iterative procedure described above. The intersection point is at 12.4 gold grains/μm² with 0.45 prevalence of GABA-immunopositive profiles.

3.3 Quantitative analysis of the subcellular targets of VIP interneurons

This section includes three parts: section 3.3.1 characterizes the structures and their distribution of the subcellular targets of VIP-positive boutons across layers; in section 3.3.2 GABA-immunopositive rate was determined in each type of targeted structure; in section 3.3.3, the targeting of VIP cells was further compared in a layer-dependent manner.

3.3.1   Quantifying the postsynaptic targets in terms of structure

In total 200 boutons of VIP interneurons were sampled: 12 in layer I, 74 in layer II/III, 45 in layer IV, 37 in layer V, and 32 in layer VI. The specific laminar distribution of this sample was inspired by soma localization of VIP cells as quantified in VIP-ires-Cre transgenic mice (Prönneke et al., 2015). All of these boutons formed symmetric Type II synapses. Figure 14 details the proportion with which postsynaptic structures were targeted by these boutons and their distribution across cortical layers. In total, the 200 boutons formed 207 synapses. Of these, 80% (165 /207) were on dendrites, 7% (15 /207) on spines, and 13% (27 /207) on somata. This confirms that neocortical VIP interneurons target mainly dendrites, like previously shown for the hippocampus (Ascády et al., 1996). In agreement with the results from serial sectioning, most of the boutons had only one synaptic contact, however, 7.5% (15 /200) of the boutons had two targets and these were mainly found in layer II/III (53%, 8 /15). Most of the postsynaptic targets were innervated by one bouton; whereas roughly 5% of the targets (7 /207) were found to be decorated with more than one synapse in any single or serial ultrathin section. Such a multiple innervation usually occurred on somata.

When cortical layers were separated, a layer-dependent difference in the proportion of target structures was found (Figure 14). In layer I, interestingly, all of the boutons exclusively formed synapses with dendritic targets (12 /12). Layers II/III, IV and V showed a comparable distribution of postsynaptic subcellular structures. In layer II/III, the targets of the boutons amounted to 80% (61 /76) for dendrites, 12% (9 /76) for spines, and 8% (6 /76) for somata. In layer IV, dendrites were the most frequently innervated subcellular profile (84%; 41 /49). Innervation on spines and somata amounted to only 4% (2 /49) and 12% (6 /49). Similarly, in layer V, 84% (32 /37) of contacts were on dendrites, whereas spines and somata both received the input of VIP cells only at a ratio of 8% (3

/37). Unlike the other layers, in layer VI, nearly 40% (12 /32) of the synapses of VIP cells were on somata, which was much higher than in all the other layers. Nevertheless, dendrites were still the major targeted profile (58%) (18 /32). Only 3% (1 /32) of the synapses were found on spines.

Fractions of the three postsynaptic structures
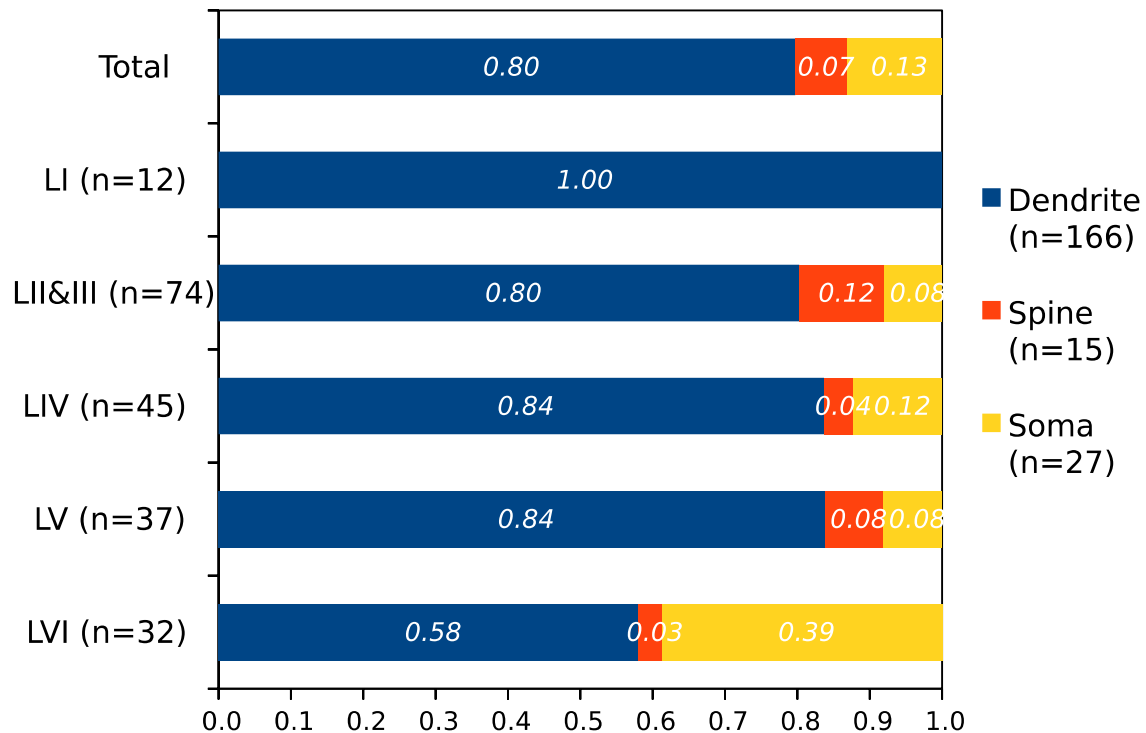
Figure 14. Fractions of postsynaptic targets of VIP-positive boutons.
Axonal boutons of VIP cells target three subcellular structures, namely dendrites (blue; n=166), spines (red; n=15), and somata (yellow; n=27). The presynaptic profiles are the 200 boutons collected across layers as shown to the left. Please note that dendritic targets dominate in all layers.

3.3.2 Calculating GABA-immunopositive ratio among the subcellular targets

To quantify the GABA-immunopositive ratio among the targets, 11.1 grains/μm^2 and 8.5 grains/μm^2 were taken as the thresholds for GABA-immunopositive dendrites (spines) and somata. In the meantime, the ratios were compared with the ones using the other cut-off methods. As shown in Figure 15, only 37% of the dendrites innervated by the axonal boutons were GABA-immunopositive when pooled over all cortical layers. As expected,

most of the spines (93%) were GABA-immunonegative. The other three methods, "equal false rate", "double thresholds at 0.1 false rate" and "prevalence based adaptive threshold", resulted in even lower GABA-immunopositive rates to respectively 32%, 30%, 25%. For the targeted spines, the other three methods gave the same GABA-immunopositive rate (7%). It was found that 26% of the targeted somata were GABA-immunopositive. The other methods generated the same result except for the double thresholds which rose to 35%.
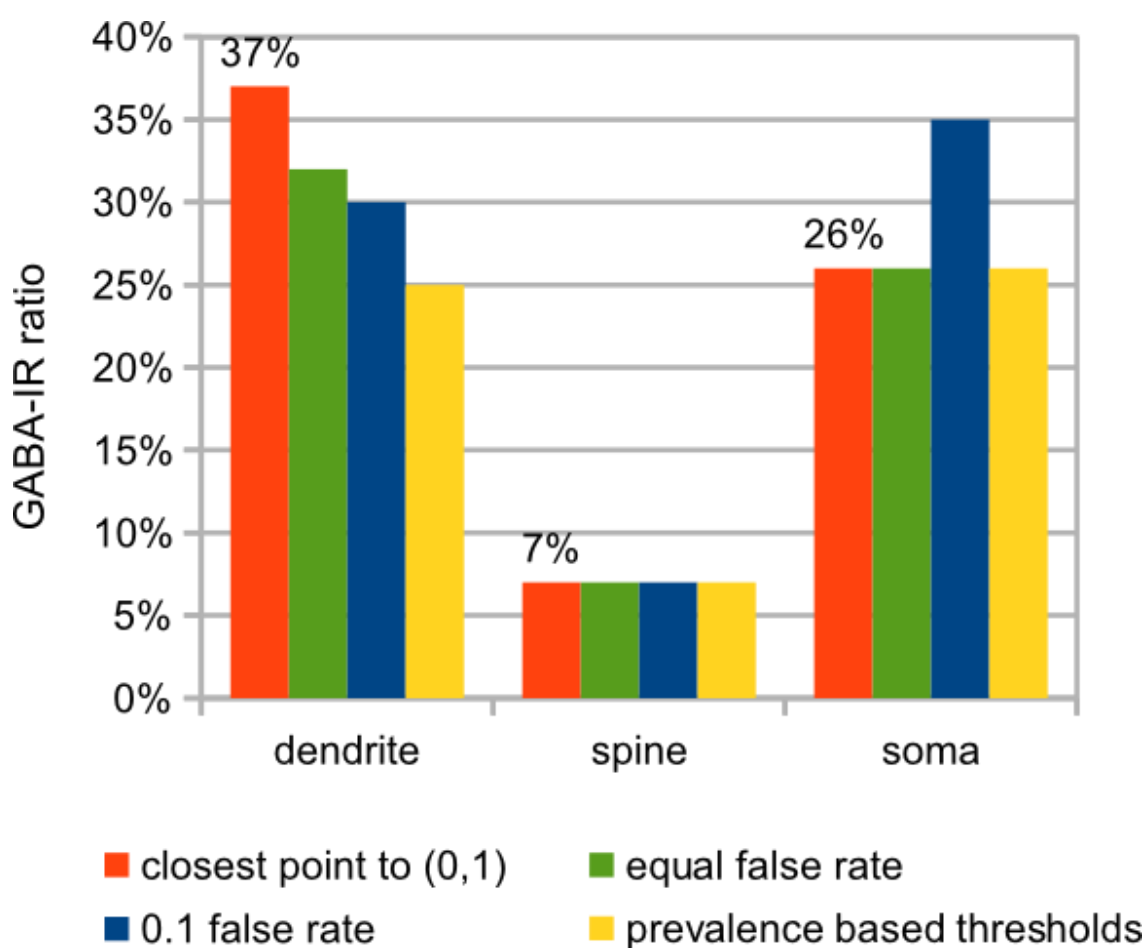
Figure 15. GABA-immunopositive ratio of the targets of VIP-positive boutons.
The other three cut-off methods are used to calculate such a ratio for comparison.

Since dendrites were the main targets of VIP interneurons across layers, the GABA-immunopositive rates were further calculated for the targeted dendrites in each layer. As Figure 16 shows, using again 11.1 grains/μm^2 as the threshold, in layer I only 29% of the

targeted dendrites were GABA-immunopositive whereas in layers II/III and IV the ratio slightly increased to 34%, similar to layer VI (39%). In layer V this value showed a peak of 48%. For comparison, the other three methods ubiquitously gave lower GABA-immunopositive rates in superficial layers, while in deep layers the results were similar. For the somatic targets, the immunopositive rate also varied across layers: none in layer I, 17% (1/6) in layer II/III, 50% (3/6) in layer IV, 67% (2/3) in layer V and 8% (1/12) in layer VI. Due to the limited sample of axosomatic synapses, the targeting specificity onto interneuron somata needs to be scrutinized in future studies.
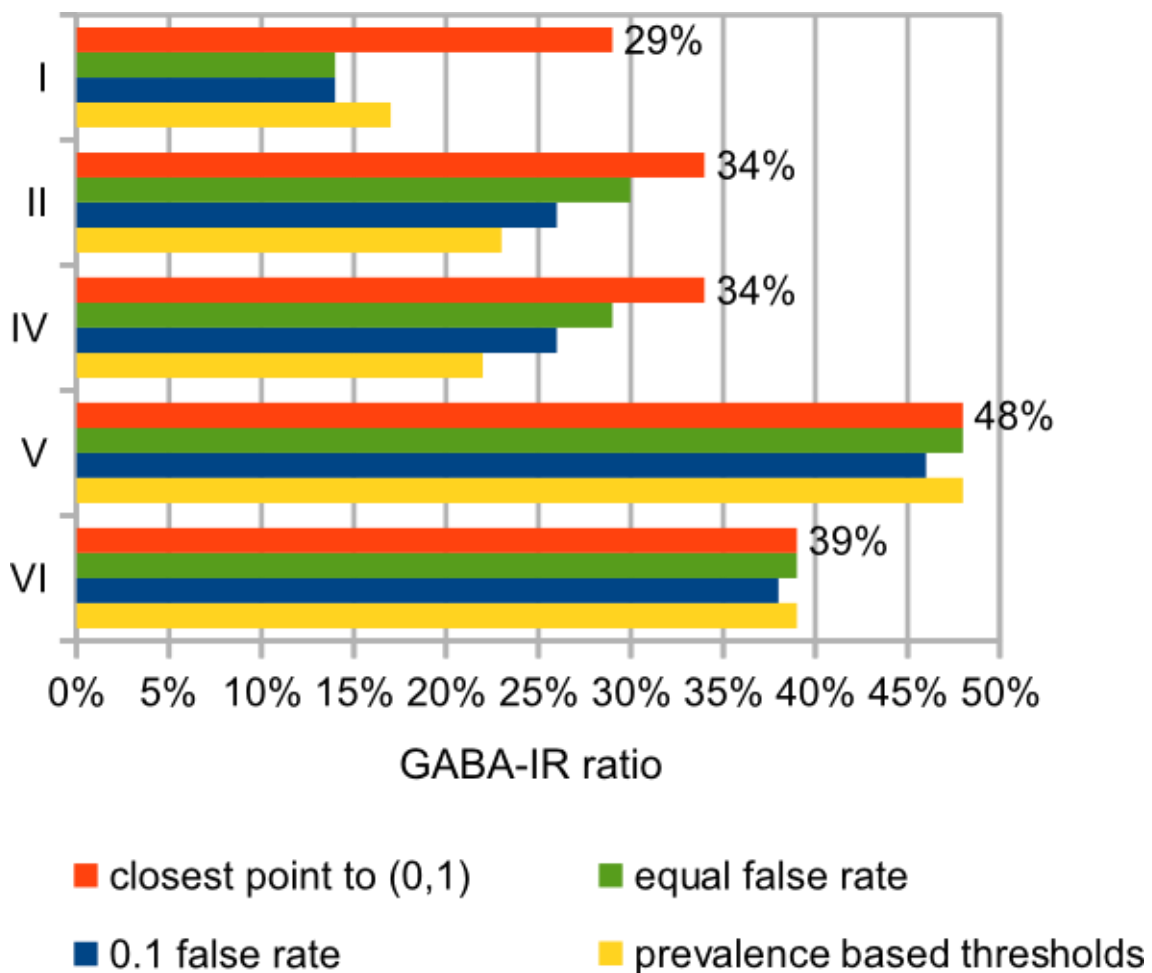
Figure 16. GABA-immunopositive ratio of the main target "dendrite" in different layers.
The other three cut-off methods are used to calculate such a ratio for comparison.

50

3.3.3 Characterizing the targeting across cortical layers

Superficial layers:

Layer I: This layer houses numerous "top-down" inputs and the somata of several types of GABAergic interneurons. Thus, it presented an intensive gold labeling of the rich neuropil (Figure 17A). In layer I, a third of the targets were GABA-immunopositive dendrites (Figure 17B) and two-thirds were GABA-immunonegative dendrites (Figure 17C). From the sampled synapses, none of the VIP boutons targeted the cell bodies of GABAergic interneurons in layer I.
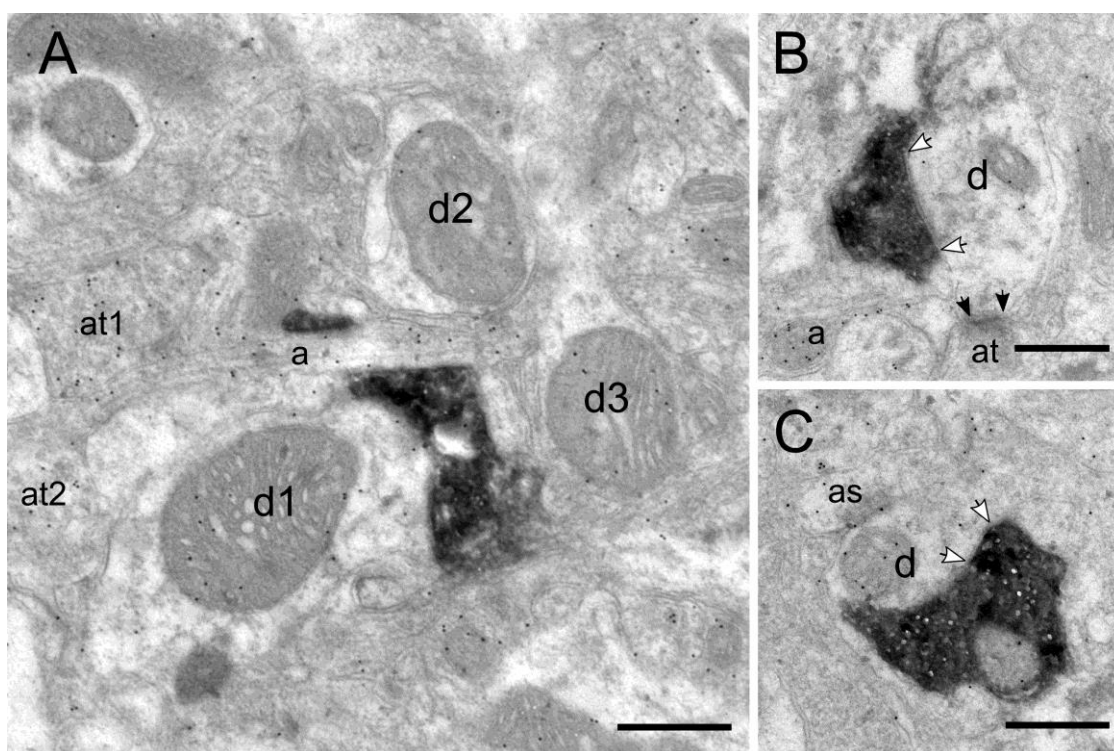
Figure 17. Targets of VIP cells in layer I.
(A) Immunogold labeling of GABA in the neuropil of layer I. The labeled structures above the threshold are an axon (a), two axonal terminals (at1, at2), and two dendrites (d1, d3); d2 is the unlabeled dendrite. (B) A bouton targets a GABA-immunonegative dendrite (d), which further receives an asymmetric axonal terminal (at). (C) A bouton targets a GABA-immunopositive dendrite (d). as: astrocytic profile. Scale bars = 0.5 μm in A-C.

Layer II/III: In this "associative" layer, it was found that the GABA-immunopositive rate was also only around one-third in the main target "dendrite". On visual inspection, the targeted GABA-immunonegative dendrites (Figure 18A-B) had much less labeling than the targeted GABA-immunopositive dendrites (Figure 18D-F). Serial sections of the targeted large caliber GABA-immunonegative dendrite in Figure 18B showed a spine protrusion on the opposite site of the synapse (data not shown), implying that they belong to apical dendrites of pyramidal cells. Although there exist sparsely spiny GABAergic non-pyramidal cells in the primary sensory cortex (DeFelipe et al., 2013), the very sparse labeling on the targeted spines (Figure 18C) indicates that they also belong to non-GABAergic pyramidal cells. For the targeted GABA-immunopositive dendrites, asymmetric excitatory synapses were usually found in the vicinity of the symmetric synapses formed by VIP cells (Figure 18F). For the axosomatic innervation, VIP boutons targeted preferentially immunonegative neurons, which are likely to be layer II/III pyramidal neurons. This finding is supported by the axosomatic synapse found on the cell body of an identified layer II/III pyramidal neuron in separate correlated light and electron microscopic studies (Figure 25).
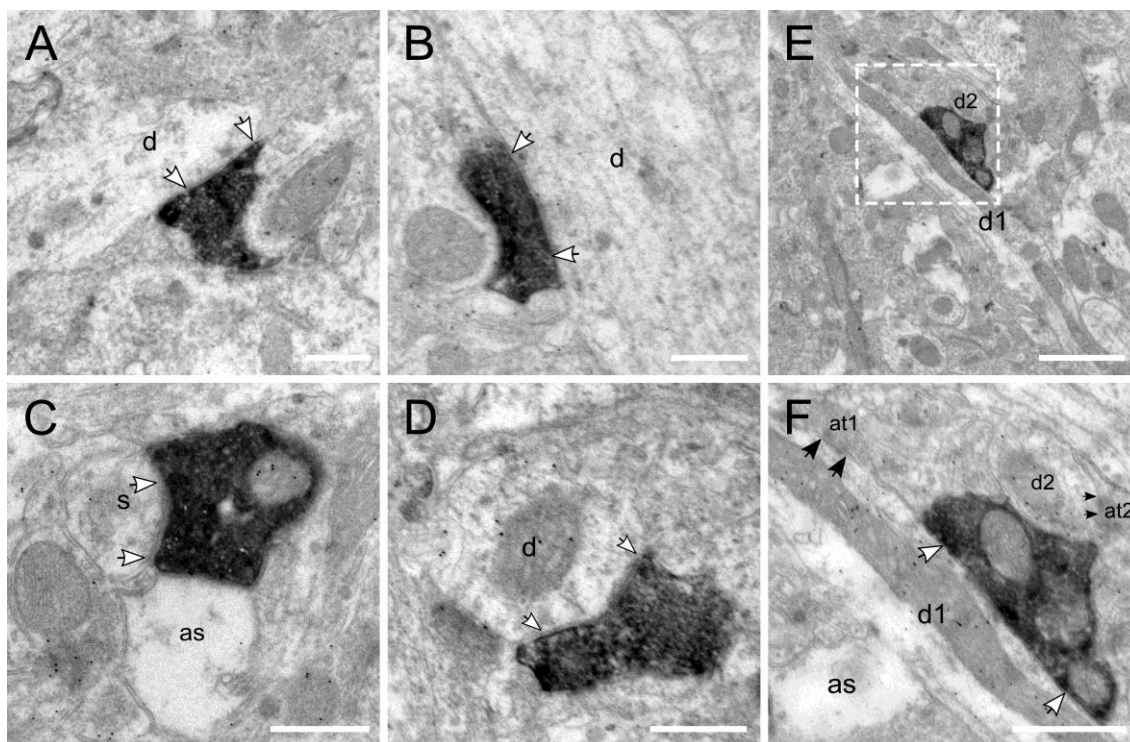
Figure 18. Targets of VIP cells in layer II/III.

(A) A bouton forms a symmetric synapse (white arrows) on a GABA-immunonegative dendrite (d). (B) Another symmetric synapse is formed on a thick GABA-immunonegative dendrite by a single bouton. (C) A synapse on GABA-immunonegative spine (s). as: astrocytic process. (D) A bouton targets a GABA-immunopositive dendrite. (E-F) A bouton innervates a longitudinally-cut small-caliber dendrite (d1); for the cross-sectional dendrite (d2), a synaptic cleft is not clear due to an oblique cutting angle. Both dendrites are GABA-immunopositive and receive asymmetric synapses (black arrows) from excitatory axonal terminals (at1, at2) in the vicinity. Scale bars = 0.5 μm in A-D, F; 1 μm in E.

Layer IV: In this major input layer to cortical columns, similar to layer II/III, the axonal boutons targeted mainly GABA-immunonegative dendrites (Figure 19A1,A2,B). Small GABA-immunopositive dendrites (Figure 19C) as well as spines and somata were innervated as minor groups. For the somatic innervation, GABAergic interneurons were targeted with an increasing ratio in layer IV as compared with layer II/III.
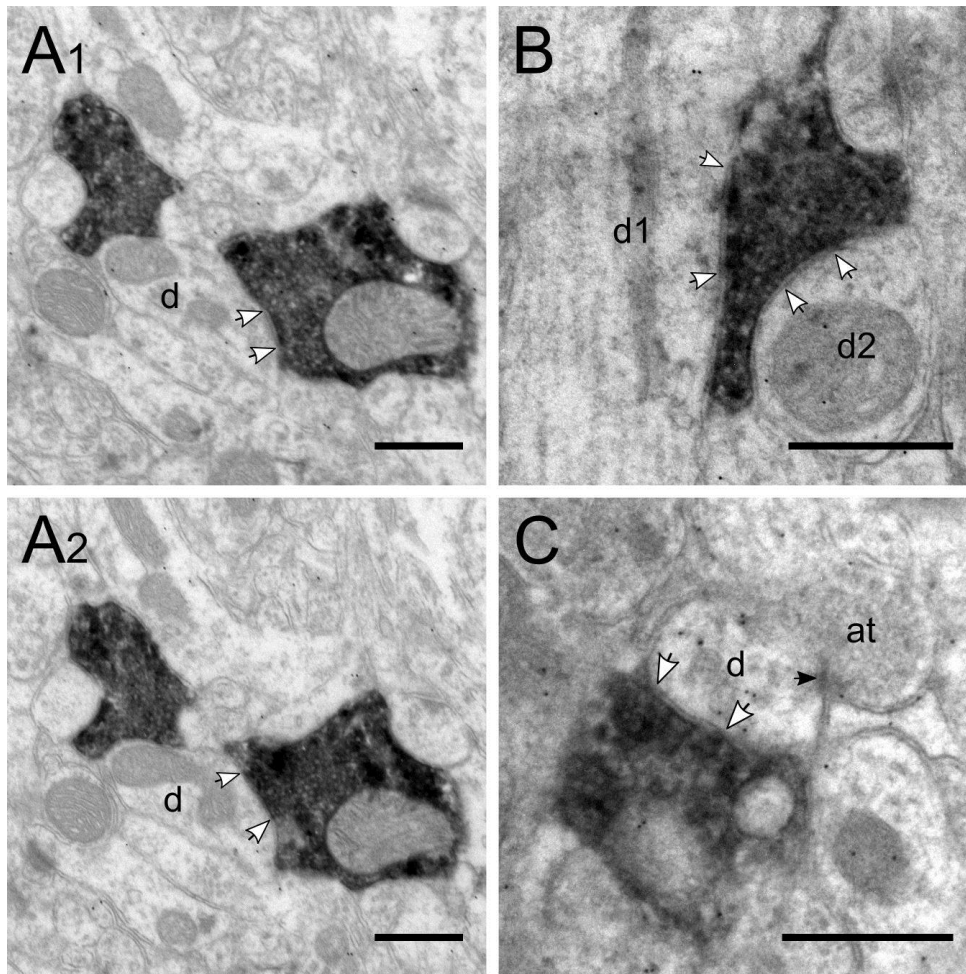
Figure 19. Targets of VIP cells in layer IV.

(A1-2) Consecutive sections of a large bouton making a symmetric synapse (white arrows) on a GABA-immunonegative dendrite (d). (B) A bouton forms two synapses on GABA-immunonegative dendrites (d1, d2). (C) A very small GABA-immunopositive dendrite is innervated by a bouton and an excitatory axonal terminal (at) (black arrow). Scale bars = 0.5 μm in A-C.

Deep layers:

Layer V: This layer is considered to be the major output layer of the neocortex. Compared with other layers, a much higher proportion of VIP targets were found on GABA-immunopositive dendrites. Labeling was rarely found over GABA-immunonegative dendrites with spine protrusions (Figure 20A1,A2); while intensive labeling was found over aspiny GABA-immunopositive dendrites (Figure 20B1,B2,C).

54

Since layer V is strongly populated by Martinotti cells, which are SST expressing interneurons (Wang et al., 2004; Muñoz et al., 2017), the targeted GABA-immunopositive dendrites might be from the Martinotti cells. Interestingly, correlated light and electron microscopic examination showed a synapse onto an identified layer VI pyramidal neuron at its distal apical dendritic domain, which might be a representative of the synapses onto immunonegative dendrites in layer V in the quantitative EM study (Figure 26). Similar to the finding in layer II/III, the targeted GABA-immunopositive dendrites in layer V tend to receive excitatory input close to the symmetric VIP synapses (Figure 20C).
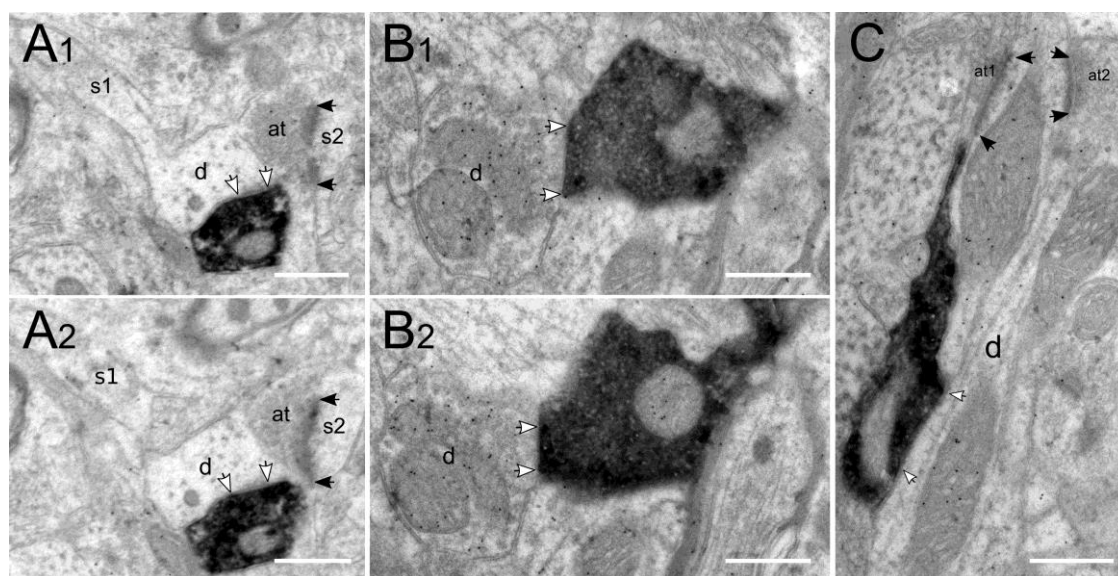
Figure 20. Targets of VIP cells in layer V.
(A1-2) Consecutive sections show a bouton which innervates a GABA-immunonegative dendrite (d; white arrows indicate the active zone). In (A1) the dendrite protrudes an elongated spine (s1). Right above there is an excitatory axospinous synapse and the postsynaptic density (black arrows in A1) has a perforation. (B) Consecutive sections show one large bouton which forms a symmetric synapse with a GABA-immunopositive dendrite, densely labeled by gold grains. (C) A bouton targets a GABA-immunopositive dendrite which is also innervated by two excitatory axonal terminals in the vicinity (at1, at2). Scale bars = 0.5 µm in A-C.
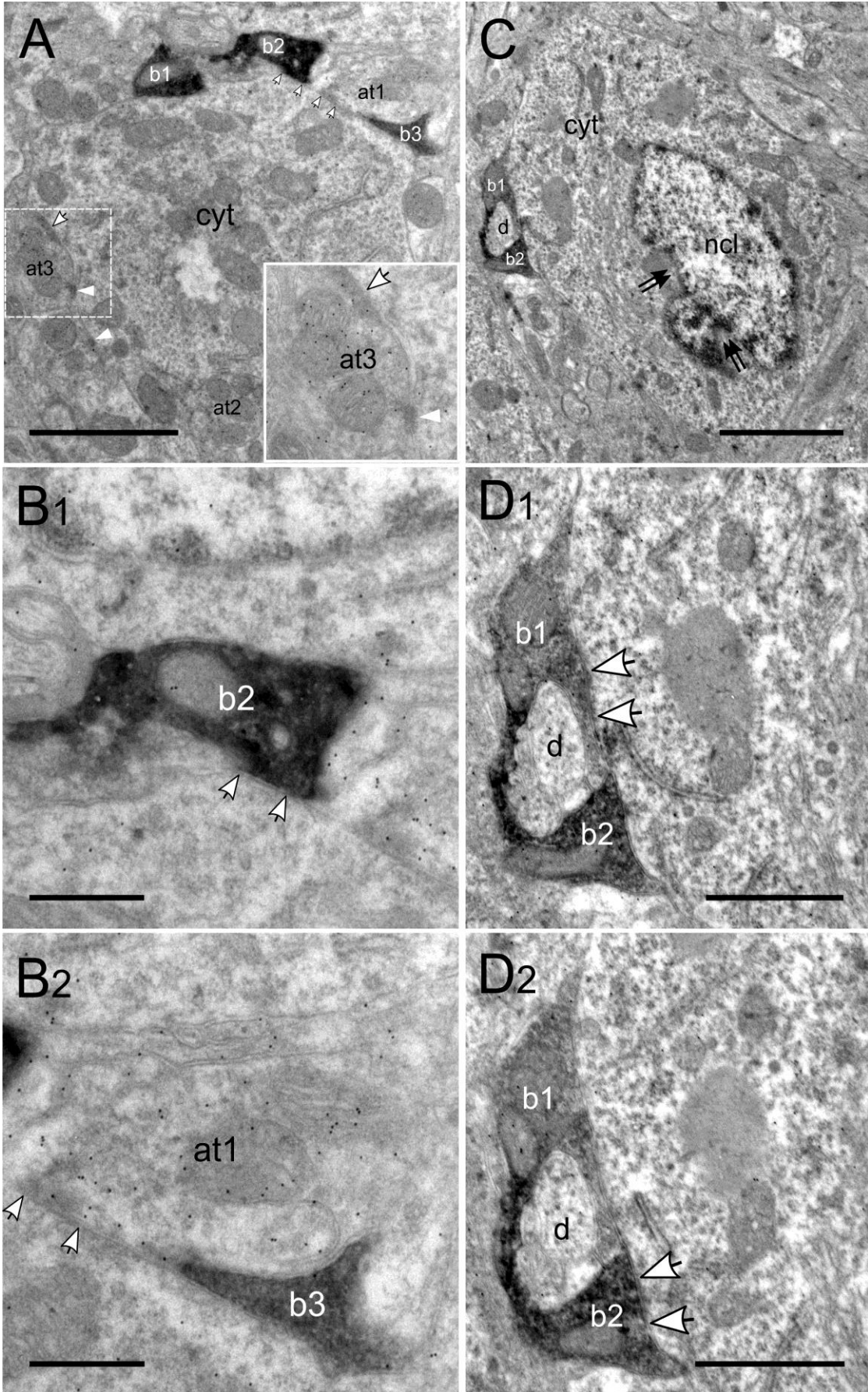
Figure 21. Targets of VIP cells in layer VI.

(A) Low magnification image of a peripheral part of an excitatory cell soma surrounded by three boutons (b1-b3) and three GABA-immunopositive axonal terminals (at1-at3). Puncta adherentes (white arrowheads) are differentiated from synaptic junctions (white arrows) as shown in the inset. (B1-2) Ultrastructure of somatic synapses formed by a bouton (b2) in (B1) and the GABA-immunopositive axonal terminal (at1) in (B2). (C) Low magnification image of an interneuron soma targeted by two boutons (b1, b2), which enwrap a dendrite (d). Double arrows indicate indentations of the nucleus (ncl). (D1-2) Higher magnification images of two consecutive sections through the boutons in (C) showing the axosomatic synaptic junctions. cyt: cytoplasm. Scale bars = 2 µm in A; 0.5 µm in B1-2; 2.5 µm in C; 1 µm in D1-2.

Layer VI: Interestingly, in this "gain control" layer, as shown in Figure 21, somatic synapses were usually formed by more than one bouton per soma, for both non-GABAergic principal cells (Figure 21A,B1,B2) and GABAergic neurons (Figure 21C,D1,D2). In contrast to layer V, the somatic immunopositive ratio was the lowest among cortical layers. This result indicates VIP interneurons preferentially target perisomatic regions of excitatory principal neurons in layer VI. Since layer VI has the morphologically most diverse principal neurons (Andjelic et al., 2009), it will be interesting to know which subtypes they innervate.

Superficial layers versus deep layers

For the main innervated structure, dendrites, GABA labeling was compared across layers in order to know whether there is a layer-dependent difference in dendritic targeting by VIP interneurons. Table 3 reports the 1st quartile (Q_{25}), Q_{50}, and 3rd quartile (Q_{75}) of gold grain density, which measured GABA labeling. However, no significant difference was found across layers (Figure 22A,B, One-way ANOVA on ranks, $H = 8.63$, df = 4, p = 0.07). The reason was possibly due to the variations of the background labeling between different animals and experimental batches. Then, normalized gold grain density was used instead of the original density. Normalization was performed by dividing the gold grain

density of a targeted dendrite by the mean density of the surrounding spines. Again Table 3 shows 1st quartile (Q$_{25}$-N), Q$_{50}$ (Q$_{50}$-N), and 3rd quartile (Q$_{75}$-N) of the normalized density. Similarly one-way ANOVA on ranks test was used to compare the GABA labeling for each layer. A significant difference existed across layers (H = 21.28, df = 4, p < 0.001) (Figure 22C,D). It can be assumed that there is a layer-dependent difference in dendritic targeting by VIP interneurons.

To further evaluate which specific layers might cause this difference, a post hoc Dunn's test with Bonferroni correction was used to compare each layer. There was a highly significant difference between layers II/III and V (z = -3.77, p < 0.001) and layers II/III and VI (z = -3.12, p < 0.001). Between layers I and V, there was also significant difference (z = -2.75, p = 0.03). For the rest of the layers, no statistically significant differences were found. Furthermore, GABA labeling of the dendritic targets was significantly stronger in deep than in superficial layers when Mann-Whitney U test was used to compare the grouped normalized density of the targeted dendrites (U $_{VIP\ cell:\ superficial\ layers\ vs\ deep\ layers}$ = 1608, p < 0.001).

In addition, we did not find a difference in terms of GABA labeling over the sampled interneuron dendrites between superficial and deep layers (data not shown). The additional test suggests the significance difference in terms of the labeling among the targeted dendrites should not be due to a variance of GABA expression of different interneurons. Thus, these results together indicate that VIP interneurons have a layer-dependent dendritic targeting property: compared with superficial layers, in deep layers a higher proportion of innervation is found on GABAergic than non-GABAergic dendrites.

Table 3. Labeling density (grains/µm^2) and normalized density (-N) of the targeted dendrites

Layer / Quartile	I	II/III	IV	V	VI
Q_{25}	3.9	2.9	4.1	7.9	5.9
Q_{50}	5.4	7.2	7.0	10.9	7.3
Q_{75}	10.7	12.9	12.9	17.2	18.5
Q_{25}-N	0.6	0.5	0.7	1.2	1.2
Q_{50}-N	0.8	1.0	1.3	2.3	3.1
Q_{75}-N	1.7	1.9	2.1	6.0	4.2
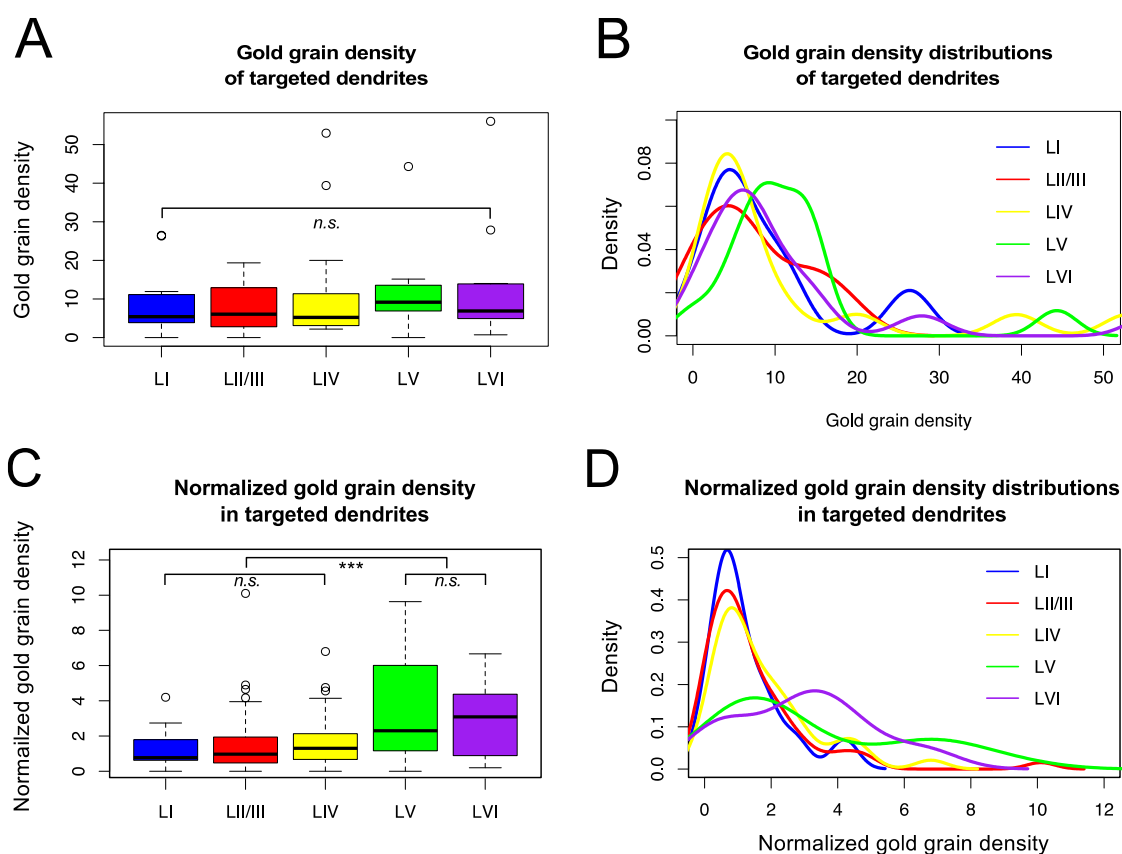
Figure 22. GABA labeling of the postsynaptic targets.

(A) Box plot of the gold grain density of the targeted dendrites. Mann-Whitney U test shows no significant difference across layers. **(B)** Probability density distributions of the dataset in (A) by kernel density estimation. **(C)** Box plots of the normalized gold grain density of the boutons targeting dendrites. Mann-Whitney U test shows a significant difference between superficial layers (layers I-IV) and deep layers (layers V-VI) with p value (superficial layers vs deep layers) <0.001 and no significant difference (n.s.) within the superficial and deep layers. **(D)** Probability density distributions of the dataset in (C) by kernel density estimation. In superficial layers,

distributions are more concentrated at around 1, which equals background. In deep layers, however, distributions are more dispersed and most of the values are shifted to larger than 1, indicating the labeling density in deep layers to be higher than background.

3.4 Self-innervation of VIP interneurons

Besides other interneurons and pyramidal neurons, VIP interneurons can also make synapses on themselves. According to the previous studies, one subgroup of VIP cells targeted another subgroup (Acsády et al., 1996), and the ultrastructure showed most of the "self-innervating" synapses located on dendritic shafts (Paspalas and Papadopoulos, 1998). During systematic sampling, additional 33 boutons were found to locate in close proximity of other VIP expressing profiles. It is expected that they were the putative self-innervating synapses, although it was difficult to identify the synaptic specializations due to the dense DAB reaction in the cytoplasm of both presynaptic and postsynaptic structures. The prevalence of the self-innervating synapses among all synapses was 14% (33/233). The presynaptic boutons localized to layer IV with the highest proportion (39%, 13/33), followed by both layers II/II and V (27%, 9/33), and with the lowest proportion in layer VI (6%, 2/33). In layer I no self-innervation of VIP interneurons was found. The postsynaptic structures were often VIP expressing dendrites. As shown in Figure 23A, a DAB stained dendrite extended vertically in layer IV. According to the morphology of VIP cells in deep layers (Prönneke et al., 2015), it might belong to a primary dendrite of a layer IV bipolar VIP cell. Figure 23B-D showed several VIP-positive boutons converging their synapses on the long dendritic segment, representing the self-innervating synapses.
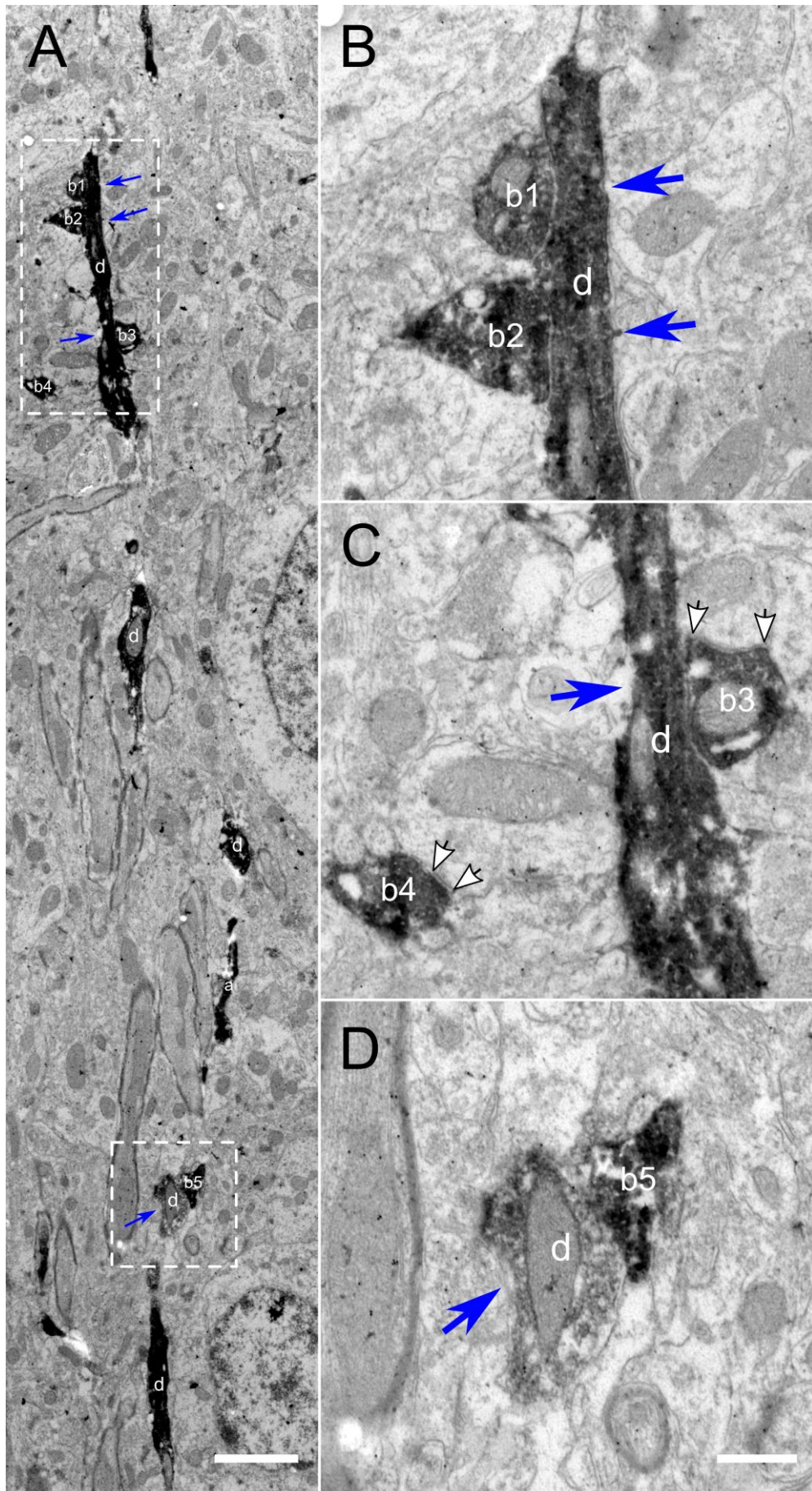
Figure 23. Self-targeting of VIP cells.

(A) In the neuropil of layer IV, a long segment of a VIP positive dendrite (d) receives innervation from VIP positive axonal boutons. (B-D) Higher magnification electron micrographs of the two insets in (A). The boutons (b1, b2, b3, b5) form putative self-innervating synapses (blue arrows) on segments of the dendrite. B3 (additionally) and b4 synapse on dendrites of other cells (white arrows). a: axon. Scale bars = 2 µm in A; 0.5 µm in D (applies also for B and C).

3.5   VIP cells get in close contact with non-neuronal structures

Besides neuronal targets, VIP cells are known to contact non-neuronal structures such as astrocytes and blood vessels and play a role in neurovascular and neurometabolic coupling (Chédotal et al., 1994; Paspalas and Papadopoulos, 1998; Cauli et al., 2004). During the systematic sampling, it was found that some axonal boutons occasionally targeted somata and processes of astrocytes (Figure 24A-C) as well as blood vessels (Figure 24D). Since innervation onto non-neuronal structures is not the main focus of the study, these contacts were not quantified. Unlike the symmetric synapses, there was no membrane specialization at the contact sites of VIP boutons onto either astrocytic profiles or blood vessels. It is suggested that VIP interneurons may regulate neurovascular and neuroglial coupling by volume transmission of VIP or GABA (Cauli et al., 2014). Previous studies also found that VIP positive presynaptic terminals indirectly innervated microvessels by contacting the endfeet of astrocytes that form a thin leaflet surrounding the microvessels (Chédotal et al., 1994; Paspalas and Papadopoulos, 1998). However, this particular ultrastructure could not be clearly demonstrated in our electron micrographs (Figure 24D), maybe due to an oblique plane of sectioning.
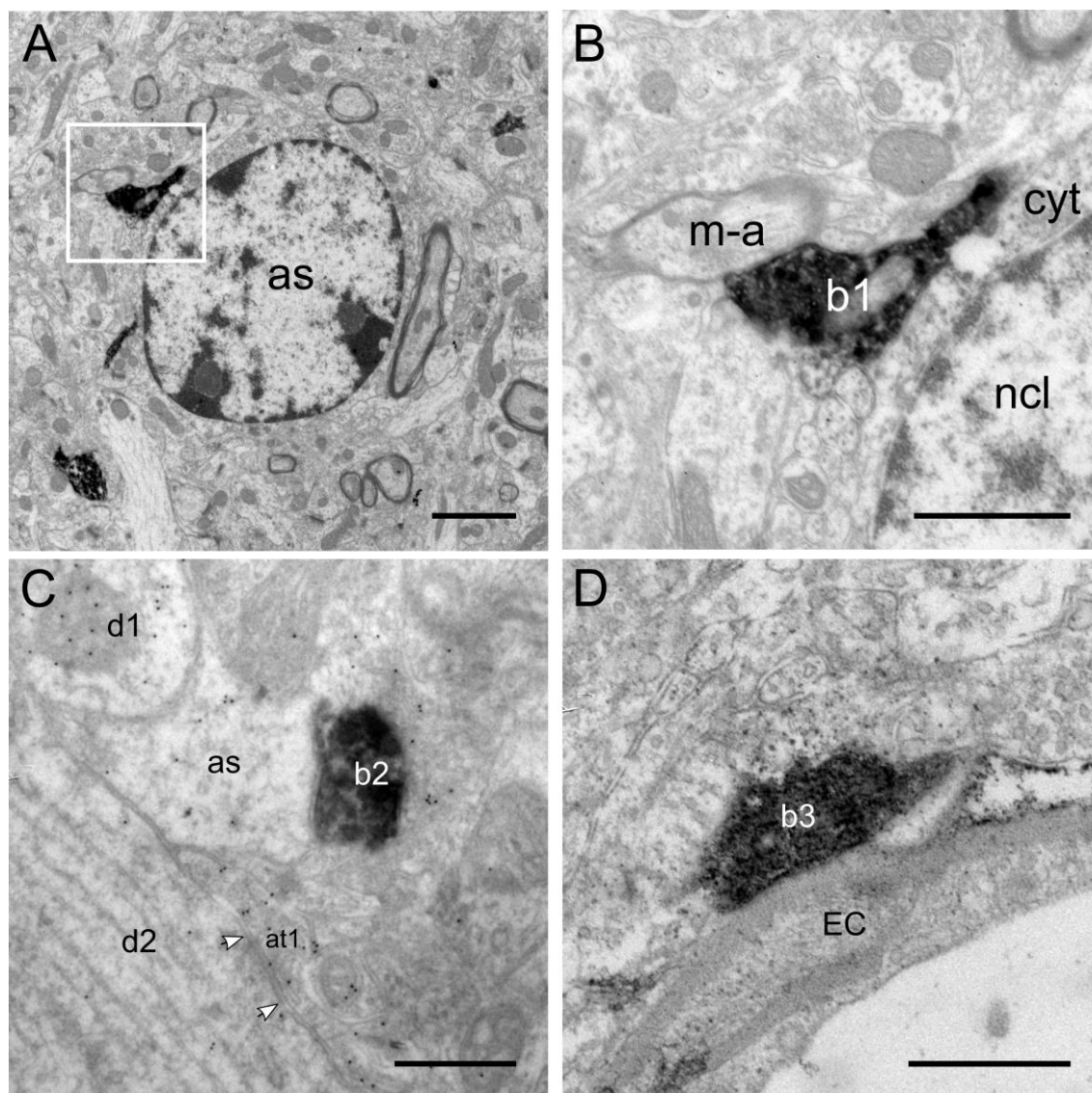
Figure 24. Non-neuronal targets of VIP interneurons.

(A) Soma of an astrocyte (as) is identified by its typical ultrastructure. (B) The inset of (A) shows in high magnification that a VIP positive bouton contacts the soma. (C) Another example of the bouton (b2) innervating astrocyte. There are gold grains accumulating over the inhibitory presynaptic terminal (at1, white arrows) and a putative GABAergic dendrite (d1) but not the thick dendritic shaft (d2). The astrocytic process (as) is also moderately labeled by gold grains. (D) VIP positive bouton (b3) innervating blood vessel. cyt: cytoplasm; EC: endothelial cell; m-a: myelinated axon; ncl: nucleus. Scale bars = 2 μm in A; 1 μm in B; 0.5 μm in C and D.

3.6   VIP boutons innervate pyramidal cells

According to the results of quantitative EM study, most of the targets are GABA-

immunonegative dendrites, and thus preferentially belong to excitatory neurons, i.e. pyramidal neurons. In order to obtain a direct evidence of the connection of VIP interneurons to pyramidal cells, I performed proof-of-principle experiments with the collaboration of another PhD student Georg Hafner. By stereotaxically injecting rabies virus of the SADΔG-EGFP-(CVS-G) strain (Wickersham et al., 2007) into the barrel cortex, it is possible to ipsilaterally label the population of short- and long-range projecting associative pyramidal cells as well as the ones in the contralateral side (Larsen et al., 2007).

Before doing double immunostaining, the sections at injection site were observed for the endogenous GFP expressing in order to evaluate the efficiency of virus transfection. On both injection site and contralateral site of the barrel field, there were GFP-labeled cells, suggesting the success transduction of rabies virus. However, after double immunostaining, it was found that only few pyramidal cells were stained: 3 in layer II/III and 3 in deep layers, either on the injection site or the contralateral site of the barrel cortex. The staining of VIP cells was successful and the result was similar to the staining shown by Figure 3. Since the rabies virus-labeled pyramidal cells were stained in golgi-like manner, although the color difference produced by DAB and DAB-nickel reaction was not easily discernable in the preparation, the labeled pyramidal neurons can be easily differentiated from the surrounding VIP cell processes by their distinctive morphology, e.g., spine-rich apical and basal dendrites and pyramidal shaped cell bodies (Figures 25A,B and 26A,B).

All of the putative VIP synapses along the entire soma-dendritic membrane of two labeled pyramidal cells were marked when doing live reconstruction. The one in layer II/III received in total 28 VIP synapses (Figure 25B), 3 of which were on soma and the rest were on dendrites. The one in layer VI had 21 VIP synapses (Figure 26B), all of

64

which located at dendritic domains. To prove the synaptic connection of VIP boutons onto pyramidal cells, on the basis of optimal orientation of presynaptic bouton, postsynaptic compartment as well as the synaptic cleft, two putative synapses in an orthogonal view were selected for correlation in the electron microscope. One was verified to be a somatic synapse on the layer II/III pyramidal cell (Figure 25C,D) and the other one was a synapse found in layer V on the apical dendrite of the layer VI pyramidal neuron (Figure 26C,D). These preliminary results motivate further studies to fully map the number and localization of VIP synapses on the pyramidal cells, in a subcellular manner (cf. Bloss et al., 2016).
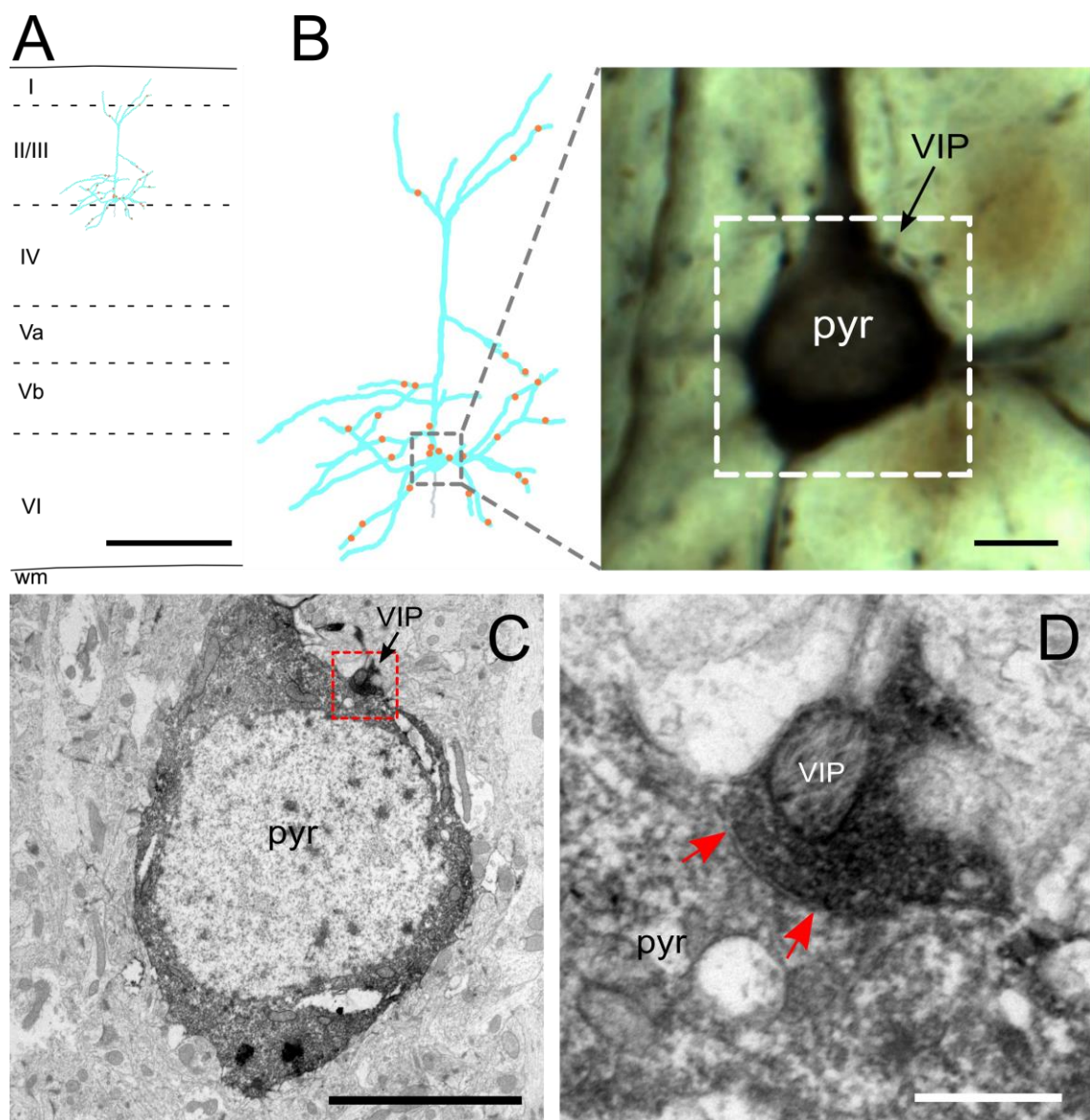
Figure 25. Synapse on apical dendrite of pyramidal neuron.

(A) Somatodendritic reconstruction of the pyramidal neuron (cyan). (B) Red dots represent 28 putative presynaptic VIP boutons, 3 of which were on the soma and 25 of which were on dendrites. Perisomatic region of the pyramidal cell (left, rectangle) was imaged in a 50 μm-thick section. An example VIP bouton (arrow) forms a putative synapse with the cell body of the pyramidal cell (pyr). (C-D) Correlated EM micrographs verify an axosomatic synapse (red arrows). Insets in (B, right) and (C) are shown in (C) and (D), respectively. Scale bars = 250 μm in A; 5 μm in B, C; 0.5 μm in D.
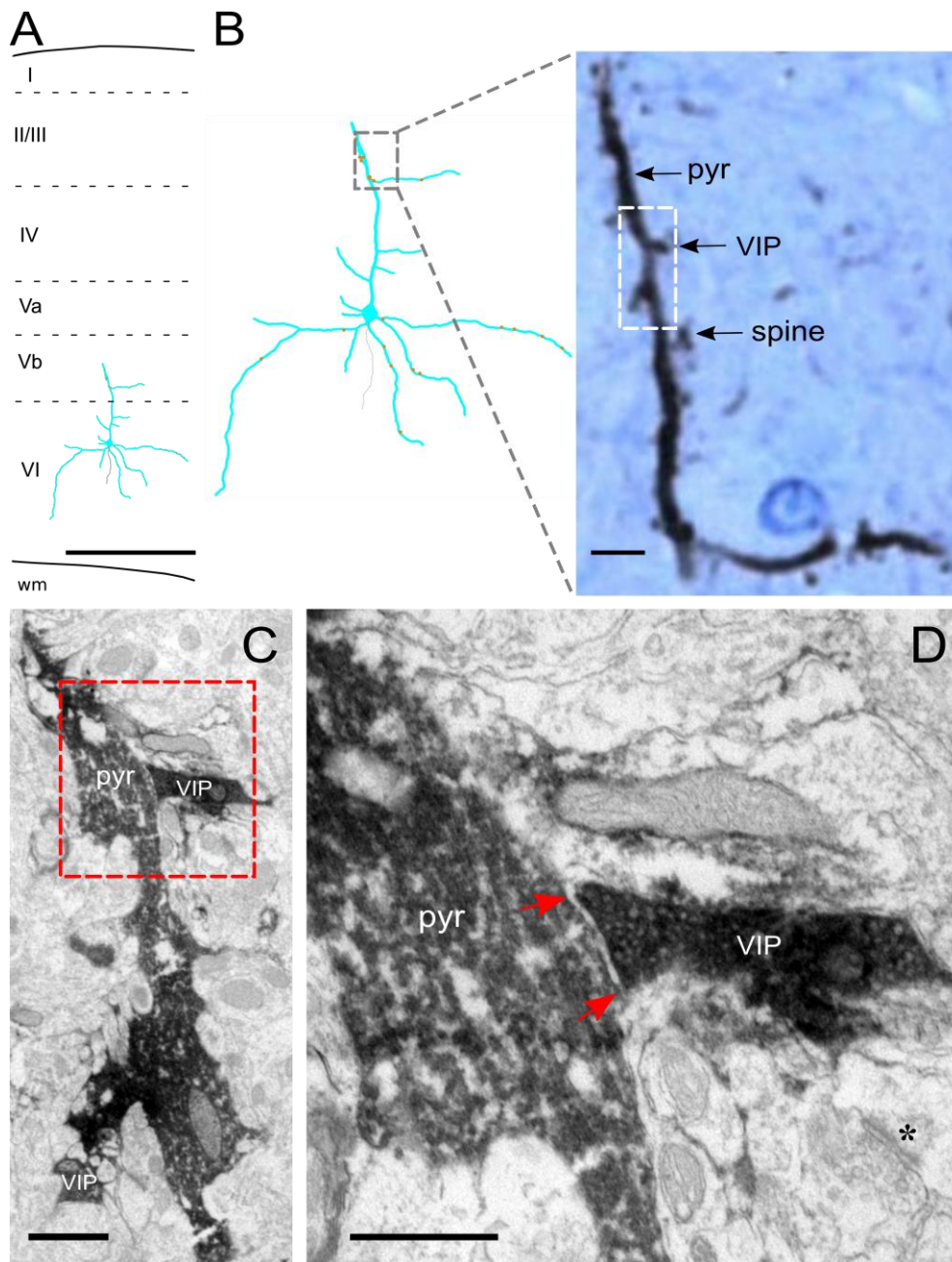
Figure 26. Synapse on soma of pyramidal neurons.

(A) Somatodendritic reconstruction of the pyramidal neuron (cyan). (B) Red dots represent 21 putative presynaptic VIP boutons, all of which were on various portions of the dendritic tree. Distal apical dendrite with several putative VIP synaptic contacts was selected for correlated light and electron microscopy study (left, rectangle). An example VIP bouton forms a putative synapse with the apical dendrite of the pyramidal cell (pyr) on a correlated semithin section (right). However, it is difficult to clearly separate the boutons (VIP) from the dendritic spines at the light microscopy level due to reduced color contrast in semithin section. (C) Correlated EM micrograph of the region (white rectangle in B) shows the apical dendrite and two VIP boutons. (D) The vesicle-rich VIP bouton (within the red rectangle in C) synapses onto the apical dendrite (red arrows). Asterisk marks an asymmetric axospinous synapse in the vicinity. Scale bars = 250 μm in A; 5 μm in B; 1 μm in C; 0.5 μm in D.

4   Discussion

4.1   Technical considerations

The study characterizes the output of VIP interneurons and the main results come from the quantitative EM approach. Before interpreting the results, the main underlying techniques, pre-embedding anti-YFP staining and post-embedding anti-GABA immunogold staining are first discussed.

4.1.1   Pre-embedding anti-YFP staining

The morphology of VIP interneurons and their cortical distribution was consistent with previous studies in rodents (Bayraktar et al., 2000; Prönneke et al., 2015). Prönneke et al (2015) recently confirmed the specificity and sensitivity of Cre expression in VIP cells of the VIP-ires-Cre driver mouse line, as proposed by Taniguchi et al (2011). Therefore, the anti-YFP immunostaining in VIP$_{cre}$/YFP mice is very likely to detect the entire population of VIP cells in every cellular detail. Using an osmium-intensified DAB reaction, sections contained extensively stained subcellular structures, from which somata, dendrites, and axons with their boutons could be easily discerned by correlated light and electron microscopy. Compared with previous work using non-genetic means (Acsády et al., 1996; Bayraktar et al., 2000), the staining yielded a complete visualization of axons and boutons. Even at the high concentration of fixative, which is necessary to obtain a suitable GABA labeling efficiency, the antigenicity of YFP was well preserved and could be reliably detected by the pre-embedding anti-YFP staining protocol.

4.1.2   Post-embedding anti-GABA immunogold labeling

68

Anti-GABA immunogold labeling is sensitive to various factors of the histological procedure, including fixative concentration, embedding material and antibody efficiency (Griffiths and Lucocq, 2014). In order to label small molecules like GABA, it is necessary to use a sufficiently high concentration of glutaraldehyde (Bergersen et al., 2008). Anti-GABA staining failed to work in the single cell approach and one possible explanation is that the glutaraldehyde concentration was not high enough to fix GABA in the cytoplasm. For the quantitative EM study, after increasing glutaraldehyde concentration to 1% during perfusion, a reliable GABA immunolabeling was achieved. Since conventional dehydration and epoxy embedding were used, the labeling efficiency is not as high as obtained by freeze substitution and cryo-embedding (Bergersen et al., 2008). However, the conventional method maintains a better ultrastructure and thus allows for better identification of more delicate subcellular structures.

Antibody-antigen affinity considerably affects immunogold labeling efficiency. Although the primary anti-GABA antibody was performing well in labeling GABAergic profiles (Bickford et al., 2008), the well-established receiver operating characteristic (ROC) statistics was adopted in order to evaluate sensitivity and specificity of the staining and to obtain statistically validated thresholds for GABA-immunogold labeling of the targets of VIP cells. For dendritic targets, at the chosen threshold (11.1 gold grains/µm²), false positive rate (0.16) and false negative rate (0.14) were close to each other, therefore the determined ratios of GABA-immunopositive dendrites should be a reasonable approximation to the real biological ones. Technically it cannot be avoided that some small-caliber dendrites of GABAergic interneurons might not contain GABA or GABA immunoreactivity is too low to be detected (Gonchar and Burkhalter, 1999; Beaulieu et al., 1994). Thus, GABA labeling was most likely underestimated. However, the vast majority of targeted GABAergic dendrites should have been detected because of the high

labeling sensitivity suggested by ROC curve analysis. For somatic targets, at the chosen threshold (8.5 gold grains/μm²), false positive rate is lower (0.17) than false negative rate (0.29). This might result in a potential underestimation, which, however, should not affect much of the final conclusion.

GABA localization: Anti-GABA post-embedding immunogold labeling has been used to localize GABAergic neurons in the central nervous system, and the GABA immunoreactivity is found in different subcellular compartments of cortical GABAergic interneurons including cell bodies, dendrites, axons and boutons (Somogyi and Hodgson, 1985). Our study is the first to quantify the immunoreactivity of different subcellular compartments in mouse barrel cortex. Structures with the strongest labeling were axon terminals, which is consistent with previous findings (Storm-Mathisen et al., 1983; Bergersen et al., 2003). A decrease in GABA immunoreactivity was detected from axon terminals to dendrites, and further to somata. This decline is probably due to the active axonal transport of GABA from the soma to axon terminals where GABA is released during synaptic transmission. On dendrites, not only GABA but also GABA transporter 2 (GAT2) was found (Conti et al., 1999). Localization of GAT2 in dendrites indicates its involvement in transporting GABA from either the extracellular space or glial cells into dendrites. Dendritic GABA may act as a retrograde messenger and retrogradely regulate synaptic transmission (Zilberter et al., 1999). This may explain why interneuron dendrites show stronger GABA immunoreactivity than somata.

Although VIP cells are GABAergic interneurons, immunogold labeling was hard to be detected over their cytoplasm because the dense DAB reaction product hid the epitope of GABA and obscured the visibility of gold grains. However, it is possible to detect gold grains over mitochondria of VIP cell processes, as the mitochondria are largely free of DAB reaction product. In fact, previous anti-GABA immunogold studies found that gold

70

grains were likely to accumulate over mitochondria of various GABA-immunopositive subcellular compartments (Beaulieu et al., 1994; Collman et al., 2015). This is probably due to GABA metabolism that requires GABA to be transferred into mitochondria to be incorporated into the tricarbonic acid cycle (Roth and Draguhn, 2012; Waagepetersen et al., 2003). GABA immunoreactivity on subcellular compartments of non-GABAergic principal cells is considered as unspecific staining and served for background determination.

4.2 Target structure distribution

Among the three different subcellular compartments, which can serve as possible postsynaptic targets (dendrites, spines, and somata), dendrites are the main structures innervated across all cortical layers. This is in consistence with the previous knowledge of VIP interneurons in the hippocampus (Acsády et al., 1996) and in agreement with the notion that VIP interneurons are dendrite-targeting cells (Markram et al., 2004). It should be noted that many inhibitory interneurons innervate the dendritic shaft as their major target domain (Kubota et al., 2016). Interestingly, however, nearly 40% of the innervation by VIP cells in layer VI was found onto the somatic region. A previous study showed for so-called perisomatic interneurons, like basket cells, that the axosomatic synapses comprise only 10–37% in rat frontal cortex (Kawaguchi and Kubota 1998). Thus, according to the target structure distribution, not all VIP interneurons should be considered as dendrite-targeting interneurons, at least not in layer VI, being partially in agreement with recent literature (He et al., 2016). Compared with the other two targets, there was rare innervation of spines, indicating that VIP interneurons are not spine-targeting interneurons. This would speak against VIP boutons being the primary substrate

of experience-dependently remodeled inhibitory spine synapses, as recently demonstrated in the visual cortex (Villa et al., 2016).

4.3   GABAergic versus non-GABAergic target structures

It was found that only 37% of the targeted dendrites belong to GABAergic neurons and most of the targeted dendrites should belong to non-GABAergic principal cells. This finding seems to be unexpected because electrophysiological data showed that VIP interneurons provide a much stronger inhibition to SOM interneurons than local pyramidal neurons and the connectivity ratio of VIP-to-pyramidal neurons is also much lower (around 12.5%) than that of VIP-to-SOM interneurons (63%) (Lee et al., 2013; Pfeffer et al., 2013). One explanation might be that VIP interneurons in barrel cortex preferentially innervate yet-to-be-determined subpopulations of pyramidal neurons and avoid the other subpopulations. The preferential innervation, if presents, can result in a low connectivity ratio when studied by paired recordings. However, for quantifying the number of synapses, the total number of synapses formed onto principal cells might be higher than onto interneurons since in neocortex ca. 80% of neurons are non-GABAergic principal cells and only ca. 20% are GABAergic interneurons. A recent study supports this hypothesis by showing a pull-push circuit computation in layer II/III of mouse prefrontal cortex, in which during arousal, activation of VIP interneurons decreased the activity of a subpopulation of pyramidal neurons via direct inhibition whereas it increased the activity of another subpopulation via disinhibition (Garcia-Junco-Clemente et al., 2017).

72

Another possible explanation could be that VIP interneurons preferentially inhibit layer V and mostly avoid layer II/III pyramidal neuron dendrites in mouse barrel cortex. Some innervated immunopositive dendrites clearly resembled apical dendrites of pyramidal neurons as they had a large caliber, spine protrusions and a radial orientation. Functional studies showed that layer II/III interneurons inhibit the apical dendrites of layer V pyramidal neurons (Jiang et al., 2013). Unfortunately, we cannot provide direct morphological evidence for the precise origin of the immunonegative dendrites and which cell types they belong to, as it was not possible to fully reconstruct the dendrites in our large-sized serial ultrathin sections. However, the proof-of-principle VIP synapses onto different membrane domains of rabies virus-labeled pyramidal neurons partially compensates this drawback and opens an avenue to quantitatively analyze the layer-specific innervation of pyramidal cells by VIP boutons.

For the innervation of interneurons, proximal dendrites as well as somata are more likely to be targeted by VIP boutons (Dávid et al., 2007; Hioki et al., 2013; Muñoz et al., 2017). The targeted cell types could belong to both SOM and PV interneurons, however, we cannot differentiate them without further specific labeling. The neighboring excitatory synapses usually have a close geometric distance to the VIP synapses onto the targeted GABAergic dendrites. The cluster of excitatory and inhibitory synapses should let VIP interneurons efficiently attenuate the dendritic excitability of the targeted cells (Kubota et al., 2016). Interestingly, a novel type of PV expressing interneuron in layer VI has recently been described, which is a central node for gain control in visual processing (Bortone et al., 2014). It remains however to be shown whether VIP boutons directly synapse on this type of layer VI interneuron.

The targeted GABA-immunonegative somata probably belong to pyramidal or other types of excitatory neurons, like star pyramidal or spiny stellate cells (Andjelic et al.,

2009). In agreement with this proposition, studies in rat frontal and somatosensory cortex have shown that some VIP interneurons are small basket cells and form multiple synapses on cell bodies of pyramidal neurons (Kawaguchi and Kubota 1996; Wang et al., 2002; Markram et al., 2004; He et al., 2016). Different from the typical bipolar VIP cells which are usually CR-positive and locate in layers I to IV, VIP small basket cells are usually multipolar shaped, express CCK instead of CR and also exist in deep layers besides upper layer II/III (He et al., 2016). It is expected that the innervation of GABA-immunonegative somata comes from the local axonal arborizations of VIP small basket cells in deep layers.

4.3   Layer-dependent targeting

There is a differential targeting of VIP cells in superficial versus deep layers, suggesting that there is more than one motif recruiting VIP interneurons into local intra- and translaminar circuits of mouse barrel cortex. Compared to the two morphological studies on the partially overlapping population of CR interneurons in monkey and rat visual cortex (Meskenaite, 1997; Gonchar and Burkhalter, 1999), the main difference here is that the interneuron-targeting rates are lower in superficial layers. This might be due to species differences. However, most likely it is caused by non-CR expressing VIP interneurons. As mentioned in the introduction, VIP interneurons also co-express other markers such as corticotropin-releasing factor (CRF) or cholecystokinin (CCK). In rat frontal cortex, a study showed layer II/III to have a higher proportion of VIP interneurons co-expressing either CRF or CCK or both whereas in layers V and VI, more VIP interneurons are CR-positive (Kubota et al., 2011). CCK/CRF expressing VIP cells were found to mainly form synapses with pyramidal neurons (Kubota et al., 2016; He et al., 2016), which may result in the lower interneuron-targeting rates in superficial layers in

the present study.

Considering the heterogeneity of VIP cells in terms of their axonal projection patterns (Prönneke et al., 2015), in superficial layers, VIP cells can be primarily classified as translaminar interneurons but at least partially also as local or less so as lateral inhibitors (Helmstaedter et al., 2009a,b,c). Their innervation of local inhibitory interneurons, presumably Martinotti cells (most of which are SST expressing interneurons), has been demonstrated (Lee et al., 2013; Karnani et al., 2016; Walker et al., 2016). Furthermore, Jiang et al (2015) reported that bitufted VIP interneurons also inhibit layer II/III pyramidal cells. In addition, VIP interneurons in layer II/III also innervate layer V pyramidal cells, mainly at their distal apical dendrites (Jiang et al., 2013). Taken all available evidence together, there might exist three different output patterns of CR expressing VIP interneurons in layer II/III (Figure 27): innervation on the dendrites of local interneurons, local pyramidal cells, and layer V pyramidal cells. The hypothetical scheme of the output may explain why only around a third of the targeted dendrites in superficial layers are GABA-immunopositive.

In deep layers, with their specific set of GABAergic interneurons (Naka and Adesnik, 2016), a substantial portion of VIP cells is morphologically distinct from superficial VIP cells, and their axons largely remain in deep layers (Prönneke et al., 2015). Since CR expressing VIP interneurons in layer II/III also send a strong translaminar projection to deep layers, it is impossible to differentiate the output of deep layer VIP cells from that of the descending axonal collaterals of superficial VIP cells in the study. Apart from still to be characterized types, it is suggested that the CCK expressing VIP small basket cells in deep layers innervate primarily the perisomatic regions of layer V and VI pyramidal neurons and other interneuron somata in addition. Therefore four different output schemes of VIP interneurons in deep layers are proposed (Figure 27): innervation on

dendrites of interneurons and pyramidal cells by the descending axons of CR expressing VIP cells; innervation on the somata by the local axons of VIP small basket cells. The proposed output may explain the GABA-immunopositive ratios of the targeted dendrites and somata in deep layers.
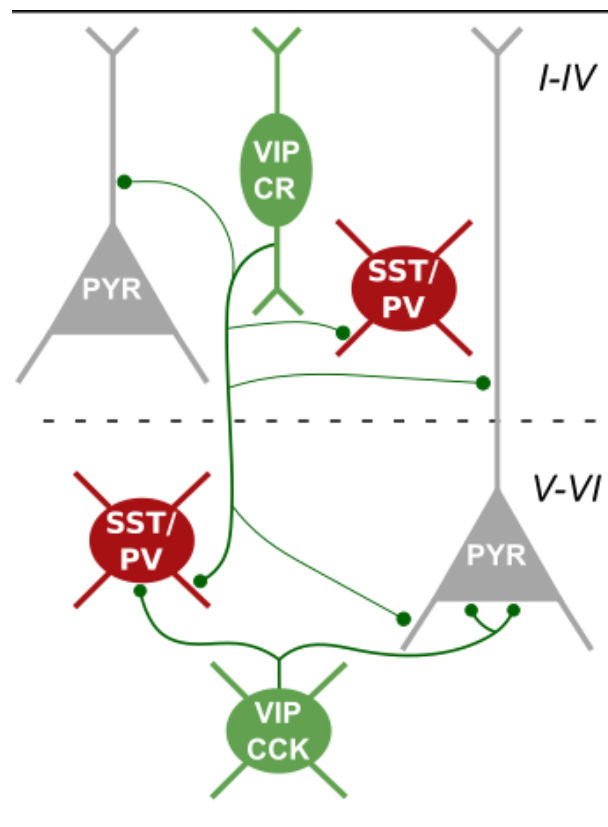
Figure 27. A hypothetical scheme for the output of VIP interneurons across layers.
Bipolar CR expressing VIP neuron as the main subtype in superficial layers innervates dendrites of other interneurons (SST/PV) in all layers, in addition to local pyramidal cells (PYR), and apical dendrites of deep layer pyramidal cells. As the minority, multipolar CCK expressing VIP interneurons in deep layers, some of which are likely small basket cells, form somatic synapses on the local pyramidal cells as well as other interneurons (SST or PV cells) in deep layers.

4.4 Self-innervation of VIP interneurons

In the hippocampus, there are three subpopulations of VIP interneurons according to their neurochemical expression, location and targeting property. The subtype that exists

76

in stratum radiatum innervates the one in stratum pyramidale by making multiple synapses per one presynaptic bouton (Acsády et al., 1996). In mouse neocortex, a dual recording of CR expressing interneurons reported that bipolar CR interneurons have a very high connectivity to multipolar CR interneurons, followed by a lower connectivity to other bipolar CR interneurons (Caputi et al., 2009). In their study, the bipolar CR interneurons resemble very much CR expressing VIP interneurons, while multipolar CR interneurons are likely to be CR expressing SST interneurons according to their morphology and firing patterns. Therefore, some "self-innervating" synapses might probably come from bipolar CR expressing VIP interneurons that target each other. As suggested by Caputi et al (2009), the self-connectivity is lower than the connectivity of VIP interneurons to SST interneurons and thus self-innervating synapses account for only 14%. Because most of the postsynaptic structures were found in layers IV to VI, it is speculated that bipolar VIP interneurons in superficial layers descend with their axons and innervate other bipolar VIP cells in deep layers, especially the ones in layer IV.

4.5 Functional implications, limitations and future perspective

The disinhibitory output circuit of VIP interneurons has been highlighted since the morphological studies on VIP interneurons and the overlapping population CR interneurons in the hippocampus and neocortex showed that they are likely to target other GABAergic interneurons, which innervate excitatory principal cells (Acsády et al., 1996; Gulyás et al., 1996; Staiger et al., 2004b). Such an interneuron-selective innervation property has also been demonstrated by in vitro electrophysiological recordings as well as *in vivo* studies in different cortical regions under various behavioral paradigms (Pfeffer

et al., 2013; Pi et al., 2013; Lee et al., 2013; Fu et al., 2014; Zhang et al., 2014; Kamigaki and Dan, 2017). One underlying microcircuit is a disinhibitory motif, which relies on the inhibition of inhibitory interneurons, preferentially SOM expressing Martinotti cells, and results in a selective increase of pyramidal neuron activity. However, the disinhibitory motif failed to explain all neuronal computations when studied under refined behavioral conditions (Pakan et al., 2016). Due to the diversity of the axonal innervation of VIP interneurons (Prönneke et al., 2015), it is unlikely to expect a singular VIP-to-Martinotti cell circuit. In fact, both *in vivo* and *in vitro* functional studies showed besides disinhibition, VIP cells also directly innervate and inhibit specific sets of pyramidal neurons (Jiang et al., 2015; Garcia-Junco-Clemente et al., 2017) and have a layer-dependent targeting across cortical layers in rat and monkey primary visual cortex (Meskenaite, 1997; Gonchar and Burkhalter, 1999). The present work is the first study that used quantitative EM methods to explore the output of VIP interneurons in all laminae of mouse barrel cortex. The results found that besides GABAergic interneurons, a substantial proportion of the targets are GABA-immunonegative subcellular structures, which is consistent with earlier studies by Peters (1990) but inconsistent with the idea of a singular VIP-to-Martinotti cell circuit motif (Pfeffer et al., 2014; Karnani et al., 2016). These results suggest that multiple cortical circuit motifs of VIP interneurons do exist and that the notion that VIP interneurons are primarily interneuron-specific interneurons (Klausberger and Somogyi, 2008) has to be discarded.

Using GABA labeling, it is not possible to tell which specific classes of GABAergic interneurons are innervated. Laminar location of the targets is difficult to be determined on ultrathin sections even when a serial sectioning approach was used. Although the rabies virus tracing enabled the complete labeling of pyramidal cells, these retrogradely transfected pyramidal cells are only parts of principal cells and not necessarily to be

innervated by VIP interneurons. Because VIP interneurons are diverse, using the VIP-ires-Cre mouse line, it cannot allow us to separate the innervation patterns of distinct subpopulations of VIP interneurons. For example, the subpopulation of CR expressing VIP cells cannot be differentiated from the CCK expressing VIP small basket cells. Bearing these limitations in mind, in the future study it is recommended to use more specific mouse lines e.g. the VIP-Flp crossed with either CR-ires-Cre or CCK-ires-Cre mouse line as described by He et al (2016), to enable cell targeting of specific subpopulations of VIP cells. It is also necessary to combine electrophysiological experiments with correlated light and electron microscopy investigation together, to map the individual connectivity between VIP cells and their potential targets. By this way, a precise relationship between functional connectivity and detailed morphology can be conclusively studied.

5   Summary

Vasoactive intestinal polypeptide (VIP) expressing GABAergic interneurons are thought to primarily inhibit other types of interneurons and thus possess a disinhibitory function by VIP-to-Martinotti cell motif in cortical circuits. However, their targeting specificity at the subcellular level is still unknown and therefore was studied anatomically at single cell and population level in mouse barrel cortex. For single VIP cell approach, correlated light and electron microscopy method was used to study the synaptic innervation of the individual VIP cells after electrophysiological recordings and reconstruction. The ultrastructure of the postsynaptic targets indicated besides interneurons non-GABAergic excitatory neurons could also be targeted by VIP boutons.

Based on this preliminary result, a quantitative immunoelectron microscopy study was adopted to comprehensively characterize the output of VIP interneurons across the whole laminae of mouse barrel cortex. Using VIP_{cre}/YFP transgenic mice, by pre-embedding anti-YFP staining combined with DAB visualization, all VIP cells as well as their processes were stained in black. By systematically sampling the axonal boutons across all layers, it was found that their targets were preferentially dendrites (80%) but also spines (7%) and somata (13%). This distribution remained similar in layers II to V. In layer I, all of the targets were dendrites; in layer VI, innervation over the somata rose up to 39% although dendrites still represented the majority of the targets (58%). Post-embedding anti-GABA immunogold staining was used to find the GABAergic profiles among the targets. The staining efficacy in terms of sensitivity and specificity was evaluated using ROC analysis. Based on the ROC curves, the optimal cut-off points were determined by the method "closest point to (0,1)". It generated the GABA-

immunopositive thresholds for dendrites (spines) and somata at 11.1 and 8.5 gold grains/μm² respectively.

Using the thresholds, the GABA-immunopositive rates among the subcellular targets were calculated: only 37% of the dendrites, 7% of the spines, and 26% of the somata showed above-threshold immunogold labeling. Among the targeted dendrites, around a third were GABA-immunopositive in layers I to IV, while in layers V and VI, the rates rose to 48% and 39% respectively. Statistical analysis showed a layer-dependent targeting existed: a higher proportion of innervation was localized on GABAergic dendrites in deep layers than in superficial layers. Besides the non-VIP positive neuronal targets, 14% of the axonal boutons formed self-innervating synapses on other VIP expressing subcellular structures, mainly on the dendrites. This self-innervation existed in all layers except layer I and had the highest incidence in layer IV. Occasionally, the boutons were found to contact the non-neuronal profiles like astrocytes and blood vessels.

In sum, the study shows the main targets of VIP interneurons are dendrites with the majority belonging to non-GABAergic principal cells at subcellular level. The dendritic targeting is layer-dependent. The results disagree with the notion that VIP interneurons are interneuron-specific interneurons and argue against the uniform disinhibitory VIP-to-Martinotti cell circuit motif. Besides innervation on dendrites, VIP interneurons play an important role in regulating both pyramidal neurons and interneurons by targeting their somata in layer VI. In conclusion, the study provides the anatomical evidence for the diverse output of VIP interneurons and suggests multiple functionalities of VIP interneurons in cortical circuitry.

6   References

Acsády L, Görcs TJ, Freund TF. 1996. Different populations of vasoactive intestinal polypeptide-immunoreactive interneurons are specialized to control pyramidal cells or interneurons in the hippocampus. Neuroscience. 73: 317–334.

Alloway KD. 2008. Information processing streams in rodent barrel cortex: the differential functions of barrel and septal circuits. Cereb Cortex. 18: 979–989.

Andjelic S, Gallopin T, Cauli B, Hill EL, Roux L, Badr S, Hu E, Tamás G, Lambolez B. 2009. Glutamatergic Nonpyramidal Neurons From Neocortical Layer VI and Their Comparison With Pyramidal and Spiny Stellate Neurons. J Neurophysiol. 101: 641–654.

Ascoli GA, Alonso-Nanclares L, Anderson SA, Barrionuevo G, Benavides-Piccione R, Burkhalter A, Buzsáki G, Cauli B, DeFelipe J, Fairén A, Feldmeyer D, Fishell G, Fregnac Y, Freund TF, Gardner D, Gardner EP, Goldberg JH, Helmstaedter M, Hestrin S, Karube F, Kisvárday ZF, Lambolez B, Lewis DA, Marin O, Markram H, Muñoz A, Packer A, Petersen CCH, Rockland KS, Rossier J, Rudy B, Somogyi P, Staiger JF, Tamas G, Thomson AM, Toledo-Rodriguez M, Wang Y, West DC, Yuste R. 2008. Petilla terminology: nomenclature of features of GABAergic interneurons of the cerebral cortex. Nat Rev Neurosci. 9: 557–568.

Bayraktar T, Welker E, Freund TF, Zilles K, Staiger JF. 2000. Neurons immunoreactive for vasoactive intestinal polypeptide in the rat primary somatosensory cortex: Morphology and spatial relationship to barrel-related columns. J Comp Neurol. 420: 291–304.

Beaulieu C, Campistron G, Crevier C. 1994. Quantitative aspects of the GABA circuitry in the primary visual cortex of the adult rat. J Comp Neurol. 339: 559–572.

Bergersen L, Ruiz A, Bjaalie JG, Kullmann DM, Gundersen V. 2003. GABA and GABAA receptors at hippocampal mossy fibre synapses. Eur J Neurosci. 18: 931–941.

Bergersen LH, Storm-Mathisen J, Gundersen V. 2008. Immunogold quantification of amino acids and proteins in complex subcellular compartments. Nat Protoc. 3: 144–152.

Bickford ME, Wei H, Eisenback MA, Chomsung RD, Slusarczyk AS, Dankowsi AB. 2008. Synaptic Organization of Thalamocortical Axon Collaterals in the Perigeniculate Nucleus and Dorsal Lateral Geniculate Nucleus. J Comp Neurol. 508: 264–285.

Bloss EB, Cembrowski MS, Karsh B, Colonell J, Fetter RD, Spruston N. 2016. Structured Dendritic Inhibition Supports Branch-Selective Integration in CA1 Pyramidal Cells. Neuron. 89:1016–1030.

Bortone DS, Olsen SR, Scanziani M. 2014. Translaminar Inhibitory Cells Recruited by Layer 6 Cortico-Thalamic Neurons Suppress Visual Cortex. Neuron. 82: 474–485.

Caputi A, Rozov A, Blatow M, Monyer H. 2009. Two Calretinin-Positive GABAergic Cell Types in Layer 2/3 of the Mouse Neocortex Provide Different Forms of Inhibition. Cereb Cortex. 19: 1345–1359.

Cauli B, Tong X-K, Rancillac A, Serluca N, Lambolez B, Rossier J, Hamel E. 2004. Cortical GABA Interneurons in Neurovascular Coupling: Relays for Subcortical Vasoactive Pathways. J Neurosci. 24: 8940–8949.

Cauli B, Zhou X, Tricoire L, Toussay X, Staiger JF. 2014. Revisiting enigmatic cortical calretinin-expressing interneurons. Front Neuroanat. 8: 52.

Chédotal A, Umbriaco D, Descarries L, Hartman BK, Hamel E. 1994. Light and electron microscopic immunocytochemical analysis of the neurovascular relationships of choline acetyltransferase and vasoactive intestinal polypeptide nerve terminals in the rat cerebral cortex. J Comp Neurol. 343: 57–71.

Collman F, Buchanan J, Phend KD, Micheva KD, Weinberg RJ, Smith SJ. 2015. Mapping Synapses by Conjugate Light-Electron Array Tomography. J Neurosci. 35: 5792–5807.

Colonnier M. 1968. Synaptic pattern on different cell types in the different laminae of the cat visual cortex. An electron microscope study. Brain Res. 9: 268–287.

Conti F, Zuccarello LV, Barbaresi P, Minelli A, Brecha NC, Melone M. 1999. Neuronal, glial, and epithelial localization of γ-aminobutyric acid transporter 2, a high-affinity γ-aminobutyric acid plasma membrane transporter, in the cerebral cortex and neighboring structures. J Comp Neurol. 409: 482–494.

Cruikshank SJ, Urabe H, Nurmikko AV, Connors BW. 2010. Pathway-specific feedforward circuits between thalamus and neocortex revealed by selective optical stimulation of axons. Neuron. 65: 230–245.

Dávid C, Schleicher A, Zuschratter W, Staiger JF. 2007. The innervation of parvalbumin-containing interneurons by VIP-immunopositive interneurons in the primary somatosensory cortex of the adult rat. Eur J Neurosci. 25: 2329–2340.

DeFelipe J, López-Cruz PL, Benavides-Piccione R, Bielza C, Larrañaga P, Anderson S, Burkhalter A, Cauli B, Fairén A, Feldmeyer D, Fishell G, Fitzpatrick D, Freund TF, González-Burgos G, Hestrin S, Hill S, Hof PR, Huang J, Jones EG, Kawaguchi Y, Kisvárday Z, Kubota Y, Lewis DA, Marín O, Markram H, McBain CJ, Meyer HS, Monyer H, Nelson SB, Rockland K, Rossier J, Rubenstein JLR, Rudy B, Scanziani M, Shepherd GM, Sherwood CC, Staiger JF, Tamás G, Thomson A, Wang Y, Yuste R, Ascoli GA. 2013. New insights into the classification and nomenclature of cortical GABAergic interneurons. Nat Rev Neurosci. 14: 202–216.

Fawcett T. 2006. An introduction to ROC analysis. Pattern Recogn Lett. 27: 861–874.

Feldmeyer D, Lübke J, Silver RA, Sakmann B. 2002. Synaptic connections between layer 4 spiny neurone-layer 2/3 pyramidal cell pairs in juvenile rat barrel cortex: physiology and anatomy of interlaminar signalling within a cortical column. J Physiol. 538: 803–822.

Feldmeyer D, Brecht M, Helmchen F, Petersen CCH, Poulet JFA, Staiger JF, Luhmann HJ, Schwarz C. 2013. Barrel cortex function. Prog Neurobiol. 103: 3–27.

Ferezou I, Cauli B, Hill EL, Rossier J, Hamel E, Lambolez B. 2002. 5-HT3 receptors mediate serotonergic fast synaptic excitation of neocortical vasoactive intestinal peptide/cholecystokinin interneurons. J Neurosci. 22: 7389–7397.

Fu Y, Tucciarone JM, Espinosa JS, Sheng N, Darcy DP, Nicoll RA, Huang ZJ, Stryker MP. 2014. A Cortical Circuit for Gain Control by Behavioral State. Cell. 156: 1139–1152.

Garcia-Junco-Clemente P, Ikrar T, Tring E, Xu X, Ringach DL, Trachtenberg JT. 2017. An inhibitory pull-push circuit in frontal cortex. Nat Neurosci. 20: 389-392.

Gonchar Y, Burkhalter A. 1999. Connectivity of GABAergic calretinin-immunoreactive

neurons in rat primary visual cortex. Cereb Cortex. 9: 683–696.

Griffiths G, Lucocq JM. 2014. Antibodies for immunolabeling by light and electron microscopy: not for the faint hearted. Histochem Cell Biol. 142: 347–360.

Gulyás AI, Hájos N, Freund TF. 1996. Interneurons Containing Calretinin Are Specialized to Control Other Interneurons in the Rat Hippocampus. J Neurosci. 16: 3397–3411.

Hájos N, Acsády L, Freund TF. 1996. Target selectivity and neurochemical characteristics of VIP-immunoreactive interneurons in the rat dentate gyrus. Eur J Neurosci. 8: 1415–1431.

Harris KD, Mrsic-Flogel TD. 2013. Cortical connectivity and sensory coding. Nature. 503: 51–58.

He M, Tucciarone J, Lee S, Nigro MJ, Kim Y, Levine JM, Kelly SM, Krugikov I, Wu P, Chen Y, Gong L, Hou Y, Osten P, Rudy B, Huang ZJ. 2016. Strategies and Tools for Combinatorial Targeting of GABAergic Neurons in Mouse Cerebral Cortex. Neuron. 91: 1228–1243.

Helmstaedter M, Sakmann B, Feldmeyer D. 2009a. Neuronal Correlates of Local, Lateral, and Translaminar Inhibition with Reference to Cortical Columns. Cereb Cortex. 19: 926–937.

Helmstaedter M, Sakmann B, Feldmeyer D. 2009b. L2/3 Interneuron Groups Defined by Multiparameter Analysis of Axonal Projection, Dendritic Geometry, and Electrical Excitability. Cereb Cortex. 19: 951–962.

Helmstaedter M, Sakmann B, Feldmeyer D. 2009c. The Relation between Dendritic Geometry, Electrical Excitability, and Axonal Projections of L2/3 Interneurons in Rat Barrel Cortex. Cereb Cortex. 19: 938–950.

Hioki H, Okamoto S, Konno M, Kameda H, Sohn J, Kuramoto E, Fujiyama F, Kaneko T. 2013. Cell Type-Specific Inhibitory Inputs to Dendritic and Somatic Compartments of Parvalbumin-Expressing Neocortical Interneuron. J Neurosci. 33: 544–555.

Jensen KF, Killackey HP. 1987. Terminal arbors of axons projecting to the somatosensory cortex of the adult rat. I. The normal morphology of specific thalamocortical afferents. J Neurosci. 7: 3529–3543.

Jiang X, Wang G, Lee AJ, Stornetta RL, Zhu JJ. 2013. The organization of two novel cortical interneuronal circuits. Nat Neurosci. 16: 210–218.

Jiang X, Shen S, Cadwell CR, Berens P, Sinz F, Ecker AS, Patel S, Tolias AS. 2015. Principles of connectivity among morphologically defined cell types in adult neocortex. Science. 350: aac9462.

Kamigaki T, Dan Y. 2017. Delay activity of specific prefrontal interneuron subtypes modulates memory-guided behavior. Nat Neurosci. 20:854–863.

Karnani MM, Jackson J, Ayzenshtat I, Sichani AH, Manoocheri K, Kim S, Yuste R. 2016. Opening Holes in the Blanket of Inhibition: Localized Lateral Disinhibition by VIP Interneurons. J Neurosci. 36: 3471–3480.

Kawaguchi Y, Kubota Y. 1996. Physiological and morphological identification of somatostatin- or vasoactive intestinal polypeptide-containing cells among GABAergic cell subtypes in rat frontal cortex. J Neurosci. 16: 2701–2715.

Kawaguchi Y, Kubota Y. 1998. Neurochemical features and synaptic connections of large physiologically-identified GABAergic cells in the rat frontal cortex. Neuroscience. 85: 677–701.

Klausberger T, Somogyi P. 2008. Neuronal Diversity and Temporal Dynamics: The Unity of Hippocampal Circuit Operations. Science. 321: 53–57.

Koralek KA, Olavarria J, Killackey HP. 1990. A real and laminar organization of corticocortical projections in the rat somatosensory cortex. J Comp Neurol. 299: 133–150.

Kubota Y, Hatada SN, Kawaguchi Y. 2009. Important Factors for the Three-Dimensional Reconstruction of Neuronal Structures from Serial Ultrathin Sections. Front Neural Circuits. 3.

Kubota Y, Shigematsu N, Karube F, Sekigawa A, Kato S, Yamaguchi N, Hirai Y, Morishima M, Kawaguchi Y. 2011. Selective Coexpression of Multiple Chemical Markers Defines Discrete Populations of Neocortical GABAergic Neurons. Cereb Cortex. 21: 1803–1817.

Kubota Y, Karube F, Nomura M, Kawaguchi Y. 2016. The Diversity of Cortical Inhibitory Synapses. Front Neural Circuits. 10.

86

Lake BB, Ai R, Kaeser GE, Salathia NS, Yung YC, Liu R, Wildberg A, Gao D, Fung HL, Chen S, Vijayaraghavan R, Wong J, Chen A, Sheng X, Kaper F, Shen R, Ronaghi M, Fan JB, Wang W, Chun J, Zhang K. 2016. Neuronal subtypes and diversity revealed by single-nucleus RNA sequencing of the human brain. Science. 352: 1586–1590.

Larsen DD, Wickersham IR, Callaway EM. 2007. Retrograde tracing with recombinant rabies virus reveals correlations between projection targets and dendritic architecture in layer 5 of mouse barrel cortex. Front Neural Circuits. 1:5.

Lefort S, Tomm C, Floyd Sarria JC, Petersen CC. 2009. The excitatory neuronal network of the C2 barrel column in mouse primary somatosensory cortex. Neuron. 61: 301–316.

Lee S, Kruglikov I, Huang ZJ, Fishell G, Rudy B. 2013. A disinhibitory circuit mediates motor integration in the somatosensory cortex. Nat Neurosci. 16: 1662–1670.

Lübke J, Feldmeyer D. 2007. Excitatory signal flow and connectivity in a cortical column: focus on barrel cortex. Brain Struct Funct. 212: 3–17.

Ma PM. 1991. The barrelettes--architectonic vibrissal representations in the brainstem trigeminal complex of the mouse. I. Normal structural organization. J Comp Neurol. 309: 161–199.

Madisen L, Zwingman TA, Sunkin SM, Oh SW, Zariwala HA, Gu H, Ng LL, Palmiter RD, Hawrylycz MJ, Jones AR, Lein ES, Zeng H. 2010. A robust and high-throughput Cre reporting and characterization system for the whole mouse brain. Nat Neurosci. 13: 133–140.

Markram H, Toledo-Rodriguez M, Wang Y, Gupta A, Silberberg G, Wu C. 2004. Interneurons of the neocortical inhibitory system. Nat Rev Neurosci. 5: 793–807.

Meskenaite V. 1997. Calretinin-immunoreactive local circuit neurons in area 17 of the cynomolgus monkey, Macaca fascicularis. J Comp Neurol. 379: 113–132.

Meyer HS, Wimmer VC, Hemberger M, Bruno RM, de Kock CP, Frick A, Sakmann B, Helmstaedter M. 2010. Cell type-specific thalamic innervation in a column of rat vibrissal cortex. Cereb Cortex. 20: 2287–2303.

Mountcastle V, Berman A, Davies P. 1955. Topographic organization and modality

representation in first somatic area of cat's cerebral cortex by method of single unit analysis. Am J Physiol. 183: 10.

Muñoz W, Tremblay R, Levenstein D, Rudy B. 2017. Layer-specific modulation of neocortical dendritic inhibition during active wakefulness. Science. 355: 954–959.

Naka A, Adesnik H. 2016. Inhibitory Circuits in Cortical Layer 5. Front Neural Circuits. 10.

Ottersen OP. 1987. Postembedding light- and electron microscopic immunocytochemistry of amino acids: description of a new model system allowing identical conditions for specificity testing and tissue processing. Exp Brain Res. 69: 167–174.

Pakan JM, Lowe SC, Dylda E, Keemink SW, Currie SP, Coutts CA, Rochefort NL. 2016. Behavioral-state modulation of inhibition is context-dependent and cell type specific in mouse visual cortex. Elife. 5.

Paspalas CD, Papadopoulos GC. 1998. Ultrastructural Evidence for Combined Action of Noradrenaline and Vasoactive Intestinal Polypeptide Upon Neurons, Astrocytes, and Blood Vessels of the Rat Cerebral Cortex. Brain Res Bull. 45: 247–259.

Perkins NJ, Schisterman EF. 2006. The inconsistency of "optimal" cut-points using two ROC based criteria. Am J Epidemiol. 163: 670–675.

Peters A. 1990. The axon terminals of vasoactive intestinal polypeptide (VIP)-containing bipolar cells in rat visual cortex. J Neurocytol. 19: 672–685.

Peters A, Palay SL, Webster HD. 1991. The fine structure of the nervous system. Neurons and their supporting cells. New York: Oxford University Press.

Pfeffer CK, Xue M, He M, Huang ZJ, Scanziani M. 2013. Inhibition of inhibition in visual cortex: the logic of connections between molecularly distinct interneurons. Nat Neurosci. 16: 1068–1076.

Pfeffer CK. 2014. Inhibitory Neurons: Vip Cells Hit the Brake on Inhibition. Curr Biol. 24: R18–R20.

Pi H-J, Hangya B, Kvitsiani D, Sanders JI, Huang ZJ, Kepecs A. 2013. Cortical interneurons that specialize in disinhibitory control. Nature. 503: 521–524.

Porter JT, Cauli B, Staiger JF, Lambolez B, Rossier J, Audinat E. 1998. Properties of bipolar VIPergic interneurons and their excitation by pyramidal neurons in the rat neocortex. Eur J Neurosci. 10: 3617–3628.

Porter JT, Cauli B, Tsuzuki K, Lambolez B, Rossier J, Audinat E. 1999. Selective excitation of subtypes of neocortical interneurons by nicotinic receptors. J Neurosci. 19: 5228–5235.

Prönneke A, Scheuer B, Wagener RJ, Möck M, Witte M, Staiger JF. 2015. Characterizing VIP Neurons in the Barrel Cortex of VIPcre/tdTomato Mice Reveals Layer-Specific Differences. Cereb Cortex. 25: 4854–4868.

Richardson KC, Jarett L, Finke EH. 1960. Embedding in epoxy resins for ultrathin sectioning in electron microscopy. Stain Technol. 35: 313–325.

Roth FC, Draguhn A. 2012. GABA Metabolism and Transport: Effects on Synaptic Efficacy. Neural Plast. 2012.

Rudy B, Fishell G, Lee S, Hjerling-Leffler J. 2011. Three groups of interneurons account for nearly 100% of neocortical GABAergic neurons. Dev Neurobiol. 71: 45–61.

Schindelin J, Arganda-Carreras I, Frise E, Kaynig V, Longair M, Pietzsch T, Preibisch S, Rueden C, Saalfeld S, Schmid B, Tinevez JY. 2012. Fiji: an open-source platform for biological-image analysis. Nat Meth. 9: 676–682.

Schubert D, Kötter R, Zilles K, Luhmann HJ, Staiger JF. 2003. Cell type-specific circuits of cortical layer IV spiny neurons. J Neurosci. 23: 2961–2970.

Schubert D, Kötter R, Staiger JF. 2007. Mapping functional connectivity in barrel-related columns reveals layer- and cell type-specific microcircuits. Brain Struct Funct. 212: 107–119.

Sing T, Sander O, Beerenwinkel N, Lengauer T. 2005. ROCR: visualizing classifier performance in R. Bioinformatics 21: 3940–3941.

Sloviter RS, Valiquette G, Abrams GM, Ronk EC, Sollas AL, Paul LA, Neubort S. 1989. Selective loss of hippocampal granule cells in the mature rat brain after adrenalectomy. Science. 243: 535–538.

Somogyi P, Hodgson AJ. 1985. Antisera to gamma-aminobutyric acid. III. Demonstration

of GABA in Golgi-impregnated neurons and in conventional electron microscopic sections of cat striate cortex. J Histochem Cytochem. 33: 249–257.

Staiger JF, Zilles K, Freund TF. 1996. Innervation of VIP-immunoreactive neurons by the ventroposteromedial thalamic nucleus in the barrel cortex of the rat. J Comp Neurol. 367: 194–204.

Staiger JF, Flagmeyer I, Schubert D, Zilles K, Kötter R, Luhmann HJ. 2004a. Functional diversity of layer IV spiny neurons in rat somatosensory cortex: quantitative morphology of electrophysiologically characterized and biocytin labeled cells. Cereb Cortex. 14: 690–701.

Staiger JF, Masanneck C, Schleicher A, Zuschratter W. 2004b. Calbindin-containing interneurons are a target for VIP-immunoreactive synapses in rat primary somatosensory cortex. J Comp Neurol. 468: 179–189.

Staiger JF, Bojak I, Miceli S, Schubert D. 2015. A gradual depth-dependent change in connectivity features of supragranular pyramidal cells in rat barrel cortex. Brain Struct Funct. 220: 1317–1337.

Storm-Mathisen J, Leknes AK, Bore AT, Vaaland JL, Edminson P, Haug F-MŠ, Ottersen OP. 1983. First visualization of glutamate and GABA in neurones by immunocytochemistry. Nature. 301: 517–520.

Taniguchi H, He M, Wu P, Kim S, Paik R, Sugino K, Kvitsani D, Fu Y, Lu J, Lin Y, Miyoshi G. 2011. A Resource of Cre Driver Lines for Genetic Targeting of GABAergic Neurons in Cerebral Cortex. Neuron. 71: 995–1013.

Tasic B, Menon V, Nguyen TN, Kim TK, Jarsky T, Yao Z, Levi B, Gray LT, Sorensen SA, Dolbeare T, Bertagnolli D, Goldy J, Shapovalova N, Parry S, Lee C, Smith K, Bernard A, Madisen L, Sunkin SM, Hawrylycz M, Koch C, Zeng H. 2016. Adult mouse cortical cell taxonomy revealed by single cell transcriptomics. Nat Neurosci. 19: 335–346.

Tremblay R, Lee S, Rudy B. 2016. GABAergic Interneurons in the Neocortex: From Cellular Properties to Circuits. Neuron. 91: 260–292.

Van Der Loos H. 1976. Barreloids in mouse somatosensory thalamus. Neurosci Lett. 2: 1–6.

Villa KL, Berry KP, Subramanian J, Cha JW, Oh WC, Kwon HB, Kubota Y, So PTC, Nedivi E. 2016. Inhibitory Synapses Are Repeatedly Assembled and Removed at Persistent Sites In Vivo. Neuron. 89: 756–769.

Waagepetersen HS, Sonnewald U, Schousboe A. 2003. Compartmentation of Glutamine, Glutamate, and GABA Metabolism in Neurons and Astrocytes: Functional Implications. Neuroscientist. 9: 398–403.

Walker F, Möck M, Feyerabend M, Guy J, Wagener RJ, Schubert D, Staiger JF, Witte M. 2016. Parvalbumin- and vasoactive intestinal polypeptide-expressing neocortical interneurons impose differential inhibition on Martinotti cells. Nat Commun. 7: 13664.

Wall NR, De La Parra M, Sorokin JM, Taniguchi H, Huang ZJ, Callaway EM. 2016. Brain-Wide Maps of Synaptic Input to Cortical Interneurons. J Neurosci. 36: 4000–4009.

Wang Y, Gupta A, Toledo-Rodriguez M, Wu CZ, Markram H. 2002. Anatomical, physiological, molecular and circuit properties of nest basket cells in the developing somatosensory cortex. Cereb Cortex. 12: 395–410.

Wang Y, Toledo-Rodriguez M, Gupta A, Wu C, Silberberg G, Luo J, Markram H. 2004. Anatomical, physiological and molecular properties of Martinotti cells in the somatosensory cortex of the juvenile rat. J Physiol. 561: 65–90.

Wickersham IR, Lyon DC, Barnard RJO, Mori T, Conzelmann K, Young JAT, Callaway EM. (2007). Monosynaptic Restriction of Transsynaptic Tracing from Single Genetically Targeted Neurons. Neuron. 53: 639–647.

Wimmer VC, Bruno RM, de Kock CP, Kuner T, Sakmann B. 2010. Dimensions of a projection column and architecture of VPM and POm axons in rat vibrissal cortex. Cereb Cortex. 20: 2265–2276.

Wright AK, Ramanathan S, Arbuthnott GW. 2001. Identification of the source of the bilateral projection system from cortex to somatosensory neostriatum and an exploration of its physiological actions. Neuroscience. 103: 87–96.

Woolsey TA, Van der Loos H. 1970. The structural organization of layer IV in the somatosensory region (SI) of mouse cerebral cortex. The description of a cortical field composed of discrete cytoarchitectonic units. Brain Res. 17: 205–

242.

Xu X, Roby KD, Callaway EM. 2010. Immunochemical characterization of inhibitory mouse cortical neurons: Three chemically distinct classes of inhibitory cells. J Comp Neurol. 518: 389–404.

Zeisel A, Muñoz-Manchado AB, Codeluppi S, Lönnerberg P, Manno GL, Juréus A, Marques S, Munguba H, He L, Betsholtz C, Rolny C, Castelo-Branco G, Hjerling-Leffler J, Linnarsson S. 2015. Cell types in the mouse cortex and hippocampus revealed by single-cell RNA-seq. Science. 347: 1138–1142.

Zhang S, Xu M, Kamigaki T, Do JPH, Chang W-C, Jenvay S, Miyamichi K, Luo L, Dan Y. 2014. Long-range and local circuits for top-down modulation of visual cortex processing. Science. 345: 660–665.

Zilberter Y, Kaiser KMM, Sakmann B. 1999. Dendritic GABA Release Depresses Excitatory Transmission between Layer 2/3 Pyramidal and Bitufted Neurons in Rat Neocortex. Neuron. 24: 979–988

Zingg B, Hintiryan H, Gou L, Song MY, Bay M, Bienkowski MS, Foster NN, Yamashita S, Bowman I, Toga AW, Dong HW. 2014. Neural networks of the mouse neocortex. Cell. 156: 1096–1111.

7   Acknowledgements

Curriculum Vitae

Personal information

Xiaojuan Zhou

Born in Wuhan, China

Address: Albrecht-Thaer-Weg 8, 37075, Göttingen

Email: j.zhou.neuronanatomy@gmail.com

Education

04.2013 – now	Doctorate in Sensory Motor Neuroscience program of GGNB
	Georg-August University, Göttingen, Germany
	Supervior: Prof. Jochen Staiger
2009 – 2012	M.Sc. in Fundamental Psychology
	East China Normal University, Shanghai, China
	Title of thesis: Regulatory Role of Histone Acetylation on Neurodegenerative Phenotypes of PS1/PS2 Double Knockout Mice
2005 – 2009	B.A. in Animal Science
	Huazhong Agricultural University, Wuhan, China
2005 – 2009	B.Sc. in Psychology
	Central China Normal University, Wuhan, China

Professional activities

01.2017	Oral presentation in SMN/SFB 889 internal retreat in Austria
12.2016	Poster presentation in GGNB Science Day in Göttingen, Germany
07.2016	FENS meeting 2016, Copenhagen, Denmark, with poster presentation
10.2015	Oral presentation in SMN/SFB 889 internal retreat in Dresden, Germany

09.2015	Attended Microscopy Conference 2015, Göttingen, Germany
05.2014	Organized Barrel Conference 2014, Göttingen, Germany

Funds and Awards

2017	GGNB Bridging fund – PhD-stipend
2014	GGNB Travel Grant for FENS meeting 2016, Copenhagen, Denmark
2013 – 2016	DAAD scholarship for doctoral study
2012	Poster prize for 2nd best poster in 9th Chinese Neuroscience Conference in Heinan, China

Teaching experience

02.2017	Provided technical supports (perfusion, immunohistochemical staining, EM procedures) to Dr. Talapka Petra for her post-doc research project
10.2015	Participated in teaching the practical course of transmission electron microscopy for Neuroscience study program in winter semester 2015/2016

Language

Native speaker in Chinese; fluent in English; B1 level in German

Software skills

Working knowledge of OpenOffice, ImageJ, GIMP, Inkscape, and R. Notation of blender and Octave.

Publications

Zhou X, Rickmann M, Hafner G, Staiger JF. 2017. Subcellular Targeting of VIP Boutons in Mouse Barrel Cortex is Layer-Dependent and not Restricted to Interneurons. Cereb Cortex. 27:5353–5368.

Cauli B, **Zhou XJ**, Tricoire L, Toussay X, Staiger JF. 2014. Revisitig enigmatic cortical calretinin-expressing interneurons. Front Neuroanat. 8:52.